DOCTOR OF PHILOSOPHY

Chaos pass filtering in chaos communication systems

Lea, Samuel

Award date:
2010

Awarding institution:
Bangor University

Chaos Pass Filtering in

Chaos Communication Systems

By Sam Lea

A thesis submitted in candidature for the degree of

Doctor of Philosophy

2010

Summary

This thesis presents the findings of a numerical study into the chaos synchronization and current modulation of semiconductor lasers. A system of coupled semiconductor lasers is simulated using a complex set of coupled differential equations.

The initial focus of the investigations is the chaos synchronization process. A proportion of the chaotic output of the first semiconductor laser is injected into a second and if the parameters of the lasers are sufficiently similar the dynamics of the second laser can lock to the dynamics of the first. The simulation model is verified by producing time domain outputs that can easily be compared with previous studies. The synchronization quality is assessed via the correlation coefficient and this is then used to obtain the widely used injection locking diagram.

The injection locking regime is studied in the frequency domain and, for the first time, frequency based injection locking diagrams are presented, providing added insight into the synchronization process. The subtle variations in the correlation of the laser dynamics observed across the injection locking region are attributed to low power spectral components at high frequencies.

The second half of the thesis focuses on the current modulation of a semiconductor laser and the use of chaos to mask the applied message. The extraction process at the receiver, commonly referred to as chaos pass filtering, is analysed. The difference between the frequency dependent current and optical modulation responses of the

semiconductor lasers used in the transmitter and receiver is shown to be key to the extraction process.

A realistic digital message is applied to the transmitter laser and the simulations have shown that a fine balance exists between the quality of extraction of the message at the receiver and the masking of the message in the transmitted signal.

Acknowledgements

Firstly, thanks to Prof. Paul Spencer for his continued support throughout these rather elongated studies. His confidence in my work and calm leadership is much appreciated. I must also thank Prof. Alan Shore and Dr. Iestyn Pierce for valued discussions throughout my time in Bangor.

I would also like to acknowledge my fellow PhD students. Thanks Anoop, Elias and Marek for providing a little light relief, a few over-competitive games of Badminton and a lot of strong coffee whenever it was required!

Thanks to my parents for always being there for support when required and believing I'd get there in the end. Better late, than never. Lastly to Maz, your support over the last few months has kept me going. I wouldn't be where I am without you, sweet as bro.

Contents

Structure of Thesis

Chapter 1 introduces the background semiconductor laser theory required to create the simulation framework used in all the numerical simulations in this thesis. The widely used Lang-Kobayashi rate equations are derived for the temporal dynamics of a semiconductor laser subject to optical feedback from an external mirror. The Lang-Kobayashi model is then extended to include optical injection from an external optical source. This provides the basis for the numerical model of a master semiconductor laser whose chaotic optical output is injected into a second, slave, laser diode.

The second Chapter introduces the numerical model. The operation of the numerical model is verified by simulating the widely studied phenomenon of chaos injection locking. A sufficient proportion of the master laser optical output is injected into the slave laser to allow the slave dynamics to lock to the dynamics of the master. The degree of synchronization between the master and slave dynamics is calculated using a cross-correlation function. The correlation of the optical intensity and carrier dynamics for varying injection strengths and detuning frequencies is collated to create injection-locking diagrams. Motivated by the eventual aim of simulating a communications

system utilizing chaotic masking, injection locking diagrams are presented, for the first time, of a current modulated master laser.

Chaos injection locking is examined in the frequency domain in Chapter 3. The optical intensity spectra of the master and slave laser diodes are presented. The slave laser spectrum is divided by the master laser spectrum to create the response gain. The spectral variation in the phase difference between the master and slave lasers is also calculated. The response gain and phase difference are calculated for both single simulations and the ensemble average of a large number of simulations with different initial conditions. The frequency domain analysis allows the identification of the spectral components required for good synchronization.

Frequency based chaos injection locking diagrams are presented for the first time and provide added insight into the chaos synchronization process. Trends in synchronization quality observed using these frequency domain techniques are compared to those seen in the time domain injection locking diagrams. The trends observed in the time domain correlation are also observed in the response gain characteristic, and these trends are shown to be dependent upon the coupling parameters. The frequency based injection locking diagrams also shows that the small changes in correlation observed in the injection locking region are highly dependent upon the low power high frequency distortion components induced in the slave by the injected signal.

Chaos Pass Filtering in Chaos Communication Systems

The addition of a message via the modulation of the semiconductor laser diode drive current is introduced in Chapter 4. Firstly, the current modulation of a solitary laser diode is explored to validate the numerical model and to also provide baseline results for later discussion. Secondly, the current modulation of a chaotic laser diode subject to external optical feedback is calculated. The frequency dependent output characteristic of the modulated solitary laser and external cavity laser are also presented. The degree to which the average background chaos and an applied sinusoidal message contribute towards the laser output is studied.

Chapter 5 adds a receiver (slave) laser diode which is subject to optical injection from the modulated transmitter (master) laser diode. The frequency domain techniques established in earlier Chapters are used to study the chaotic masking of an applied sinusoidal message and the extraction process of the message in the receiver. The optical amplitude and phase modulation responses of the receiver to the sinusoidal messages applied to the transmitter injection current are presented and shown to be frequency dependent.

A strongly applied message may be extracted in the receiver laser via the subtraction of the receiver output from that of the transmitter input in a process known as 'chaos pass filtering'. The response gain characteristic for chaos synchronization of a master and slave laser system from Chapter 3 is compared to that of a communication system utilizing a current modulated transmitter laser with and without chaos masking. It is shown that the difference in the optical and current modulation characteristics give rise to frequency dependent attenuation and gain of the message, while the high power

background chaos components receive a uniform gain in the receiver. This synchronization of the background chaos and attenuation or gain of the message allows the message to be extracted in the receiver by subtraction of the receiver output from the incoming transmission.

Three regions of operation of the current modulated communications system employing chaos masking are defined and are related to the transmitted message security and the quality of extraction in the receiver. A trade off between message security and extraction is observed whereby a strongly applied message may be easily extracted via subtraction of the optical fields in the receiver laser but is susceptible to possible detection in the transmission by an eavesdropper. Meanwhile, a securely applied message that is not distinguishable from the background chaos is also indistinguishable from the chaos in the receiver and cannot be extracted successfully.

A more complex and realistic pseudo random bit sequence message is applied to the transmitter in Chapter 6. The pseudo random bit stream message is subject to the same response in the transmitter and receiver lasers as for individually applied sinusoidal messages. The complex pseudo random bit sequence (PRBS) message has time varying spectral content and is more difficult to identify in the transmission spectrum than a simple sinusoidal message. The PRBS message is not easily extracted due to the interaction with the fluctuating spectral power of the background chaos and some deterioration of the message at the receiver must be accepted if the message is to be securely transmitted.

Chapter 1

Semiconductor Lasers

1.1 Introduction

This chapter details the semiconductor laser theory required for the simulations presented later in this thesis.

The widely used Lang-Kobayashi set of equations [1] are derived and terms representing optical feedback from an external mirror and optical injection from an external source are added to the model. This extended form of the Lang-Kobayashi equations forms the basis for the numerical simulations presented in later chapters.

1.2 Semiconductor Laser Dynamics

The charge carrier number in the semiconductor laser diode, N, can be shown to be given by [2]:

$$\frac{\partial N}{\partial t} = \frac{I}{eV} + D\nabla^2 N - r_{st}(N,P) - \frac{N}{\tau_N} \qquad 1.1$$

where the terms on the right hand side of the equation represent from left to right the pumping rate, diffusion rate $D\nabla^2 N$, $r_{st}(N,P)$ the rate of stimulated emission which is

dependent upon both the carrier (N) and photon (P) number, and the rate of spontaneous emission. Following standard practice diffusion effects will be neglected, [3] and hence Eqn. 1.1 simplifies to:

$$\frac{dN}{dt} = \frac{I}{eV} - r_{st}(N,P) - \frac{N}{\tau_N} \qquad 1.2$$

The pumping rate populates the excited energy levels while the other processes depopulate it. The rate of stimulated emission can be written as:

$$r_{st} = G(N)P = \frac{g_N P c}{n_g} \qquad 1.3$$

where $G(N)$ is the optical gain term and can be assumed to be linear. g_N is the gain coefficient of the carriers. The optical field is not necessarily confined to the active region unlike the carriers and as a result only a fraction of the optical field can contribute towards stimulated emission. We can define the optical field confinement factor, Γ, so that $g_P = \Gamma g_N$ [3,4]:

$$\Gamma \approx \frac{(\omega^2/c^2)(n_1^2 - n_2^2)d^2}{2 + (\omega^2/c^2)(n_1^2 - n_2^2)d^2} \qquad 1.4$$

It is often assumed that there is complete overlap between the optical field and the active region, setting the confinement factor to unity $\Gamma = 1$. The optical and carrier gain term are then equal $g_P = g_N = g$ and the carrier rate equation becomes:

$$\frac{dN}{dt} = \frac{I}{eV} - \frac{gPc}{n_g} - \frac{N}{\tau_N} \qquad 1.5$$

1.2.1 The Linewidth Enhancement Factor

The refractive index, n ,of the active region is known to be carrier dependent and will be assumed to vary linearly with the carrier number [3]:

$$n(N) = n_b + \frac{\partial n}{\partial N} N \tag{1.6}$$

This then leads to the pump induced susceptibility χ_p which is linearly dependent upon the carrier number so that:

$$\chi_p(N) = n_b \left(2\frac{\partial n}{\partial N} + i\frac{c}{\omega}\Gamma\frac{\partial g}{\partial N} \right) N \tag{1.7}$$

The linewidth enhancement factor or α -factor can now be defined by the ratio of the real and imaginary parts of the susceptibility:

$$\alpha \equiv -2\frac{\omega}{c\Gamma}\frac{\partial n / \partial N}{\partial g / \partial N} \tag{1.8}$$

The linewidth enhancement factor is a consequence of the existence of a range of possible energy levels within the valence and conduction bands. The linewidth enhancement factor enhances the linewidth of the optical field spectrum and plays a significant role in the temporal and spectral dynamics of semiconductor laser [5].

1.3 Semiconductor Laser Dynamics – Optical Field

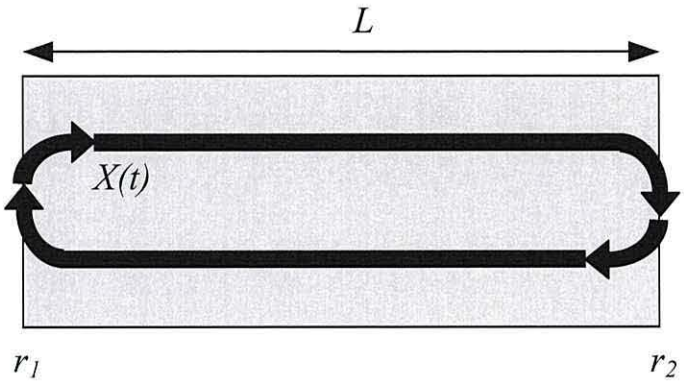

Figure 1.1. Complex E-Field within semiconductor laser active region of length *L* and facet reflectivities r_1 and r_2.

Expressions for the temporal dynamics of a semiconductor laser E-Field and carrier number will now be derived following the procedure described by Petermann in [6].

The round-trip gain G_r can be defined:

$$G_r = r_1 r_2 \exp\left[-i2\beta L + (g - \alpha_s)L\right] \tag{1.9}$$

where r_1 and r_2 are the reflectivities of the laser diode facets and L is the length of the active region, Figure 1.1. The optical loss constant is given by β, g is the optical gain coefficient and all the non-contributory losses are grouped together and given by α_s.

The losses α_s are assumed to be independent of frequency, however the optical phase constant β depends upon both the threshold frequency ω_{th} and carrier density N_{th} such that [3, 6]:

$$\beta = \frac{\omega}{c} n \approx \frac{n_{th}\omega_{th}}{c} + \frac{\omega_{th}}{c}\frac{\partial n}{\partial N}(N - N_{th}) + \frac{1}{c} n_g(\omega - \omega_{th}) \tag{1.10}$$

where c is the speed of light, n is the refractive index and n_g is the group refractive index.

Substituting Eqn. 1.10 into Eqn. 1.9 and given that the round-trip gain operator may be written as $G_r = G_{rI}G_{r\omega}$ the intensity dependent operator G_{rI} and the frequency dependent operator $G_{r\omega}$ can be defined by Eqn. 1.11 and Eqn. 1.12 respectively:

$$G_{rI} = r_1 r_2 \exp\left[(g(N) - \alpha_s)L - 2i\frac{\omega_{th}L}{c}\frac{\partial n}{\partial N}(N - N_{th})\right] \quad 1.11$$

$$G_{r\omega} = \exp\left[-2i\frac{n_{th}\omega_{th}L}{c} - 2i\frac{n_g L}{c}(\omega - \omega_{th})\right] \quad 1.12$$

Since $\omega n / c = \beta$ and $\beta L = m\pi$ the first component in the exponent of Eqn. 1.12 disappears over a complete round-trip. The resonant cavity linear mode spacing ∂f is defined as:

$$\partial f = \frac{c}{2Ln_g} = \frac{1}{\tau_{in}} \quad 1.13$$

where τ_{in} is the internal cavity round-trip time. Eqn. 1.13 can now be substituted into Eqn. 1.12 giving:

$$G_{r\omega} = \exp\left[-i(\omega - \omega_{th}\tau_{in})\right] \quad 1.14$$

and a further substitution $d / dt = i\omega$ gives:

$$G_{r\omega} = \exp\left[i\omega_{th}\tau_{in}\right]\exp\left[-\tau_{in}\frac{d}{dt}\right] \tag{1.15}$$

The intensity and frequency round-trip gain operators can now be applied to define the complex E-Field within the cavity, $X(t)$, and leads to:

$$X(t) = G_{rI}G_{r\omega}X(t) = G_{rI}\exp\left[i\omega_{th}\tau_{in}\right]\exp\left[-\tau_{in}\frac{d}{dt}\right]X(t) \tag{1.16}$$

The E-Field slowly varying envelope approximation given as:

$$X(t) = E(t)e^{i\omega_{th}t} \tag{1.17}$$

and can now be substituted into Eqn. 1.16 removing the fast oscillation. Also noting that $\exp\left[-\tau_{in}d/dt\right]$ is simply a time shift in the field [6]:

$$E(t) = G_{rI}E(t-\tau_{in}) \tag{1.18}$$

The variation in the E-Field envelope can be considered small over a single cavity round-trip and can be approximated to:

$$E(t-\tau_{in}) \approx E(t) - \tau_{in}\frac{dE}{dt} \tag{1.19}$$

Substituting Eqn. 1.19 into Eqn. 1.18 and rearranging an expression for the rate of change of electric field can be derived:

$$\frac{dE}{dt} = \frac{1}{\tau_{in}}\left(1-\frac{1}{G_{rI}}\right)E(t) \tag{1.20}$$

In order to substitute for $1/G_{rI}$ Eqn. 1.11 needs to be rewritten as an exponential and then the fact that $G_{rI} \approx 1$ for laser operation may be used, thus:

$$\frac{1}{G_{rI}} = \exp\left[-\ln(r_1 r_2) - (g(N) - \alpha_s)L + 2i\frac{\omega_{th}L}{c}\frac{\partial n}{\partial N}(N - N_{th})\right] \quad 1.21$$

$$\frac{1}{G_{rI}} \approx 1 + \frac{1}{2}\ln(R_1 R_2) - gL + \alpha_s L + 2i\frac{\omega_{th}L}{c}\frac{\partial n}{\partial N}(N - N_{th}) \quad 1.22$$

Substituting Eqn. 1.22 into Eqn. 1.20:

$$\frac{dE}{dt} = \frac{1}{\tau_{in}}\left(-\frac{1}{2}\ln(R_1 R_2) - gL + \alpha_s L + 2i\frac{\omega_{th}L}{c}\frac{\partial n}{\partial N}(N - N_{th})\right)E(t) \quad 1.23$$

The photon lifetime will now need to be defined:

$$\frac{1}{\tau_p} = \frac{c}{n_g}\left(\alpha_s + \frac{1}{2L}\ln(R_1 R_2)\right) \quad 1.24$$

and using Eqn. 1.24 along with the relation $2L/\tau_{in} = c/n_g$ Eqn. 1.23 becomes:

$$\frac{dE}{dt} = \left(-\frac{1}{2}\tau_p + \frac{gc}{2n_g} - i\frac{\omega_{th}}{n_g}\frac{\partial n}{\partial N}(N - N_{th})\right)E(t) \quad 1.25$$

Finally, the differential gain term is introduced $\xi = (c/n_g)\partial g/\partial N$ and substituting in the linewidth enhancement factor from Eqn. 1.8 gives:

$$\frac{dE}{dt} = \frac{1}{2}(1 + i\alpha)\xi(N - N_{th})E(t) \quad 1.26$$

Assuming that each carrier decay gives rise to a coherent photon then the rate of change of photons in the optical field can be written as:

$$\frac{dP}{dt} = G(N)P \tag{1.27}$$

and can be substituted into Eqn. 1.5 for the carrier dynamics giving:

$$\frac{dN}{dt} = \frac{I}{eV} - \frac{N}{\tau_N} - \xi(N - N_0)|E(t)|^2 \tag{1.28}$$

Eqn. 1.26 and eqn. 1.28 form the coupled rate equation model for semiconductor laser diode dynamics.

The gain G has so far been considered to be linear. Under the strong optical pumping likely to be used during laser operation, however, the gain can saturate [7]. This is due to a number of processes but the most important are spectral hole burning and dynamic carrier heating [3]. The gain term G can be modified to take these factors into account and the expression below has been shown to be a good fit to experimental data:

$$G(N,P) = \frac{g(N(t) - N_0)}{1 + \varepsilon|E(t)|^2} \tag{1.29}$$

where ε is the gain saturation coefficient. This version of the gain will now be used in the semiconductor laser rate equation model and throughout the subsequent work.

1.4 The Lang-Kobayashi Model

An external mirror is now added to the semiconductor laser diode defining an external cavity and providing optical feedback into the laser cavity, Figure 1.2. The super-scripts denote the field propagating from left-right (+) and right-left (-) in Figure 1.2.

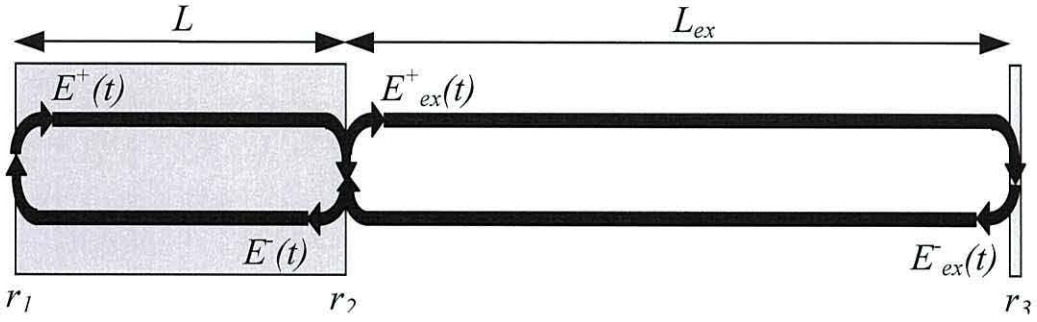

Figure 1.2. Semiconductor laser diode with feedback from an external mirror with reflectivity r_3. The length of the external cavity is L_{ex}. Superscript + (-) denotes the field propagating from left to right (right to left).

Given that $E^+(t)$ is the fraction of the field that leaves the cavity through mirror r_2. $E_{ex}^+(t)$ is then the field propagating in the external cavity and the portion fed back into the laser cavity, $E_2^-(t)$, may be written as:

$$E_{ex}^+(t) = \sqrt{(1-r_2^2)}E^+(t-\tau/2) \qquad 1.30$$

$$E_{ex}^-(t) = r_3 E_{ex}^+(t-\tau_{ex}/2) = r_3\sqrt{(1-r_2^2)}E^+(t-\tau/2-\tau_{ex}/2) \qquad 1.31$$

$$E_2^-(t) = \sqrt{(1-r_2^2)}E_{ex}^-(t-\tau_{ex}/2) = r_3(1-r_2^2)E^+(t-\tau/2-\tau_{ex}) \qquad 1.32$$

$E_2^-(t)$ gives the additional field propagating from right to left within the laser cavity due to the external optical feedback provided by the external mirror r_3. $E_2^-(t)$ can now

be expressed as a fraction of the field propagating right-to-left in the solitary laser cavity (no external cavity feedback) $E^-(t) = r_2 E^+(t-\tau/2)$ and rearranging so that $E^+(t) = E^-(t+\tau/2)/r_2$. Now substituting for $E^+(t)$ in Eqn. 1.32 yields:

$$E_2^-(t) = \frac{r_3(1-r_2^2)}{r_2} E^-(t-\tau_{ex}) \qquad 1.33$$

Eqn. 1.33 uses the single round-trip approximation [6] assuming that multiple reflections do not occur within the external cavity. The single round-trip approximation has been shown to be accurate for relatively low levels of feedback where $r_3 r_2 << 1$. To account for multiple reflections Eqn. 1.33 can be extended to give [1]:

$$E_2^-(t)e^{i\omega_0 t} = \left[r_2 + (1-r_2^2)r_3 e^{-i\omega_0\tau_{ex}} + (1-r_2^2)r_3^2 r_2 e^{-i2\omega_0\tau_{ex}} + \ldots\right] E^-(t)e^{i\omega_0 t} \qquad 1.34$$

The first term on the right hand side of Eqn. 1.34 is the optical field due to the internal cavity. Each subsequent term is a field component due to a round-trip of the external cavity.

For $r_3 r_2 << 1$ the complex optical field rate Eqn. 1.26 can be combined with Eqn. 1.33 giving [1]:

$$\frac{dE(t)}{dt} = \frac{1}{2}(1+i\alpha)\left[G(t) - 1/\tau_P\right]E(t) + \kappa E(t-\tau_{ex})e^{-i\omega_0\tau_{ex}} \qquad 1.35$$

where κ is external cavity feedback rate defined as:

$$\kappa = \frac{(1-r_2^2)r_3}{\tau_{in} r_2} \qquad 1.36$$

Eqn. 1.35 and Eqn. 1.28 along with Eqn. 1.28 together make up the Lang-Kobayashi model [1].

1.4.1 Optical Injection

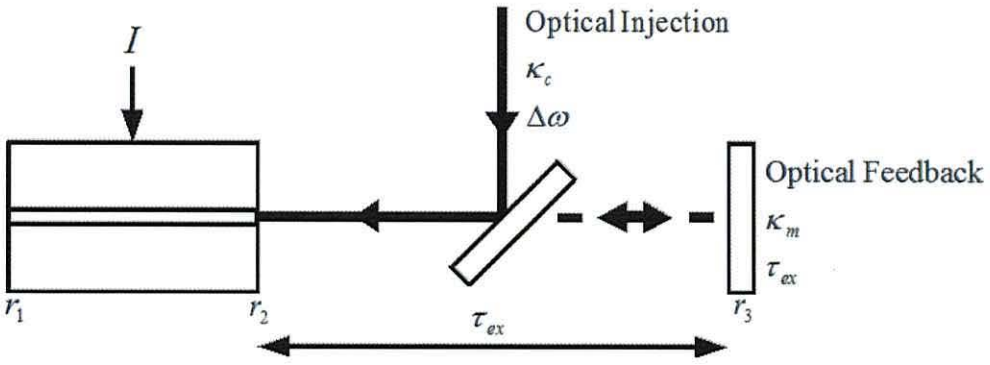

Figure 1.3. Semiconductor laser diode subject to optical injection from an external source with injection rate κ_c and detuning frequency $\Delta\omega$.

An external optical field may be injected into the laser cavity from a second laser diode, Figure 1.3. An additional term is added to the field Eqn. 1.35 to account for the optical injection [8]:

$$\frac{dE(t)}{dt} = \frac{1}{2}(1+i\alpha)\left[G(t) - 1/\tau_P\right]E(t) + \kappa E(t-\tau_{ex})e^{-i\omega_0\tau_{ex}} + \kappa_c E_c(t-\tau_c)e^{i\Delta\omega t} \qquad 1.37$$

where the transit time from the external optical source is given by τ_c . The frequency difference between the injected optical signal ω_c and the free running solitary laser at threshold ω_0 is defined as $\Delta\omega = \omega_c - \omega_0$. If the second laser diode is identical to the first then the injection rate κ_c of the optical field E_c may be defined as:

$$\kappa_c = \frac{\sqrt{(1-r_{2m}^2)}\sqrt{(1-r_2^2)}\Gamma}{\tau_{in} r_2} \tag{1.38}$$

where Γ is the transmission coefficient of the injected field and represents any attenuation experienced by the field during transmission between the generating laser diode and the laser diode subject to the injection. Complete injection of the field is given by $\Gamma = 1$. The reflectivity of the facet from which the external optical field is generated in the second laser is denoted by $r_{2,m}$ in Eqn. 1.38. If both laser diodes have identical facet reflectivities $r_{2,m} = r_2$ then Eqn. 1.38 may be reduced to:

$$\kappa_c = \frac{(1-r_2^2)\Gamma}{\tau_{in} r_2} \tag{1.39}$$

1.5 Summary and Implementation

The rate equation model to be used in the following chapters has been presented. This model may be solved using the Euler method [9] and forms the basis of the work presented in later chapters. Firstly, in the study of chaos synchronization via optical injection (Chapters 2-3). Secondly, in the study of a chaotic communications system (Chapters 4-6).

1.6 Bibliography

[1] R Lang and K Kobayashi, "External Optical Feedback Effects on Semiconductor Injection Properties," *IEEE J. Quant. Electron.*, vol. 16, no. 3, pp. 347-355, March 1980.

[2] M Yamada, "Transverse and longitudinal mode control in semiconductor injection lasers," *IEEE J. Quantum Electron.*, vol. 19, no. 9, pp. 1365-1380, September 1983.

[3] G H M van Tartwijk and D Lenstra, "Seminconductor lasers with optical injection and feedback," *Quantum Semiclass. Opt.*, vol. 7, pp. 87-143, April 1995.

[4] D Botez, "InGaAsP/InP double-heterostructure lasers: Simple expressions for wave confinement, beamwidth, and threshold current over wide ranges in wavelength (1.1-1.65 μm)," *IEEE J. Quantum Electron.*, vol. 17, no. 2, pp. 178-186, February 1981.

[5] L A Coldren and S W Corzine, *Diode Lasers and Photonic Integrated Circuits.*: Wiley, 1995.

[6] K Petermann, *Laser Diode Modulation and Noise.*: Kluwer Academic Publishers, 1988.

[7] A Bogatev, P Eliseev, and B Sverdlov, "Anomalous interaction of spectral modes in

a semiconductor laser," *IEEE J. Quantum Electron.*, vol. 11, no. 7, pp. 510-515, July 1975.

[8] V Annovazzi-Lodi and S Donati, "Synchronization of Chaotic Injected-Laser Systems and Its Application to Optical Cryptography," *IEEE Journal of Quantum Electronics*, vol. 32, no. 6, pp. 953-959, June 1996.

[9] William H Press, Brian P Flannery, Saul A Teukolsky, and William T Vetterling, *Numerical Recipes in C: The Art of Scientific Computing*, 2nd ed.: Cambridge University Press, 1992.

Chapter 2

Synchronization of Semiconductor Laser Diodes: Time Domain Analysis

2.1 Introduction

In 1665 Christiaan Huygens observed that by placing two similar unsynchronized pendulum clocks together, the two pendulums would soon become entrained via mutual coupling. Schatz et al. [1] subsequently showed that the synchronization occurred because the vibrations were being transmitted through the wooden beam that the pendulums were hung from and the closely matched properties of the pendulums allowed the mutual bi-directional coupling of the clocks. Since then there has been significant research into the synchronization of oscillators.

Synchronization is of significant technological importance and particularly so for some forms of communications. This has led to extensive investigation of the phenomenon and various stable and unstable synchronization regimes have been identified. Semiconductor lasers have been one of the physical systems used in these investigations.

2.1.1 Stable Continuous Wave Optical Injection Locking

Improvements in semiconductor laser fabrication in the late 1970s and early 1980s provided enhanced lasing characteristics and allowed the practical study of a system of coupled semiconductor lasers.

Continuous wave injection locking is achieved by injecting a proportion of the optical output of a master laser into another laser, the slave. If the injected power is sufficiently strong and the frequency detuning of the master and slave lasers is sufficiently small then the slave laser can be forced to operate at exactly the same frequency as the master laser and the lasers are said to be injection locked. An increase in the injected optical power allows injection locking to be achieved for a wider range of detuning frequencies. Continuous wave injection locking has been extensively studied in semiconductor lasers with various aims including the stabilization of a slave laser, bandwidth enhancement and noise reduction [2-4].

2.1.2 Unstable Dynamics - Chaotic Injection Locking

Chaotic operation of the master laser is possible with appropriate optical and electrical feedback or injection. It has also been shown that stable locking and synchronization can also be achieved even when the dynamics are chaotic [5]. Hayes et al [6] proposed that such a system could be used as a communications channel. Since then there has been much interest in this concept, due in part to the possibility of creating an all optical communications system with the message securely hidden by a chaotic carrier.

Chapter 2 – Synchronization of Semiconductor Laser Diodes: Time Domain Analysis

Chaotic synchronization has been reported in both electrical and optical systems and several types of chaotic synchronization have been identified [7-12]. The various synchronization regimes can be broadly assigned to one of two groups: complete or perfect chaotic synchronization [12, 13] and general or injection locking synchronization [14-18].

Semiconductor lasers have been found to be an ideal system for studying the chaotic synchronization process. Early work by Geodgebuer et al [19] demonstrated one form of chaotic synchronization scheme based on chaotic fluctuation in the emission wavelength of semiconductor lasers. Subsequent work has primarily focused on chaotic synchronization schemes based on chaotic fluctuations in the optical intensity of semiconductor lasers. Typically, these chaotic intensity fluctuations are induced in the master laser either by suitable external optical feedback from a mirror or by external optical injection. Both result in a dramatic broadening of the emission spectrum and large amplitude chaotic fluctuations in the optical intensity [20, 21]. Sivaprakasam et al [21] were the first to experimentally demonstrate optical intensity based chaotic synchronization using laser diodes and since then numerous theoretical and experimental studies of this phenomenon have been reported [22-30].

2.2 Types of Chaos Synchronization

2.2.1 Perfect Synchronization

Complete synchronization is strictly speaking a mathematical abstraction that requires the two coupled systems to be identical and places stringent requirements on the coupling strength between the coupled oscillators [12]. If the required conditions are met then the dynamics of the two oscillators become identical, except for a time delay. It is also possible for this time delay to be such that the dynamics of the slave oscillator anticipate those of the master oscillator [13].

For perfect synchronization to occur the parameters of both the master laser and the slave laser must be identical and $\kappa_c + \kappa_s = \kappa_m$, where κ_c is the slave laser injection rate and κ_m and κ_s are the master and slave laser feedback rates respectively. This condition is necessary but not sufficient for perfect synchronization. At the point where perfect synchronization is achieved, the following relationship is attained: $P_m(t) = P_s(t + (\tau_c - \tau_{ex}))$ where P_m and P_s are the master and slave laser field amplitudes. τ_c is the time of flight between the two lasers and τ_{ex} is the master external round trip time. The slave laser output is observed to anticipate the master laser output if $\tau_{ex} > \tau_c$. Anticipation has been observed in the slave laser in several published studies [23, 26]. In perfect synchronization all the frequency components are "locked" simultaneously and continuously.

2.2.2 Injection Locking Synchronization

Injection locking based synchronization is a more robust process than perfect synchronization and can tolerate considerable changes in parameter values. Injection locking synchronization may be achieved for a large range of slave laser injection rates and detuning frequencies. The quality of the injection locking synchronization is always less than that for perfect synchronization and varies according to the master and slave laser parameter values. The quality of synchronization deteriorates with increasing master-slave mismatch. In injection locking based synchronization the slave dynamics always lag those of the master oscillator: $P_s(t) = P_m(t-\tau)$ where τ is the time shift between the master and slave dynamics for which the best quality synchronization is attained [31]. It will be shown in Chapter 3, using frequency domain techniques, that in injection locking synchronization only the main frequency components are locked continuously, other frequencies are locked only intermittently at best. This is in marked contrast to perfect synchronization.

2.3 Numerical Model Framework

The numerical model used for the simulations throughout this thesis will now be outlined. Figure 2.1 illustrates the master and slave laser configuration. The master (ML) and slave (SL) lasers have internal reflectivities given by r_1 and r_2 and external mirror reflectivities r_{3m} and r_{3s} respectively. The length of the master and slave laser external cavities are defined by the round trip time τ_{ex}. The master (slave) laser injection current is given by I_m (I_s). The optical output of the master laser is coupled to the slave laser via the optical isolator (ISO).

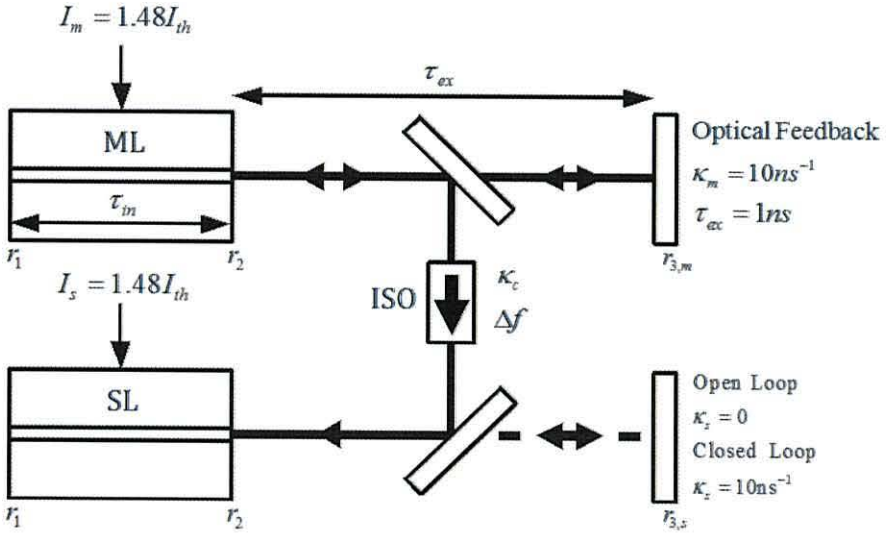

Figure 2.1. Configuration of the master (ML) and slave (SL) laser diodes. Master and slave facet reflectivities r_1 and r_2. The master is subject to optical feedback from an external mirror with reflectivity r_{3m}. The master and slave drive currents are given by I_m and I_s respectively. The optical isolator (ISO) allows unidirectional injection from the master to the slave laser.

Chapter 2 – Synchronization of Semiconductor Laser Diodes: Time Domain Analysis

The term open-loop configuration is used when the slave laser is not subject to optical feedback from an external mirror. In contrast, the closed-loop configuration contains external optical feedback from an external mirror with reflectivity, r_{3s}.

The master and slave laser dynamics can be simulated using an extended form of the Lang-Kobayashi equations [32],

$$\frac{dE_m(t)}{dt} = \frac{1}{2}(1+i\alpha)\left[G_m(t) - \frac{1}{\tau_P}\right]E_m(t) + \kappa_m E_m(t-\tau_{ex,m})e^{-i\omega_m\tau_{ex,m}} \quad 2.1$$

$$\frac{dE_s(t)}{dt} = \frac{1}{2}(1+i\alpha)\left[G_s(t) - \frac{1}{\tau_P}\right]E_s(t) + \kappa_s E_s(t-\tau_{ex,s})e^{-i\omega_s\tau_{ex,s}} + \kappa_c E_m(t)e^{i\Delta\omega t} \quad 2.2$$

$$\frac{dN_{m,s}(t)}{dt} = \frac{I_{m,s}}{e} - \frac{N_{m,s}(t)}{\tau_N} - G_{m,s}(t)\left|E_{m,s}(t)\right|^2 \quad 2.3$$

$$G_{m,s}(t) = \frac{g_0(N_{m,s}(t) - N_0)}{1+\varepsilon\left|E_{m,s}(t)\right|^2} \quad 2.4$$

Where E_m (E_s) is the slowly varying complex field amplitude of the master (slave) laser. N_m (N_s) is the master (slave) laser carrier number. The time of flight τ_c between the master and slave laser is set to $\tau_c = 0$ throughout the investigation.

$\tau_N = 2ns$ and $\tau_P = 2ps$ are the carrier and photon lifetimes respectively, $\tau_{ex} = 1ns$ is the external cavity round trip time, e is the electronic charge, $\alpha = 5$ is the linewidth enhancement factor, $N_0 = 1.5x10^8$ is the carrier number at transparency, $g_0 = 1.5x10^{-8}ps^{-1}$ is the linear gain coefficient, $\varepsilon = 5x10^{-7}$ is the gain saturation

coefficient. $\Delta\omega$ is the frequency detuning between the two lasers and determines the phase of the injected field. Spontaneous emission is not considered since the following numerical simulations occur well above threshold. The parameter set used throughout this thesis is based upon that used in [16] and [31].

The magnitude of the frequency detuning is defined by,

$$\Delta\omega = \omega_m - \omega_s \tag{2.5}$$

Where ω_m (ω_s) is the emission frequency of the ML (SL). The solitary ML and SL are assumed to support a single longitudinal mode. The nominal emission wavelength of the master is assumed to be $\lambda = 780nm$. κ_m (κ_s) is the master (slave) feedback coefficient given by,

$$\kappa_{m,s} = \frac{(1-r_2^2)r_{3m,s}}{r_2\tau_{in}} \tag{2.6}$$

Where $r_2 = r_1 = 0.548$ is the master and slave facet reflectivity, $r_{3m,s}$ is the master, slave laser external reflectivity and $\tau_{in} = 7ps$ is the internal cavity round trip time for the master and slave lasers. κ_c is the slave laser injection rate given by,

$$\kappa_c = \frac{(1-r_2^2)\Gamma}{r_2\tau_{in}} \tag{2.7}$$

Where Γ is the transmission coefficient of the injected field. $I_{m,s}$ is the master, slave laser injection current. I_{th} is the laser threshold current given by

$$I_{th} = \frac{e}{\tau_N}\left(N_0 + \frac{1}{g_0 \tau_P}\right) \qquad 2.8$$

Table 2.1 details the complete parameter set used in the following numerical simulations.

Parameter	Symbol	Value
Master laser drive current	I_m	$1.48I_{th}$
Slave laser drive current	I_s	$1.48I_{th}$
Linewidth enhancement factor	α	5
Carrier lifetime	τ_N	2ns
Photon lifetime	τ_P	2ps
Internal cavity round-trip time	τ_{in}	7ps
Master laser external cavity round-trip time	τ_{ex}	1ns
Linear gain coefficient	g	$1.5\text{x}10^{-8}\text{ps}^{-1}$
Gain saturation coefficient	ε	$5\text{x}10^{-7}$
Carrier number at transparency	N_0	$1.5\text{x}10^{8}$
Wavelength	λ	780nm
Facet reflectivity	r_1, r_2	0.548
Master laser feedback rate	κ_m	10ns^{-1}
Slave laser injection rate	κ_c	170ns^{-1}
Slave laser detuning frequency	Δf	0
Slave laser feedback rate	κ_s	0

Table 2.1. Parameter set used in the investigation is similar to that used in [16] and [31].

2.3.1 Numerical Solution of Differential Equations

The rate equations (1-4) were solved using Euler's method [33] and the master (slave) laser complex varying amplitude of the electric field E_m (E_s) is then used to determine the optical intensity P_m (P_s) since

$$P_{m,s}(t) = \left(\frac{\hbar\omega_{m,s}}{\tau_P}\right)\left|E_{m,s}(t)\right|^2 \qquad 2.9$$

where $\hbar$ is the reduced Planck constant. The optical phase is given by

$$\phi_{m,s} = \tan^{-1}\left(\frac{\Im(E_{m,s}(t))}{\Re(E_{m,s}(t))}\right) \qquad 2.10$$

In order to achieve accurate solutions to the complex set of stiff equations used a very small time step is required. Verification of the model has shown that a time step of one tenth of the size of the photon lifetime, is sufficient to ensure numerical stability and model the photon dynamics within the laser cavity.

Chapter 2 – Synchronization of Semiconductor Laser Diodes: Time Domain Analysis

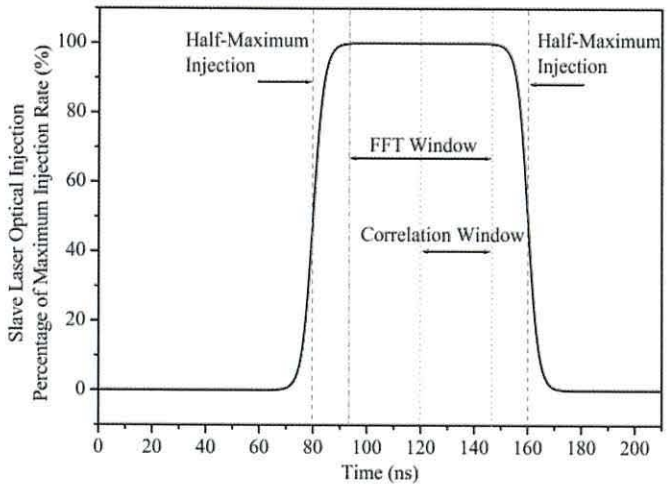

Figure 2.2. Percentage of maximum optical injection to the slave laser for a single simulation of 210ns duration.

In this thesis a single numerical simulation is run for a total duration of 210ns. During a simulation the initial transients are allowed to decay, before the master laser output is injected into the slave laser. The master laser output is then injected into the slave laser using the exponential windowing function shown in Figure 2.2. This ramps up the injection rate gradually from 0% to 100% to minimize any transients that may occur. Half the maximum injection is achieved after 80ns.

2.4 Analysis of Simulation Data

During the period at the full injection rate the correlation between the master and slave laser intensities is calculated within a 26ns window. The Fast Fourier Transform (FFT) of the master laser and slave laser intensities is also calculated using a 52ns window offset by the time difference required to obtain maximum correlation [31]. The simulation time periods used for the correlation and FFT are shown in Figure 2.2. The slave laser intensity is shifted by the optimum time shift τ to ensure that the slave laser FFT coincides with the correct time period of the injected signal. The fairest comparison of the master and slave laser spectra may then be performed. For example, at the perfect synchronization point the optimum time shift between the master and slave dynamics is equal to the master laser external cavity round trip time, in the absence of a transit time between master and slave.

The fast Fourier transform will be extensively used to investigate injection locking synchronization process in the spectral domain in Chapter 3, where the post-processing will also be outlined in more detail.

2.4.1 Correlation

The degree of temporal synchronization between the master and slave laser dynamics is determined using the cross-correlation function $C_P(\tau)$,

$$C_P(\tau) = \frac{\left\langle \left[P_m(t-\tau) - \langle P_m \rangle\right]\left[P_s(t) - \langle P_s \rangle\right] \right\rangle}{\left\{ \left\langle \left[P_m(t-\tau) - \langle P_m \rangle\right]^2 \right\rangle \left\langle \left[P_s(t) - \langle P_s \rangle\right]^2 \right\rangle \right\}^{\frac{1}{2}}} \qquad 2.11$$

where τ is the time shift between the master and slave laser outputs. At the perfect synchronization point the maximum correlation is achieved for $\tau = \tau_{ex}$ assuming the master - slave transit time $\tau_c = 0$. A correlation of zero indicates completely unsynchronized dynamics and a correlation of unity indicates complete or perfect synchronization.

The correlation between master and slave dynamics is calculated for a range of time shifts τ, from $\tau = -1\text{ns}$ to $\tau = 1\text{ns}$ in $\Delta\tau = 2\text{ps}$ time steps to ensure the maximum correlation is found. The time shift corresponding to the maximum correlation is the optimum time shift, τ_{opt}. The correlation given by Eqn. 2.11 applies to the correlation of the master and slave optical intensity dynamics, $P_m(t)$ and $P_s(t)$ respectively, but these can be substituted for other variable such as the optical phase, $\phi(t)$, or carrier number, $N(t)$.

2.5 Numerical Simulation

2.5.1 Dynamics of Synchronized Chaotic Laser Diodes

The master and slave laser diode optical intensity, optical phase and carrier dynamics for a typical simulation of injection locking synchronization will now be presented. The quality of synchronization will be calculated and the high frequency distortion induced in the slave laser optical intensity will also be highlighted.

Chaotic injection locking of the master and slave laser operating in the open-loop $(\kappa_s = 0)$ configuration may be observed for a wide range of detuning frequencies and slave laser injection rates. The time domain dynamics of the master and slave laser optical intensity (Eqn. 2.9), phase (Eqn. 2.10) and carrier number (Eqn. 2.3) are presented in Figures 2.3 (a,b) and 2.4 (a) respectively for a 5ns time period at maximum injection for a single simulation of 210ns with zero detuning, $\Delta f = 0$, and very strong slave laser injection, $\kappa_c = 170\text{ns}^{-1}$. Figure 2.4 (b) shows the optical output phase difference $\Delta\phi = \phi_m - \phi_s$ for the duration of a single simulation. The master laser dynamics are driven chaotic by the addition of optical feedback from an external mirror with feedback rate, $\kappa_m = 10\text{ns}^{-1}$, and external cavity round trip time, $\tau_{ex} = 1\text{ns}$. The ranges of the correlation and FFT windowing functions are also illustrated in Figure 2.4 (b); the half maximum injection to the slave laser is indicated by the dashed lines, the FFT window by the time range between the dash-dot line and the dotted line and the correlation window is indicated by the range between the dotted lines.

(a) – Optical Intesnity $P_{m,s}(t)$

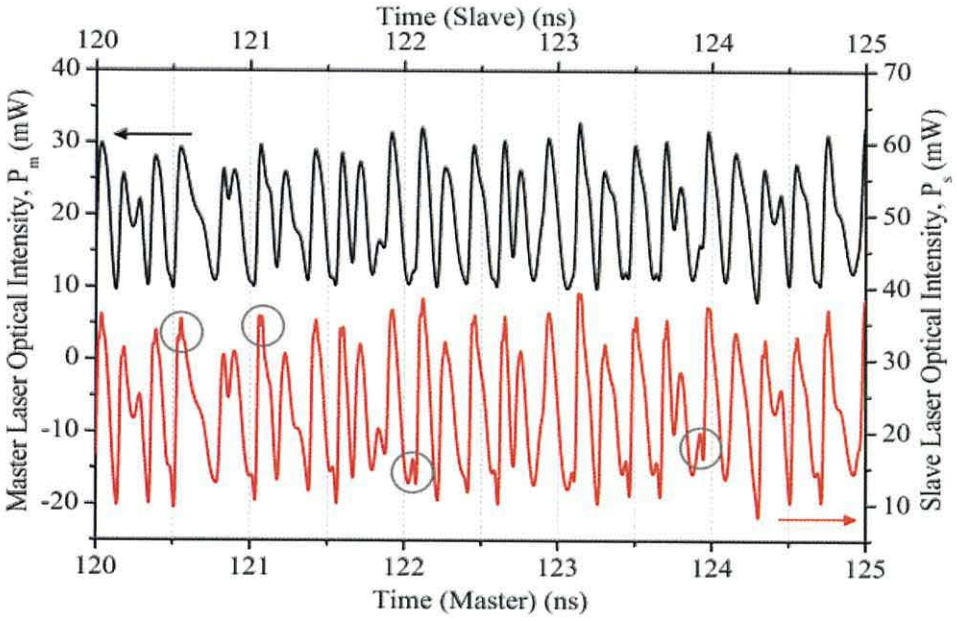

(b) – Carrier Number $N_{m,s}(t)$

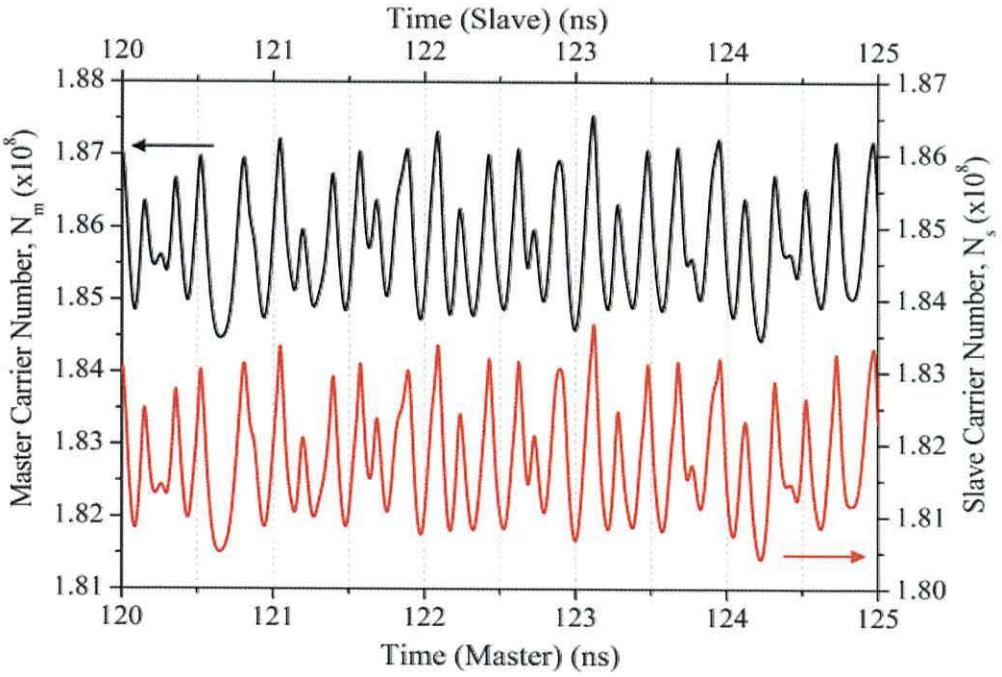

Figure 2.3. Time traces of simulation results showing injection locking synchronization. The black line represents the master laser output and the red line the slave laser output.

(a) – Optical Phase $\phi_{m,s}(t)$

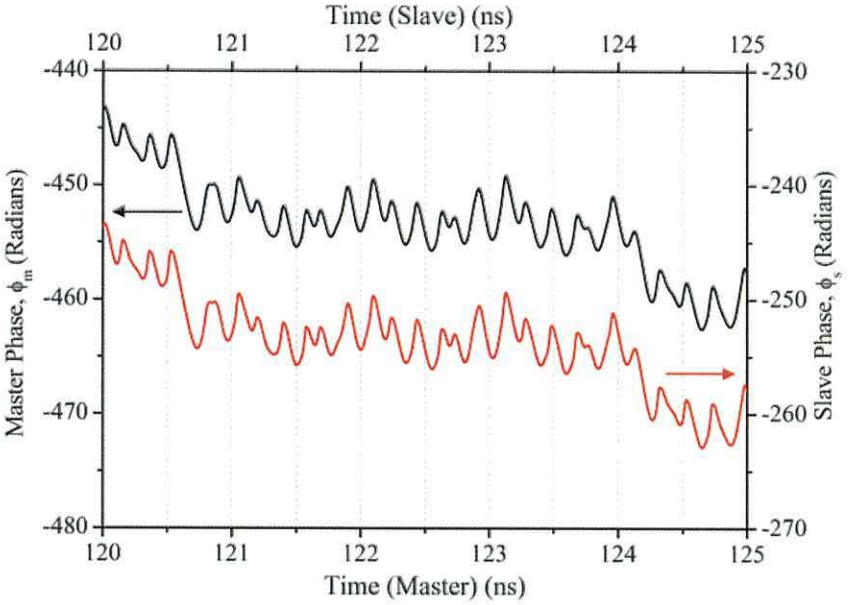

(b) – Optical Phase Difference $\phi_s(t) - \phi_m(t)$

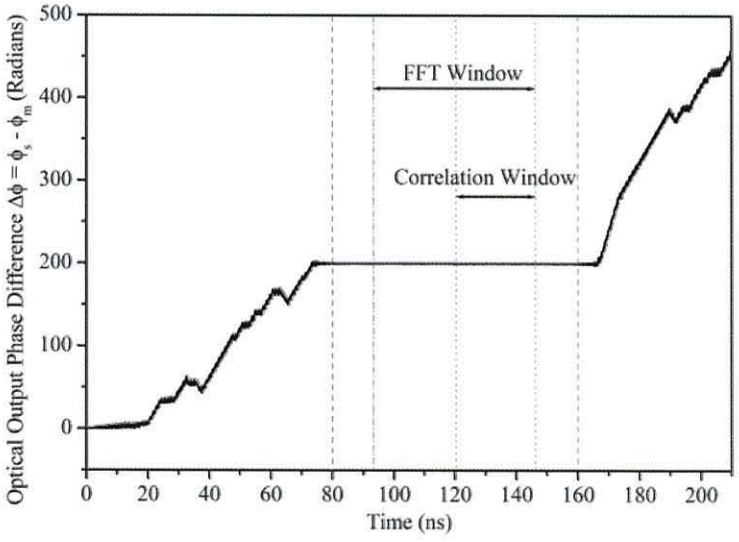

Figure 2.4. Time traces of simulation results showing injection locking synchronization. In (a) the black line represents the master laser output and the red line the slave laser output. See Figure 2.2 for slave laser injection rate.

The time range over which phase locking occurs is illustrated by a constant phase difference, Figure 2.4 (b). The constant phase difference achieved when locked is determined by the phase difference at the commencement of the locking. In the presence of a detuning frequency between the master and slave lasers the locked phase does not result in a constant phase difference but a linearly increasing or decreasing phase difference dependent upon the level of positive or negative detuning respectively. The time range in Figures 2.3 (a, b) and 2.4 (a) illustrates a 5ns time period where the optical output intensity and phase of the slave laser is locked to the master laser output. Very good reproduction of the output intensity, phase and carrier number is observed in Figures 2.3 (a, b) and 2.4 (a) however the slave laser output intensity is not identical to the master optical output intensity, as for the case of perfect synchronization. The slave laser optical intensity shows a small amount of high frequency noise due to the strong injection. Examples of this high frequency noise, which ultimately leads to a degradation of the synchronization quality, are highlighted in Figure 2.3 (a) by the grey circles. As expected, zero time difference is also observed between the injection locked synchronized output dynamics.

The calculated optical intensity correlation $C_P = 0.989$, the carrier correlation $C_N = 0.992$ and the optical phase correlation $C_\phi = 0.999$. The slave laser optical phase follows that of the master laser very closely. While both the carrier and optical intensity correlations are very high, as expected for strong injection, the carrier correlation is slightly higher than the optical intensity value. This is due to the presence of high frequency distortion, introduced to the optical intensity dynamics of the slave

laser, and highlighted in Figure 2.3 (a) by the grey circles. The slower dynamics of the carriers essentially low pass filter the chaotic dynamics resulting in a slightly improved synchronization quality. In all cases carrier correlation is higher than the intensity correlation, $C_N > C_P$.

The investigation will now be extended to test a wide range of slave laser optical injection rates and detuning frequencies to identify the region within the parameter space for which chaotic injection locking of the open-loop master-slave laser configuration is achieved. The identification of the parameter range for which chaotic synchronization is possible is an important consideration in the design of any secure communications schemes that relies on chaos pass filtering to extract the masked message and hopes to be secure. If chaotic synchronization is easily achievable for a wide parameter range then it increases the likelihood that an eavesdropper monitoring the transmission could successfully synchronize to the chaotic carrier and extract the message using a laser diode that does not have identical parameters to the transmitter master laser diode.

2.5.2 Chaotic Injection Locking of Optical Intensity

2.5.2.1 Generation of Injection Locking Diagram

The process of creating the injection locking diagram for the coupled master – slave laser diode system, given in Figure 2.1, will now be outlined.

The injection locking diagram is created for detuning frequencies from $\Delta f = -50\text{GHz}$ to $\Delta f = 30\text{GHz}$ and increasing the slave laser injection rates from $\kappa_c = 2\text{ns}^{-1}$ to $\kappa_c = 200\text{ns}^{-1}$. The injection rate $\kappa_c = 2\text{ns}^{-1}$ corresponds to a transmission coefficient $\Gamma = 7.7\text{x}10^{-3}$ and an injection rate of $\kappa_c = 200\text{ns}^{-1}$ corresponds to a transmission coefficient $\Gamma = 0.77$. The maximum correlation coefficient and associated optimum time shift is calculated for each set of detuning frequency and slave laser injection rate. The correlation is calculated over a 26ns time period at which the maximum injection rate has been applied to the slave laser for sufficient time for stable locking to be achieved and for any transients introduced by the injection rate ramping function to have subsided. The injection locking diagrams presented here are created from 8100 unique simulations; the individual correlation and optimum time shift results are then collated to create the complete injection locking map. The injection locking diagram presents correlation values from 0.8 to 1 on a colour scale. A correlation $C \geq 0.8$ (80%) is deemed to represent a good quality synchronization of the master and slave

dynamics. The darker the blue the higher the correlation and hence the better the quality of the synchronization.

The injection locking diagram for the open-loop configuration with master feedback rate $\kappa_m = 10\text{ns}^{-1}$ and external cavity round trip time $\tau_{ex} = 1\text{ns}$ and master and slave drive currents $I_m = I_s = 1.48I_{th}$ is presented in Figure 2.5 for the maximum correlation C_P (a) and corresponding optimum time shift τ_{opt} (b). All other parameters are as outlines in section 2.3.

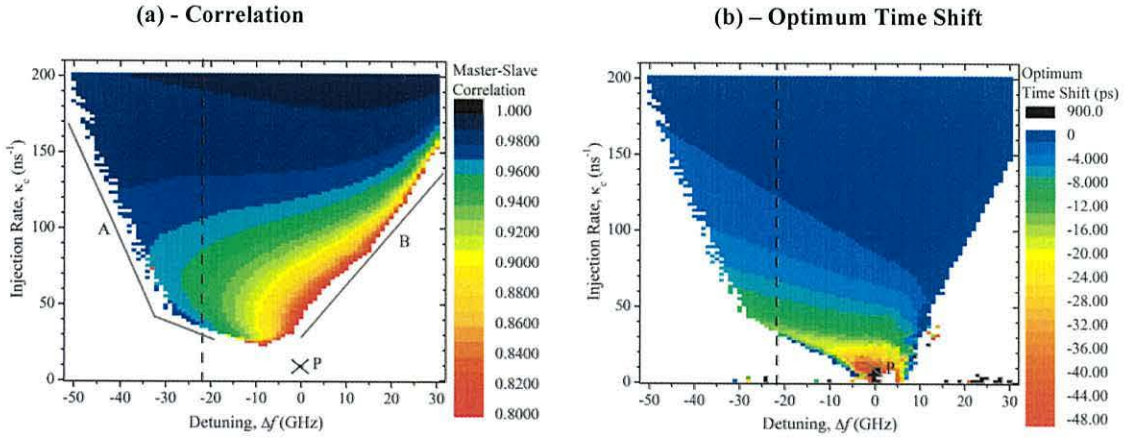

Figure 2.5. Optical intensity injection locking diagram (a) and optimum time shift (b) for $I_m = I_s = 1.48I_{th}$, $\kappa_m = 10\text{ns}^{-1}$, $\kappa s = 0\text{ns}^{-1}$. The colour bar represents (a) the degree of correlation (0 represents no synchronization and 1 represents perfect synchronization) between the master and slave dynamics and (b) gives the associated time shift. The point 'P' indicates the perfect synchronization point and the injection locking boundaries are indicated by A and B.

2.5.2.2 Trends in Chaos Injection Locking Synchronization

The overall trend in the synchronization quality across the injection locking region will now be summarized. In general, as the injection rate increases the quality of the synchronization improves. As the detuning frequency is increased the synchronization quality deteriorates.

The asymmetric injection locking boundaries and their differing nature are clearly seen in Figure 2.5 (a). For strong negative detuning frequencies, boundary A in Figure 2.5 (a), there is a abrupt change at the boundary from very low correlations, indicating no synchronization, to very high correlation, indicating very good quality synchronization. For positive detuning frequencies the boundary, B in Figure 2.5 (a), is less clear as the correlation gradually increases with injection rates.

We will now consider the vertical dashed line in Figure 2.5 for a constant detuning frequency $\Delta f = -22\text{GHz}$. The line intersects an area of very good synchronization quality, $C_P > 97\%$, at relatively small injection rates (identified by a dark blue area in Figure 2.5) [31]. Within this area a local maximum in the correlation is observed at an injection rate immediately above boundary A at $\kappa_c = 38\text{ns}^{-1}$. As the injection current is increased from $\kappa_c = 38\text{ns}^{-1}$ to $\kappa_c = 60\text{ns}^{-1}$ the correlation is observed to decrease to a minimum at $\kappa_c = 60\text{ns}^{-1}$. Further increases in the injection rate $\kappa_c > 60\text{ns}^{-1}$ result in increased master – slave laser correlation. This area of improved synchronization will be examined further using the frequency domain techniques developed in Chapter 3.

The optimum time shift for chaotic injection locking, Figure 2.5 (b), decreases as the detuning frequency or the injection rate increases. The boundary observed in the optical intensity correlation Figure 2.5 (a) for strong negative detuning frequencies coincides with that observed in the optimum time shift Figure 2.5 (b). The clear and abrupt change in the correlation coincides with a similar change in the optimum time shift. Using our correlation threshold $C_P \geq 0.8$ to define the injection locking boundary it is clear that the positive detuning boundary 'B' of the correlation (Figure 2.5 (a)) and time shift (Figure 2.5 (b)) maps do not coincide. The optimum time shift clearly identifies two abrupt boundaries.

Injection locking diagrams have also been produced for the closed loop case and compared to the open loop case. Very few differences are observed between the synchronization diagrams of the open and closed loop configurations. However, the closed loop configuration does provide a slightly stronger synchronization and slightly smaller optimum time difference across the injection locking region when the master and slave laser external cavity lengths are matched.

2.5.3 Chaos Injection Locking of Carrier Dynamics

The associated correlation of the carrier dynamics has also been calculated and the degree of correlation compared with that found in the optical intensity.

The difference in the optical intensity correlation and carrier correlation is presented in Figure 2.6 (a) and is calculated using Eqn. 2.12,

$$C_{N-P}(\Delta\omega,\kappa_c) = C_N(\Delta\omega,\kappa_c) - C_P(\Delta\omega,\kappa_c) \qquad 2.12$$

The difference in correlation, C_{N-P}, is given by the colour bar; green to dark blue correspond to a higher carrier correlation $C_N > C_P$, yellow corresponds to equal correlations $C_N = C_P$ and oranges and reds correspond to a higher optical intensity correlation $C_N < C_P$. The large green area covering the majority of the injection locking region in Figure 2.6 (a) shows the carrier dynamics to be slightly better correlated than the optical intensity, the carrier correlation is approximately 2.5% higher. The yellow area at very high injection rates indicates that the optical intensity and carrier dynamics have essentially the same synchronization quality, $C_N = C_P > 99\%$.

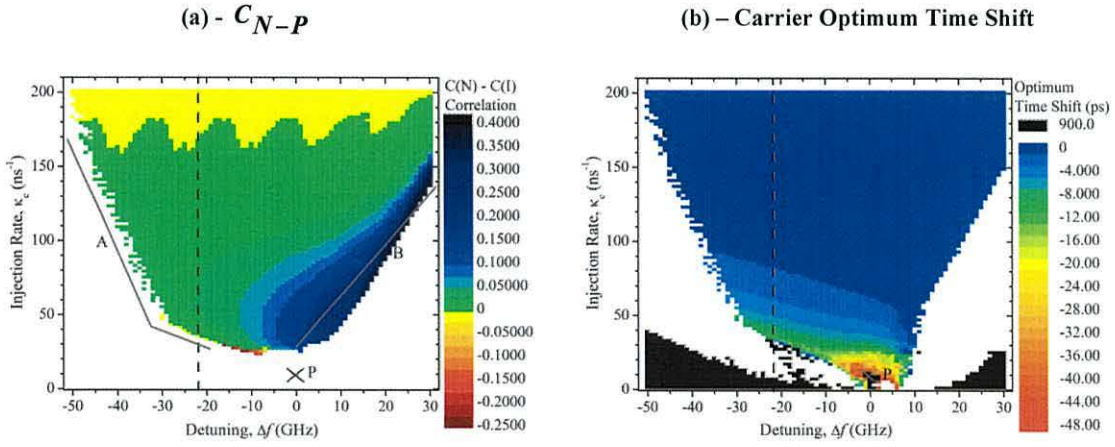

Figure 2.6. Difference in carrier and optical intensity synchronization quality C_N-C_P (a) and optimum time-shift for chaos injection locking synchronization of the carrier dynamics (b). The point 'P' indicates the perfect synchronization point. I_m=I_s=1.48I_{th}, κ_m=10ns^{-1}, κ_s=0. The optical intensity injection locking boundaries as defined in Figure 2.5 are indicated by A and B.

There is an area in Figure 2.6 (a) at positive detuning frequencies and relatively low injection rates, shown by the blue area, where a significant difference in the carrier and optical intensity correlation is observed. The carrier correlation is significantly higher than the optical intensity correlation in this area and corresponds to an area where the carrier dynamics are synchronized but the optical intensity dynamics are not. To demonstrate this the temporal variation in the optical intensity and carrier dynamics will now be presented for an injection rate $\kappa_c = 60ns^{-1}$ and detuning frequency $\Delta f =$ 10GHz. Figure 2.7 (a) presents the master (black) and slave (red) laser optical intensity dynamics and (b) presents the master (black) and slave (red) laser carrier dynamics for a 2.5ns time period during a single simulation.

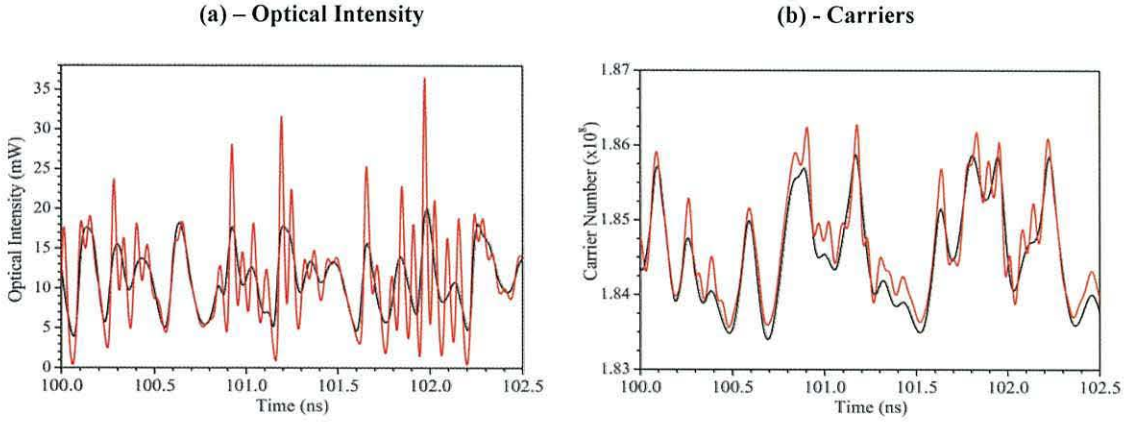

Figure 2.7. Optical Intensity (a) and Carrier Number (b) dynamics for the master laser (black line) and slave laser (red line) for simulation time period 100ns – 102.5ns. Detuning frequency $\Delta f =$ 10GHz and slave laser injection rate $\kappa_c = 60ns^{-1}$ operating close to the injection locking boundary.

The slave intensity and carrier dynamics both exhibit high frequency fluctuations that are not present in the master dynamics. These high frequency perturbation are much less pronounced in the carrier dynamics and hence the carrier correlation is higher. The

carrier correlation is $C_N = 0.94$ while the optical intensity correlation is $C_P = 0.69$. The two devices are arguably unsynchronized in the optical intensity while the carrier dynamics are well synchronized. If the majority of the spectral power appears at lower frequencies then synchronization can be improved by merely low pass filtering the slave output. This proposition will be examined further in the frequency domain analysis of chaos injection locking synchronization in Chapter 3.

As the injection rate is decreased below the injection locking boundary B, increased high frequency distortion is introduced as the injection to the slave laser perturbs rather than dominates the slave dynamics.

The optimum time shift for chaos injection locking synchronization of the carrier dynamics is presented in Figure 2.6 (b). The chaos injection locking boundaries are identical in the optimum time shift diagrams for optical intensity and carrier dynamics, Figure 2.5 (b) and Figure 2.6 (b) respectively. This shows that the optical intensity and carrier dynamics synchronize simultaneously but to differing degrees of quality.

2.5.4 Chaos Injection Locking of Optical Phase

The optical intensity and carrier correlation is now compared with the optical phase correlation for zero detuning. Figure 2.8 presents the optical intensity (black line), carrier (red line) and optical phase (green line) correlation for zero detuning and slave laser injection rates from $\kappa_c = 1\text{ns}^{-1}$ to $\kappa_c = 200\text{ns}^{-1}$.

It is observed in Figure 2.8 that the optical phase correlation is always higher than the carrier correlation which in turn is always higher than the optical intensity correlation within the injection locking region with zero detuning. Only a very small injected power is required for the optical phase of the slave laser to synchronize to the dynamics of the master laser.

The condition for perfect synchronization is attained for an injection rate $\kappa_c = 10\text{ns}^{-1}$, the three correlations are equal $C_P = C_N = C_\phi = 0.99999$.

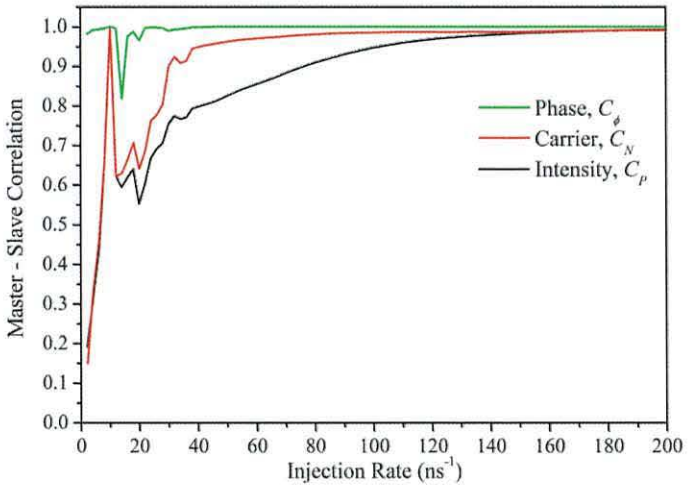

Figure 2.8. Correlation of master and slave optical intensity (black line), optical phase (green line) and carrier (red line) dynamics for zero detuning and injection rates from κ_c=1ns^{-1} to κ_c=200ns^{-1}. The perfect synchronization point occurs at κ_c=10ns^{-1}.

For detuning frequencies other than zero the optical phase dynamics diverge at a rate corresponding to the detuning frequency. If this divergence in the optical phase dynamics is compensated for and the correlation calculated the optical phase correlation remains higher than the optical intensity and carriers.

2.5.5 Variation in Master Laser Drive Current

The communications system investigated later in Chapter 5 utilizes master laser drive current modulation and relies on chaos synchronization in the slave laser to enable successful extraction of the message. It is therefore important to know how the quality of the chaotic synchronization changes when the master laser drive current is modulated. Injection locking diagrams are presented for a master laser drive current modulated with a sinusoidal message to simulate a simple message and also with a dc current higher than the slave laser drive current to simulate a master laser drive current that could be used to encode the high level of a digital message. The master laser drive current would then be switched between the two levels to encode the digital message.

Figure 2.9 (a) presents the injection locking diagram for a master drive current with the addition of a sinusoidal message $I_m = 1.48I_{th}(1 + h(\sin 2\pi f_{mod}))$ with modulation frequency f_{mod} = 1.5GHz and modulation depth h = 10%. The slave laser drive current remains unchanged $I_s = 1.48I_{th}$. All other parameters are the same as for the injection locking diagram, Figure 2.5 (a). For the majority of the injection locking region the optical intensity correlation is approximately 5% less than for the un-modulated drive current Figure 2.5 (a). This reduction in correlation is small and very good synchronization is still achieved for a large parameter range.

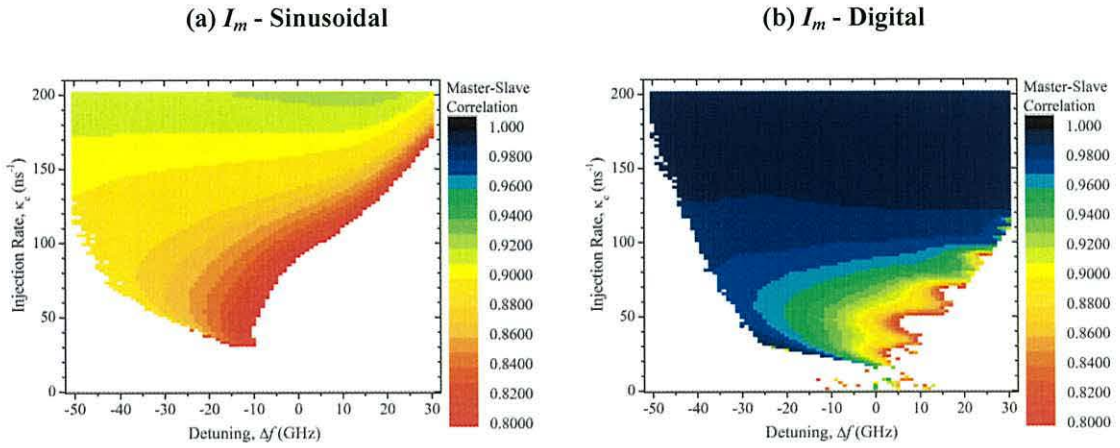

Figure 2.9. Optical intensity injection locking diagram for (a) sinusoidal modulation of master laser drive current $I_m = 1.48I_{th} + h1.48I_{th}(\sin 2\pi f_{mod})$ with $f_{mod} = 1.5$GHz and h = 10% and (b) $I_m = 1.48I_{th} + hI_{th}$ with h = 0.3. For both (a) and (b) $I_s = 1.48I_{th}$, $\kappa_m = 10ns^{-1}$, $\kappa_s = 0ns^{-1}$. The colour bar represents the degree of correlation between the master and slave dynamics.

Figure 2.9 (b) presents the case for master laser drive current $I_m = 1.48I_{th} + 30\%$. The slave laser drive current is $I_s = 1.48I_{th}$. In general an increase in correlation is observed across the injection locking region which is also extended to lower injection rates for positive and small negative detuning frequencies. This is intuitive since there is additional optical power being injected into the slave laser, and the slave lasers own lasing is suppressed, further enhancing the synchronization with the master laser dynamics.

2.6 Conclusions

The simulation model of a system of master and slave laser diodes has been outlined and the temporal dynamics of the master and slave laser diodes system operating in the chaos injection locking synchronization regime have been presented.

The master – slave laser chaos synchronization has been studied for a wide range of slave laser injection rates and detuning frequencies and from these the injection locking correlation and optimum time shift diagrams have been constructed.

The injection locking of the optical intensity, carriers and optical phase has been presented. The master – slave correlation and optimum time shift have been calculated and provide a numerical measure of the degree of synchronization. It has been shown that, for zero detuning, as the slave laser injection rate is increased the optical phase locks first, followed by the carriers and, lastly the optical intensity. The optical phase correlation remains marginally higher than the carrier correlation, which in turn is higher than the optical intensity correlation.

The quality of synchronization across the large parameter range for which injection locking is achieved has been shown to be higher for the slower carrier dynamics than for the optical intensity. This extends the carrier injection locking region to lower injection rates for positive detuning frequencies. However, within this area at low injection rates, where the optical intensity correlation is below the threshold conventionally imposed, the slave laser optical intensity is observed to follow the

master laser dynamics fairly closely but is also subject to a higher frequency distortion reducing the measured correlation. It appears as though the important chaotic frequencies are in fact reproduced along with high frequency noise. These observations will be investigated further in the frequency domain analysis of chaos injection locking synchronization in the next chapter.

The optimum time shift diagram for chaos synchronization clearly identifies the boundaries of the injection locking region since it is defined for zero or negative optimum time shift while the conventional correlation threshold determines the boundary observed in the correlation diagram.

The chaos synchronization has also been studied for the case of a modulated master laser drive current as employed in the communications system investigated laser in Chapters 5-6. A small reduction in the quality of the chaos synchronization is observed when the master laser is modulated with a sinusoidal message but very good synchronization is still achieved. Simple sinusoidal modulation of the master laser drive current has little effect upon the quality of synchronization in the slave laser, because this does not result in significant parameter mismatch. A second dc level applied to the master laser can be used to encode a digital message into the output optical intensity. A small increase in the quality of synchronization is observed for a master laser current 30% higher than that of the slave laser. This is to be expected since the overall power injected into the slave laser is increased and its influence on the output is suppressed further.

The study of the injection locking region will allow a stable operating point to be chosen in later chapters when the master laser drive current is modulated.

2.7 Bibliography

[1] M Bennett, M F Schatz, H Rockwood, and Wiesenfeld K, "Huygens's Clocks," *Mathematical, Physical and Engineering Sciences*, vol. 458, no. 2019, pp. 563-579, March 2002.

[2] L Goldberg and M K Chun, "Injection locking characteristics of 1W broad stripe laser diode," *Applied Physics Letters*, vol. 53, pp. 1900-1902, 1988.

[3] J Wang, M K Halder, L Li, and F V C Mendis, "Enhancement of modulation bandwidth of laser diodes by injection locking," *IEEE Photon. Technol. Lett.*, vol. 8, pp. 34-36, 1996.

[4] T B Simpson and J M Liu, "Bandwidth enhancemnet and broadband noise reduction in injection-locked semiconductor lasers," *IEEE Photon. Technol. Lett.*, vol. 9, pp. 1322-1324, 1997.

[5] L M Pecora and T L Carroll, "Synchronization in chaotic systems," *Phys. Rev. Lett.*, vol. 64, no. 8, pp. 821-824, 1990.

[6] S Hayes, C Grebogi, and E Ott, "Communicating with chaos," *Phys. Rev. Lett.*, vol. 70, no. 20, pp. 3031-3034, 1993.

[7] K M Cuomo and A V Oppenheim, "Circuit implementation of synchronized chaos with applications to communications," *Phys. Rev. Lett.*, vol. 71, no. 1, pp. 65-68, July 1993.

[8] H U Voss, "Anticipating chaotic synchronization," *Phys. Rev. E*, vol. 61, no. 5, pp. 5115-5119, May 2000.

[9] P Colet and R Roy, "Digital communication with synchronized chaotic lasers," *Opt. Lett.*, vol. 19, pp. 2056-2058, 1994.

[10] G D VanWiggeren and R Roy, "Optical Communication with Chaotic Waveforms," *Phys. Rev. Lett.*, vol. 81, no. 16, pp. 3547-3550, October 1998.

[11] G D VanWiggeren and R Roy, "Communication with Chaotic Lasers," *Science*, vol. 279, pp. 1198-1200, 1998.

[12] V Ahlers, U Parlitz, and W Lauterborn, "Hyperchaotic dynamics and synchronization of external-cavity semiconductor lasers," *Phys. Rev. E*, vol. 58, no. 6, pp. 7208-7213, December 1998.

[13] C Masoller, "Anticipation in synchronization of chaotic semiconductor lasers with optical feedback," *Phys. Rev. Lett.*, vol. 86, pp. 2782-2785, 2001.

[14] A Locquet, F Rogister, M Sciamanna, P Megret, and M Blondel, "Two types of synchronization regimes in unidirectionally coupled chaotic external-cavity

semiconductor lasers," *Phys. Rev. E*, vol. 64, p. 045203, 2001.

[15] J Revuelta, C R Mirasso, P Colet, and L Pesquera, "Criteria for synchronization of coupled chaotic external-cavity semiconductor lasers," *IEEE Phot. Technol. Lett.*, vol. 14, pp. 140-142, 2002.

[16] A Locquet, C Masoller, and C R Mirasso, "Synchronization regimes of optical-feedback-induced chaos in unidirectionally coupled semiconductor lasers," *Phys. Rev. E*, vol. 65, no. 5, p. 056205, April 2002.

[17] E M Shahverdiev, S Sivaprakasam, and K A Shore, "Lag synchronization in time-delayed systems," *Phys. Letts. A*, vol. 292, pp. 320-324, 2002.

[18] I V Koryukin and P Mandel, "Two regimes of synchronization in unidirectionally coupled semiconductor lasers," *Phys. Rev. E*, vol. 65, no. 2, p. 026201, January 2002.

[19] J-P Goedgebuer, L Larger, and H Porte, "Optical Cryptosystem Based on Synchronization of Hyperchaos Generated by a Delayed Feedback Tunable Laser Diode," *Phys. Rev. Lett.*, vol. 80, no. 10, pp. 2249-2252, March 1998.

[20] D Lenstra, B H Veerbeek, and A J de Boef, "Coherence Collapse in single-mode semiconductors due to optical feedback," *IEEE J. Quant. Electron.*, vol. 21, pp. 674-679, 1985.

[21] S Sivaprakasam and K A Shore, "Demonstration of optical synchronization of chaotic external-cavity laser diodes," *Opt. Lett.*, vol. 24, pp. 466-468, 1999.

[22] R Vicente, T Perez, and C R Mirasso, "Open- versus Closed loop performance of synchronized chaotic external cavity semiconductor lasers," *IEEE J. Quant. Electron.*, vol. 38, pp. 1197-1204, 2002.

[23] Y Liu et al., "Injection Locking and synchronization of Periodic and Chaotic Signals in Semiconductor Lasers," *IEEE J. Quant. Electron.*, vol. 39, pp. 269-277, 2003.

[24] S Sivaprakasam, E M Shahverdiev, and K A Shore, "Experimental verification of the synchronization condition for chaotic external cavity diode lasers," *Phys. Rev. E*, vol. 62, no. 5, pp. 7505-7507, November 2000.

[25] S Sivaprakasam et al., "Inverse synchronization in semiconductor laser diodes," *Phys. Rev. A*, vol. 64, no. 1, p. 013805, May 2001.

[26] S Sivaprakasam, E M Shahverdiev, P S Spencer, and K M Shore, "Experimental Demonstration of Anticipating Synchronization in Chaotic Semiconductor Lasers with Optical Feedback," *Phys. Rev. Lett.*, vol. 87, no. 15, p. 154101, September 2001.

[27] Y Takiguchi, H Fujino, and J Ohtsubo, "Experimental synchronization of chaotic oscillations in externally injected semiconductor lasers in the low frequency

fluctuation regime," *Opt. Lett.*, vol. 24, pp. 1570-1572, 1999.

[28] H Fujino and J Ohtsubo, "Experimental synchronization of chaotic oscillations in externally cavity semiconductor lasers," *Opt. Lett.*, vol. 25, pp. 625-627, 2000.

[29] I Fischer, Y Liu, and P Davis, "Synchronization of chaotic semiconductor laser dynamics on subnanosecond time scales and its potential for chaos communication," *Phys. Rev. A*, vol. 62, no. 1, p. 011801, June 2000.

[30] S Peters-Flynn, I Pierce, P S Spencer, and P Rees, "Synchronization recovery in unidirectionally coupled semiconductor lasers," *IEE Proc.-Optoelectron.*, vol. 153, pp. 8-12, 2006.

[31] S Peters-Flynn, P S Spencer, S Sivaprakasam, I Pierce, and K A Shore, "Identification of the Optimum Time-Delay for Chaos Synchronization Regimes of Semiconductor Lasers," *IEEE J. Quant. Elect.*, vol. 42, pp. 427-434, 2006.

[32] R Lang and K Kobayashi, "External Optical Feedback Effects on Semiconductor Injection Properties," *IEEE J. Quant. Electron.*, vol. 16, no. 3, pp. 347-355, March 1980.

[33] William H Press, Brian P Flannery, Saul A Teukolsky, and William T Vetterling, *Numerical Recipes in C: The Art of Scientific Computing*, 2nd ed.: Cambridge University Press, 1992.

Chapter 3

Synchronization of Semiconductor Laser Diodes: Frequency Domain Analysis

3.1 Introduction

This chapter further investigates the injection locking of a system of uni-directionally coupled external cavity master laser diode and slave laser diode. However, the focus will now be on the frequency domain.

The numerical framework is the same as that outlined in Chapter 2. The simulation data is then analysed in the frequency domain. The frequency domain post processing is detailed in the next section. The process of producing the output spectra using a fast Fourier transform technique is outlined along with the response gain defined as the slave spectrum divided by the master spectrum, and the master laser spectral phase lead defined as the difference in phase between the master and slave laser outputs.

The average spectra and response gain are presented and provide the overall spectral characteristic of the chaotic master laser output. In order to ascertain the relationship between the injected chaotic power and the synchronization quality individual chaotic

spectral components will be studied. The high power spectral components will be identified in the chaotic master laser optical intensity spectrum and related to the synchronization quality. The synchronization quality of the local spectral minima in the master spectrum are also analysed to determine whether any relationship exists between the relative injection power and the quality of synchronization observed.

Frequency domain techniques will be used to investigate the trends in synchronization quality observed in the correlation based injection locking diagrams seen in Chapter 2.5.2. An area of the injection locking region for positive detuning frequencies and relatively low injection rates was identified in the time domain analysis in Chapter 2.5.2.2. Within this area the correlation of the carriers is high while the correlation of the optical intensity is low indicating that the carrier dynamics are locked while the optical intensity is not. This area is also examined further in this chapter.

3.2 Frequency Domain: Response Gain

For completeness the rate equations, [1] are reproduced here,

$$\frac{dE_m(t)}{dt} = \frac{1}{2}(1+i\alpha)\left[G_m(t) - \frac{1}{\tau_P}\right]E_m(t) + \kappa_m E_m(t-\tau_{ex,m})e^{-i\omega_m\tau_{ex,m}} \qquad 3.1$$

$$\frac{dE_s(t)}{dt} = \frac{1}{2}(1+i\alpha)\left[G_s(t) - \frac{1}{\tau_P}\right]E_s(t) + \kappa_s E_s(t-\tau_{ex,s})e^{-i\omega_s\tau_{ex,s}} + \kappa_c E_m(t)e^{i\Delta\omega t} \qquad 3.2$$

$$\frac{dN_{m,s}(t)}{dt} = \frac{I_{m,s}}{e} - \frac{N_{m,s}(t)}{\tau_N} - G_{m,s}(t)\left|E_{m,s}(t)\right|^2 \qquad 3.3$$

$$G_{m,s}(t) = \frac{g_0(N_{m,s}(t) - N_0)}{1 + \varepsilon \left| Em, s(t) \right|^2} \quad 3.4$$

give a complex output that is related to the output optical intensity via the relation

$$P_{m,s}(t) = \left(\frac{\hbar \omega_{m,s}}{\tau_P} \right) \left| E_{m,s}(t) \right|^2 \quad 3.5$$

Chapter 2, Table 2.1 details the parameter set used in the following investigations unless stated otherwise (Sections 3.6.3 and 3.6.4 vary the slave laser detuning frequency and injection rate respectively).

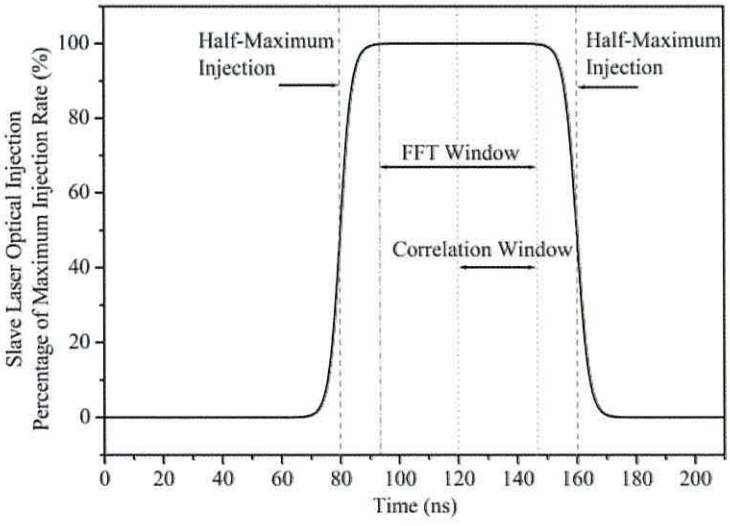

Figure 3.1. Percentage of maximum optical injection to the slave laser for a single simulation of 210ns duration.

Frequency domain post processing of the optical intensity, P, and carrier, N, dynamics is performed after the completion of each simulation. The Fast Fourier Transform (FFT) [2] of the master laser and slave laser intensities is calculated using a 52ns window offset by the time difference required to obtain maximum correlation [3].

The FFT windowing function is applied during the period at full injection rate and includes the time range for which the time domain correlation is calculated, Figure 3.1.

The complex FFT of the master laser optical intensity $\Im[P_m(t)]$ provides a magnitude and phase, A_m and φ_m respectively,

$$\Im[P_m(t)] = A_m(f)e^{i\varphi_m(f)} \tag{3.6}$$

The slave laser dynamics are shifted by the optimum time shift τ_{opt} and the shifted slave laser dynamics are calculated

$$\Im[P_s(t+\tau_{opt})] = A_s(f)e^{i\varphi_s(f)} \tag{3.7}$$

The spectral power of the master and slave optical intensity output $A_m(f)$ and $A_s(f)$ are then used to calculate the optical intensity response gain $H_A(f)$ for the system defined as

$$H_A(f) = 10\log_{10}\frac{A_s(f)}{A_m(f)} \tag{3.8}$$

The master and slave spectral phases are unwrapped and the master laser phase lead is determined. The spectral phase difference is defined as

$$\Delta\varphi = \varphi_m - \varphi_s \tag{3.9}$$

A master laser spectral phase lead close to zero indicates good synchronization, while a phase lead of π indicates completely out of phase dynamics. The overall quality of

reproduction of the master laser spectral output in the slave laser depends upon both the response gain and the master laser phase lead.

The response gain and master laser spectral phase lead are defined above and can easily be modified for the optical phase or carrier dynamics.

Now that the frequency domain post processing techniques have been described the average spectra of the master and slave laser diodes will be constructed.

3.3 Long Term Average Chaos Characteristic

3.3.1 Construction of the Average Spectrum

The spectral power of the chaotic output from a semiconductor laser subject to optical feedback fluctuates in time. However, it is possible to determine an average chaotic spectrum that gives the general trends of the chaotic response. The long term time averaged chaotic response presented here is constructed by averaging the spectral power output, $A(f)$, from the fast Fourier transforms of 50 individual simulations each with identical device parameters but different initial conditions providing a different route to chaos. The average spectra are normalized with respect to the maximum spectral power of the master laser.

3.3.2 Average Chaotic Optical Intensity Spectrum

A typical optical intensity power spectrum is presented in Figure 3.2. The master laser optical power spectrum is shown as the black line and the synchronized slave laser optical intensity power spectrum is denoted by the red line. The calculated spectral profiles from the numerical simulations presented here show good agreement with published experimental observations [4].

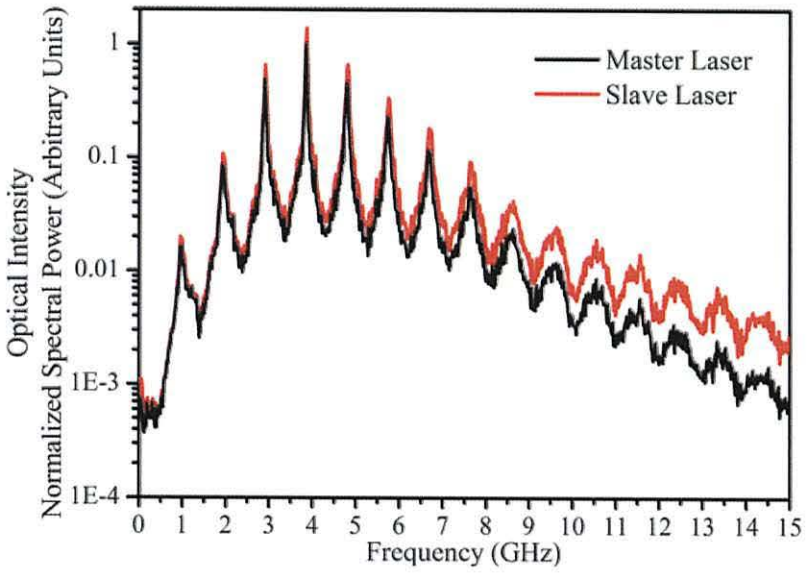

Figure 3.2. Average master (black line) and slave laser (red line) optical intensity spectra of 50 simulations for injection locking synchronization.

The parameters are as detailed in Table 2.1, Chapter 2 for chaos injection locking with a master laser optical feedback rate of $\kappa_m = 10\text{ns}^{-1}$ and external cavity round trip time of $\tau_{ex} = 1\text{ns}$. The optical feedback is sufficient to drive the master laser output chaotic. The highly periodic nature of the average chaos spectrum of the master laser optical

intensity output is a consequence of the external cavity round trip time. The very strong optical injection ($\kappa_c = 170\text{ns}^{-1}$) applied to the slave laser and matched laser parameters allows the slave laser to match the relaxation oscillation of the master laser, which ensures good synchronization is achieved (Chapter 2, Figure 2.3). The slave laser spectrum closely follows that of the master laser near to the relaxation oscillation frequency, $f_{relax} = 3.85\text{GHz}$, while gain is observed in the slave laser for frequencies above the relaxation oscillation frequency. If the master laser chaotic spectrum is subject to frequency dependent gain in the slave laser then the synchronization quality will be adversely affected. In this case for strong optical injection ($\kappa_c = 170\text{ns}^{-1}$) the distortion is minimal (a small amount of high frequency distortion is observed in the time domain optical intensity Figure 2.3(a) in Chapter 2), but the quality of the synchronization is very good with an optical intensity correlation of $C_P = 0.989$ and optimum time shift of $\tau_{opt,P} = 0$.

3.3.3 Response Gain and Phase Lead

The optical intensity response gain and master laser spectral phase lead will now be constructed from the master and slave spectra, Figure 3.2. It will be shown that the response gain and master laser phase lead provide additional information about the chaos injection locking synchronization process.

The optical intensity response gain $H_A(f)$ and master laser phase lead $\Delta\varphi$ are presented in Figure 3.3 (a) and (b) respectively.

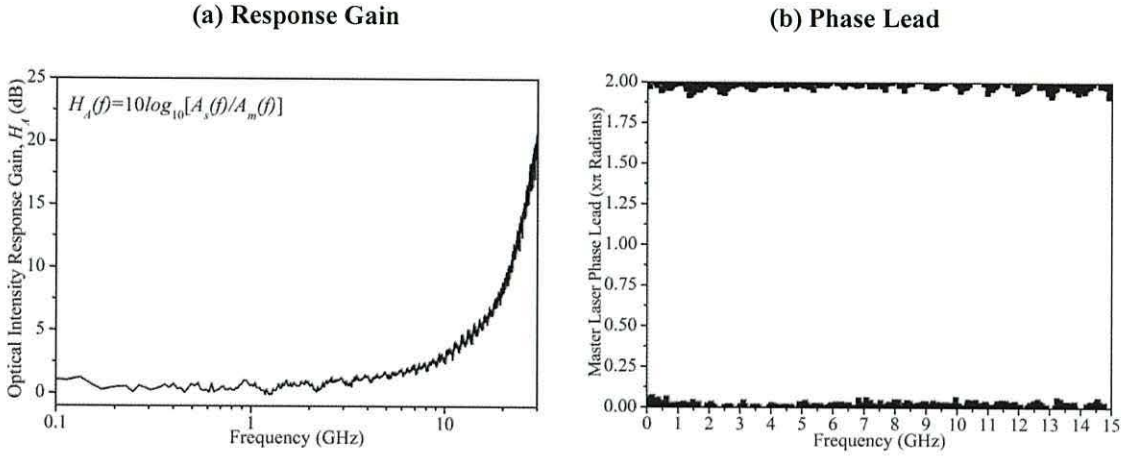

Figure 3.3. Response gain (a) and master laser phase lead (b) calculated from the average optical intensity spectral power of 50 simulations for chaos injection locking synchronization.

The response gain in Figure 3.3 (a) shows that the spectral content of the master laser optical intensity receives a small amount of almost uniform gain for frequencies up to the relaxation oscillation. For frequencies above the relaxation oscillation the distortion observed in the optical intensity (Chapter 2, Figure 2.3 (a)) is seen as additional gain in the response gain profile, Figure 3.3 (a).

The strong optical injection into the slave laser improves its modulation response as the slave laser's relaxation oscillation is suppressed resulting in a broadening of the slave laser spectrum [5]. This in turn results in the apparent high frequency gain observed in the response gain, Figure 3.3 (a).

The process behind the suppression of the relaxation oscillation response has previously been elucidated, albeit with regard to the current modulation response of the slave laser, and is based on a partial decoupling of the relationship between the carrier and photons

processes within the laser cavity [6]. In reference [6] Murakami *et al* demonstrated that the magnitude of the carrier fluctuations in a current modulated injection-locked slave laser are significantly suppressed by strong optical injection and it is this suppression, which dampens down the inherent relaxation oscillation response. In [6] the authors also demonstrated, using a linear stability analysis, that under strong optical injection the modulation response of the slave laser is effectively flat up to the cavity resonance shift frequency (of the order of 10GHz). In fact, strong optical injection suppresses the carrier fluctuations irrespective of the modulation mode of the slave laser and hence a broadened modulation response is seen in both the optical modulation and the current modulation cases.

The master laser phase lead for spectral component of the optical intensity is presented in Figure 3.3 (b). The optimum time shift $\tau_{opt,P} = 0$ means that the synchronized components must have a phase shift very close to zero and this is exactly what is observed in Figure 3.3 (b). The largest deviations from zero phase shift are observed in Figure 3.3 (b) for the local minima in the master laser average power spectrum, Figure 3.2.

For injection locking the synchronized spectral components are therefore subject to a flat response gain and zero master laser phase lead. The frequency components that deviate from this cause the distortion seen in the slave laser output.

3.4 Single Numerical Simulation

The average master and slave laser optical intensity power spectra, Figure 3.2 and corresponding response gain, Figure 3.3, show the general long term response to the chaotic dynamics generated in the master laser diode. The nature of the chaos means that the spectral power fluctuates considerably in time. From our earlier time domain analysis, Chapter 2.5, it has been shown that during chaos injection locking the master and slave dynamics are highly correlated. If the correlation is calculated using a travelling window a consistent correlation is seen. It is therefore important to study the spectra over a single short period of time to identify the spectral components that are required to achieve a good quality synchronization. The next subsection presents the master laser spectrum for a 52ns period for a single simulation. The high power components in the master laser spectrum are identified and the corresponding response gain and master laser phase lead are studied to see if these high power components are subject to the flat response gain and zero phase shift expected for good synchronization. The low power components in the master laser output are then examined to see if they are subject to the desired response, or do not have sufficient power to be reproduced accurately in the slave laser.

3.4.1 Identification of Important Spectral Components

The spectrum of the master laser optical intensity output for a 52ns period of a single simulation is presented in Figure 3.4. The corresponding optical intensity response gain and master laser phase lead are presented in Figure 3.5 (a) and (b), respectively. The parameter set given in Table 2.1 is again used.

The optical intensity correlation is calculated for a 26ns period within the 52ns fast Fourier transform window. The optical intensity correlation is very high C_P = 98.9% indicating very good quality injection locking synchronization.

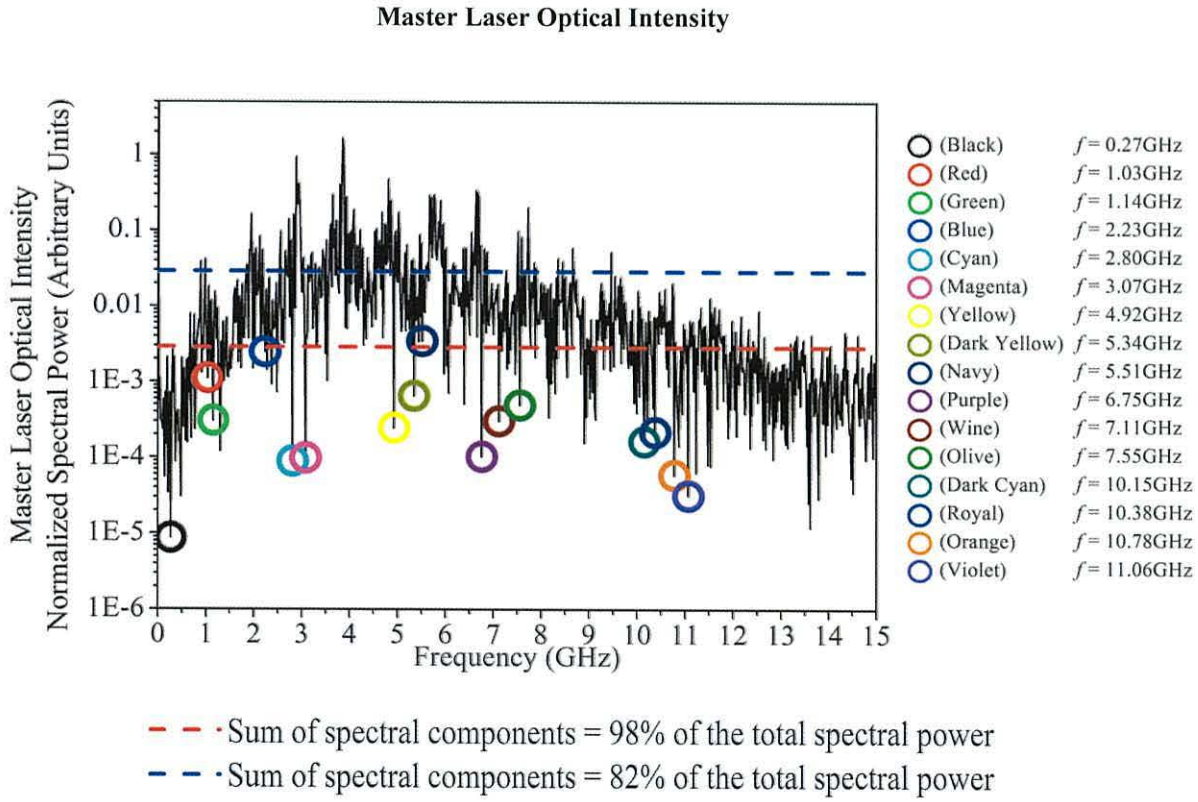

Figure 3.4. Master laser optical intensity for a single simulation with chaos injection locking synchronization.

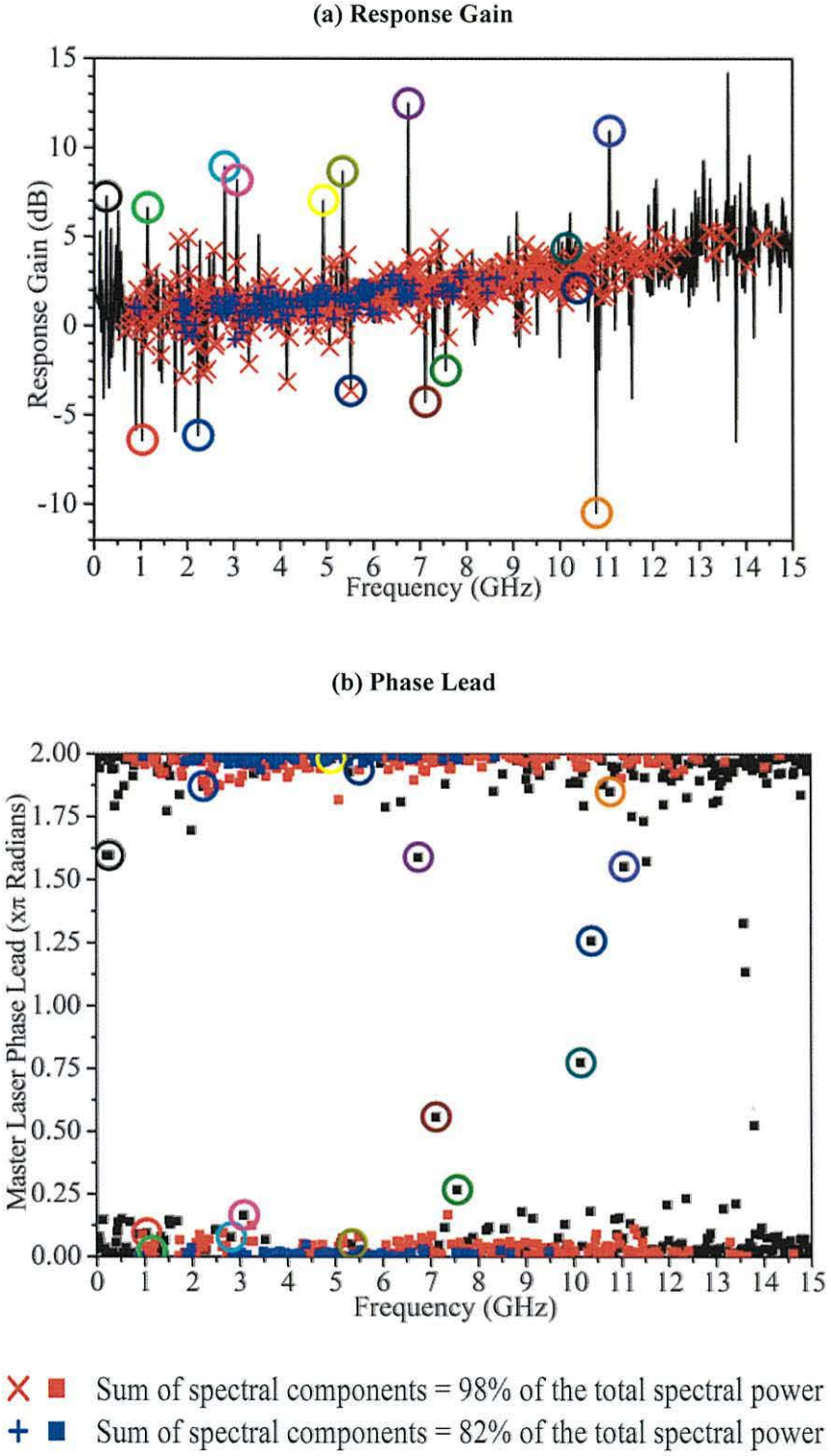

Figure 3.5. Response gain (b) and master laser phase lead (c) for a single simulation with chaos injection locking synchronization.

The master laser optical intensity spectrum is given by the black line in Figure 3.4. Significantly larger variations are observed in the master laser spectral power for a single simulation, black line in Figure 3.4, than for the averaged spectrum presented in Figure 3.2 (black line). The single simulation master laser spectrum along with the response gain and phase shift is now examined to determine which spectral components experience the constant response gain and zero master laser phase lead required for good quality injection locking synchronization. To aid further discussion two power thresholds will be utilized to identify the high power spectral components that dominate the total spectral power.

3.4.1.1 High Power Spectral Components

The first power threshold is denoted by the dashed blue line in Figure 3.4 and the spectral components above this threshold sum to 82% of the total spectral power. The spectral components above the first threshold (82% of total spectral power) are indicated by the blue drop-lines in Figure 3.4, in the response gain Figure 3.5 (a) by blue crosses, and in the master laser phase lead Figure 3.5 (b) by blue squares.

The second threshold (red dashed line, Figure 3.4) is at a lower spectral power and the sum of the spectral components above this threshold sum to 98% of the total spectral power. The spectral components above this second, lower power, threshold are indicated by the red drop-lines (as well as the blue drop-lines for the higher threshold) in Figure 3.4. The master laser spectral components with power above the lower threshold are denoted by red crosses in the response gain, Figure 3.5 (a), and by red squares in the master laser phase lead, Figure 3.5 (b).

Figure 3.5 (a) and (b) show that the high power spectral components (blue) all have the desired flat response gain profile and zero phase delay, needed for high quality synchronization.

The spectral components above the lower threshold (red) are grouped closer to the mean response gain (Figure 3.5 (a)) and phase lead (Figure 3.5 (b)) than the other lower power components (circled spectral components in Figures 3.4 and 3.5).

The navy circle in Figures 3.4 and 3.5 identifies a spectral component, $f = 5.51\text{GHz}$, with power just above the lower threshold (Figure 3.4, red dashed line). This spectral component experiences approximately 5dB attenuation with respect to the flat response experienced by the high power spectral components. However, the master laser phase lead is very close to zero and results in better reproduction of this spectral component (navy circle) than the other low power components investigated next.

3.4.1.2 Low Power Spectral Components

The response gain and the master laser phase lead of the local minima in the master laser optical intensity spectrum are now examined to determine whether these low power spectral components are well reproduced in the slave laser and contribute significantly towards the synchronization.

The local minima in the master laser spectrum are: $f = 0.27\text{GHz}$, $f = 6.75\text{GHz}$, $f = 7.11\text{Hz}$, $f = 7.55\text{Hz}$, $f = 11.06\text{GHz}$ (indicated by the black, purple, wine, olive and violet circles respectively in Figures 3.4 and 3.5), are subject to the largest deviations from both the desired flat response gain profile (Figure 3.5 (a)) and zero

master laser phase lead requirement (Figure 3.5 (b)). The other highlighted spectral components; $f = 1.03\text{GHz}$, $f = 1.14\text{GHz}$, $f = 2.23\text{GHz}$, $f = 2.80\text{GHz}$, $f = 3.07\text{GHz}$, $f = 4.92\text{GHz}$, $f = 5.34\text{GHz}$, $f = 10.15\text{GHz}$, $f = 10.38\text{GHz}$, $f = 10.78\text{GHz}$ (red, green, blue, cyan, magenta, yellow, dark yellow, dark cyan, royal and orange respectively in Figures 3.4 and 3.5) show either a large deviation from the flat response gain profile or a significant master laser phase lead, which in either case results in poor synchronization of these spectral components . A large deviation in the response gain is observed for the spectral components $f = 1.03\text{GHz}$, $f = 1.14\text{GHz}$, $f = 2.23\text{GHz}$, $f = 2.80\text{GHz}$, $f = 3.07\text{GHz}$, $f = 4.92\text{GHz}$, $f = 5.34\text{GHz}$, $f = 10.78\text{GHz}$ (red, green, blue, cyan, magenta, yellow, dark yellow and orange circles in Figures 3.4 and 3.5). Large deviation in the master laser phase lead is observed for the spectral components $f = 10.15\text{GHz}$ and $f = 10.38\text{GHz}$ indicated by the dark cyan and royal blue circles in Figures 3.4 and 3.5.

The low power spectral components of the master laser chaotic optical intensity clearly exhibit greater variability in their response gain and phase shift than the high power spectral components. These low power spectral components are not involved in the synchronization process, but also have little effect upon the overall synchronization quality.

Clearly the degree of spectral synchronization is dependent upon the spectral power, and hence will change as the spectral power changes. This means that some spectral components will have temporally intermittent synchronization.

3.4.2 Variation in Chaos Synchronization Quality over Time

The variation in the quality of the master – slave synchronization will now be closely investigated for two spectral components; the first $f = 4\text{GHz}$, close to a local maximum, and the second $f = 4.5\text{GHz}$, close to a local minimum in the average master laser spectrum, Figure 3.2. The average master laser optical intensity spectrum presented in Figure 3.2 (black line) shows that both spectral components $f = 4\text{GHz}$ and $f = 4.5\text{GHz}$ have appreciable power. It would be expected, therefore, that these spectral components would, on average, be subject to the flat response gain profile with zero phase difference and this is exactly what is observed in Figure 3.3 (a).

The variation in the spectral power at both these frequencies will now be examined for 100 individual simulations each having unique initial conditions. The parameter set is given in Table 2.1, Chapter 2. The spectral power, response gain and phase difference are calculated (during the 52ns fast Fourier transform window) for each simulation then collated and presented in Figure 3.6.

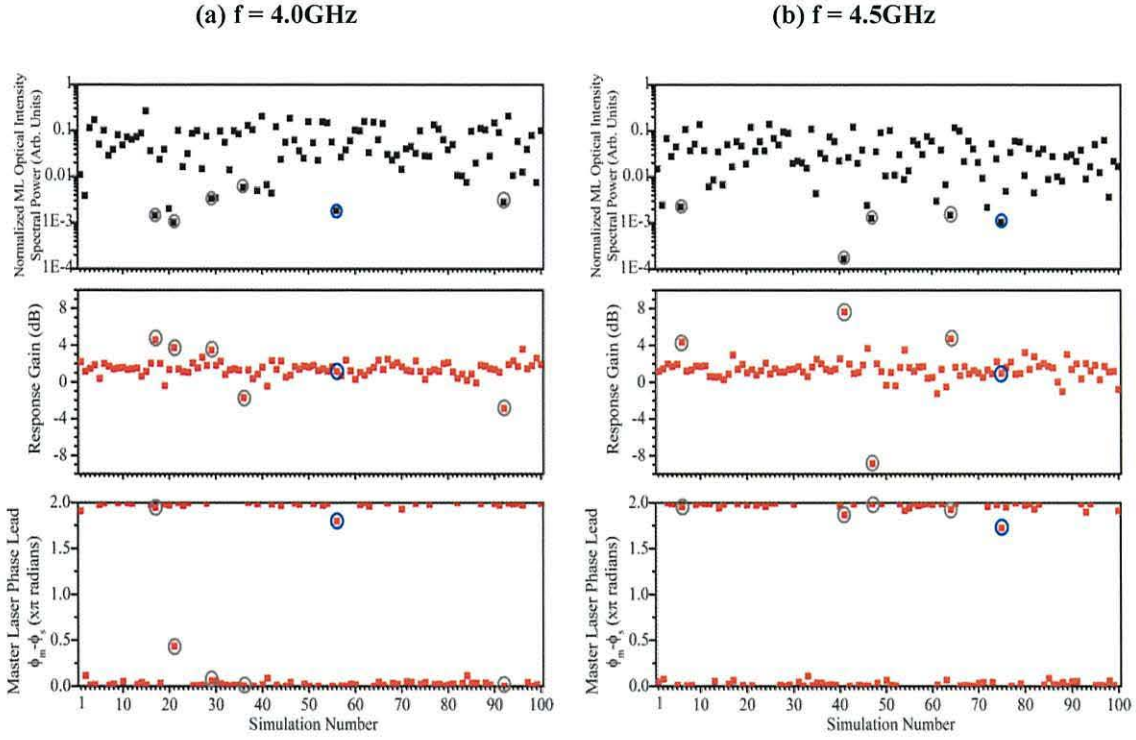

Figure 3.6. Master laser optical intensity (top pane), response gain (middle pane) and master laser phase lead (bottom pane) of two spectral components f = 4.0GHz (a) and f = 4.5GHz (b) for 100 simulations each with unique initial conditions.

The variation in spectral power at both frequencies and the corresponding response gain and phase difference for each individual simulation, with coupling parameters; injection rate $\kappa_c = 170\text{ns}^{-1}$ and zero detuning $\Delta f = 0$ is shown in Figure 3.6. Figure 3.6 shows that there is considerable variation in the spectral power (Figure 3.6, top pane), response gain (middle pane) and phase difference (bottom pane) over time.

Both spectral components (Figure 3.6 (a) - $f = 4\text{GHz}$, Figure 3.5 (b) - $f = 4.5\text{GHz}$) show spectral power (top pane of Figure 3.6) variation of over two orders of magnitude. However, the master laser power remains high enough for the majority of the

simulations to ensure a consistent flat response gain profile (middle pane of Figure 3.6) and master laser phase lead (bottom pane of Figure 3.6) close to zero.

A small number of the simulations have initial conditions that result in a significantly lower spectral power than the average, indicated by the grey circles in Figure 3.6. These master laser low power spectral components result in significant attenuation or gain away from the desired flat response gain profile. This results in a loss of synchronization at these frequencies in these simulations.

The blue circles represent low spectral power where the response gain is approximately unity (middle pane) but there is sufficient phase distortion (bottom pane) to cause a loss of synchronization.

In summary, it has been shown that it is only the high power spectral components of the master that receive uniform response gain and zero phase shift and therefore contribute to a good synchronization quality. The response to low power spectral components varies and these components only contribute to the synchronization process intermittently. The power of individual chaotic spectral frequencies in the master laser output also varies in time and can result in spectral components that may or may not be synchronized in the slave laser at any specific point in time.

3.5 Quality of Chaos Synchronization in Carrier Dynamics

3.5.1 Time Domain Observations

A significant difference in the synchronisation quality of optical intensity and carrier dynamic was observed in the time domain investigation of injection locking synchronization outlined in Chapter 2 for coupling parameters $\Delta f = 10\text{GHz}$ and $\kappa_c = 60\text{ns}^{-1}$. The difference in the carrier and intensity correlation C_{N-P} is reproduced in Figure 3.7, the dark blue area illustrates the region where the carrier correlation is significantly $(C_{N-P} > 0.2)$ higher than the intensity correlation. The synchronization of the carrier dynamics as well as the optical intensity will prove to be important in later chapters when considering how a message is be extracted in the slave laser. A frequency domain analysis will now be undertaken to investigate the difference.

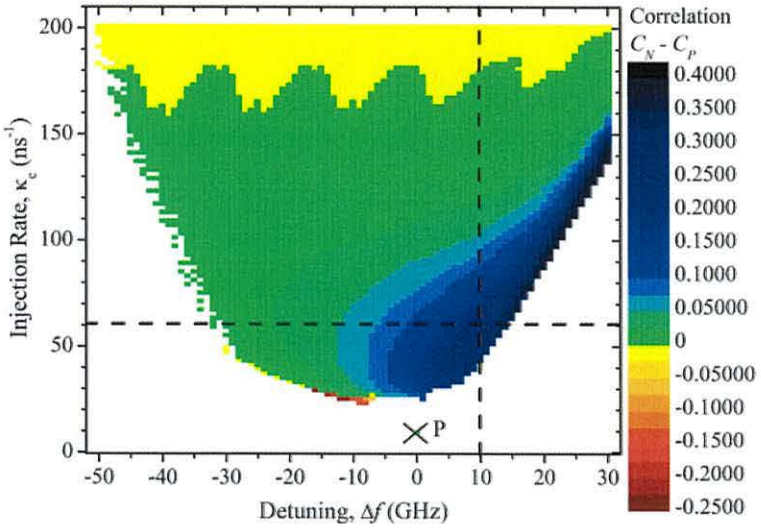

Figure 3.7. Difference in carrier and optical intensity synchronization quality C_{N-P}.

3.5.2 Frequency Domain Observations

The master laser optical intensity and carrier average spectra averaged over 50 simulations are presented in Figure 3.8 (a) by the black and red lines respectively. The corresponding optical intensity and carrier response gain for coupling parameters $\Delta f = 10\text{GHz}$ and $\kappa_c = 60\text{ns}^{-1}$ is presented in Figure 3.8 (b) by the black and red lines respectively.

The carrier spectrum of the master laser, red line in Figure 3.8 (a), contains significantly more power below the relaxation oscillation frequency than the master laser optical intensity spectrum, black line in Figure 3.8 (a). The spectral power of the carrier dynamics also drops off more rapidly than for the optical intensity above the relaxation oscillation frequency. A larger proportion of the spectral power of the carrier dynamics is situated at frequencies below the relaxation oscillation frequency than is the case for the optical intensity.

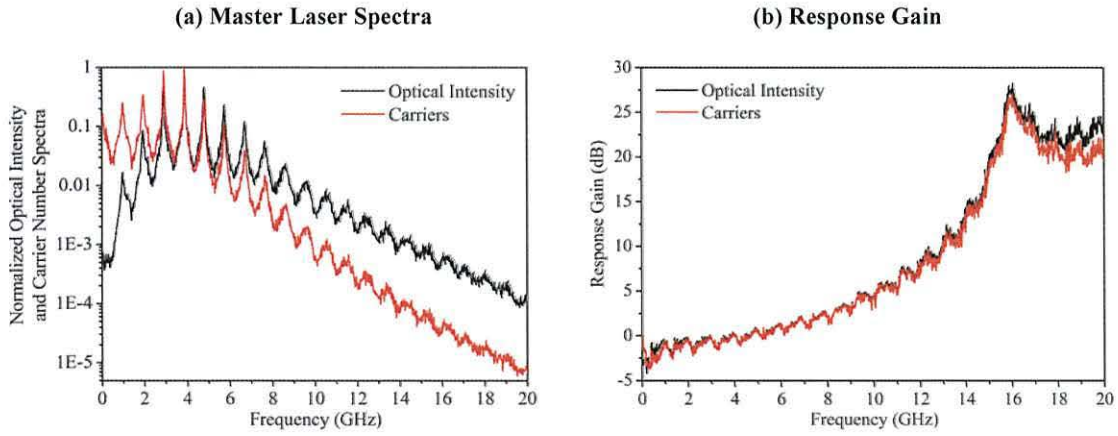

Figure 3.8. Average master laser spectrum (a) and response gain (b) for optical intensity (black line) and carrier dynamics (red line). Detuning frequency $\Delta f = 10\text{GHz}$, slave laser injection rate $\kappa_c = 60\text{ns}^{-1}$.

Figure 3.8 (b) shows that the optical intensity and carrier response gain profiles are very similar. The response gain is relatively flat for the important frequencies around the relaxation oscillation frequency. The additional spectral power above the relaxation oscillation frequency in the optical intensity with respect to the carriers is, therefore, the reason for the lower quality optical intensity synchronization. The distortion introduced above the relaxation oscillation frequency in the slave laser has a greater effect upon the optical intensity than the carrier dynamics.

In summary, the difference in the master laser optical intensity and carrier power spectra results in the differing synchronization quality observed. The optical intensity has more spectral power than the carriers above the relaxation oscillation frequency. The optical intensity is therefore more sensitive to the slave laser distortion and hence the synchronization quality is not as good as for the carrier dynamics.

The optical intensity synchronization may be improved by low pass filtering the slave laser intensity removing the high frequency noise while maintaining the important spectral components that are subject to the required flat response.

3.6 Injection Locking Diagram in the Frequency Domain

We will now use the frequency domain to investigate the injection locking region by collating individual response gain and master laser phase lead curves for the optical intensity and phase. The response gain and master phase lead will be presented as a 2D colour map plotted against frequency and a range of detuning frequencies or injection rates.

3.6.1 Response Gain

For a good synchronization we expect to observe a flat gain profile (H_A) indicating uniform gain or attenuation for the frequencies of interest around the relaxation oscillation frequency.

In the frequency domain injection locking diagrams good quality injection locking synchronization is indicated by a uniform colour vertical strip, around the important spectral components close to the relaxation oscillation frequency, where the majority of the spectral power is distributed.

Perfect synchronization is represented in the frequency domain injection locking diagram by a vertical blue strip in the response gain (H_A) corresponding to unity gain $(H_A = 0\text{dB})$.

A non uniform response gain profile (large colour variation along a vertical section) or significant gain or attenuation (dark red/black or dark blue/black) result in

unsynchronized dynamics. Poorly synchronized components close to the relaxation oscillation frequency have the greatest effect upon the overall synchronization quality.

3.6.2 Master Laser Phase Lead

The slave laser fast Fourier transform window is shifted by the time domain optical output intensity correlation optimum time shift (τ_{opt}) and therefore the well synchronized spectral components have a master phase lead ($\theta_{lead}(P)$) of zero.

Perfect synchronization in the phase is represented by a vertical black strip in the master laser phase lead plot. Unsynchronized dynamics result in a significant master phase lead (colours other than dark red/black or dark blue/black).

3.6.3 Synchronization Trends due to Frequency Detuning

The optical intensity injection locking diagram discussed in Chapter 2 is reproduced here in Figure 3.9 (a) to illustrate the parameter ranges of the frequency domain injection locking diagrams of the current parameter set. The dashed line superimposed on Figure 3.9 (a) indicates constant injection rate $\kappa_c = 60\text{ns}^{-1}$. The correlation and optimum time shift for $\kappa_c = 60\text{ns}^{-1}$ is also shown in Figure 3.9 (b). The solid black line in Figure 3.9 (b) shows the optical intensity correlation, the corresponding optimum time shift is given by the red crosses.

The optical intensity response gain (H_A) and master phase lead ($\Delta\varphi_A$) spectral profiles are presented in Figure 3.10 (a) and (b) respectively for a detuning frequency range

from $\Delta f = -50\text{GHz}$ to $\Delta f = 30\text{GHz}$ at a constant slave laser injection rate $\kappa_c = 60\text{ns}^{-1}$. Lines A ($\Delta f = -30\text{GHz}$) and B ($\Delta f = 6\text{GHz}$) are superimposed on Figure 3.10 to identify the optical intensity injection locking boundaries seen in Figure 3.9 (a).

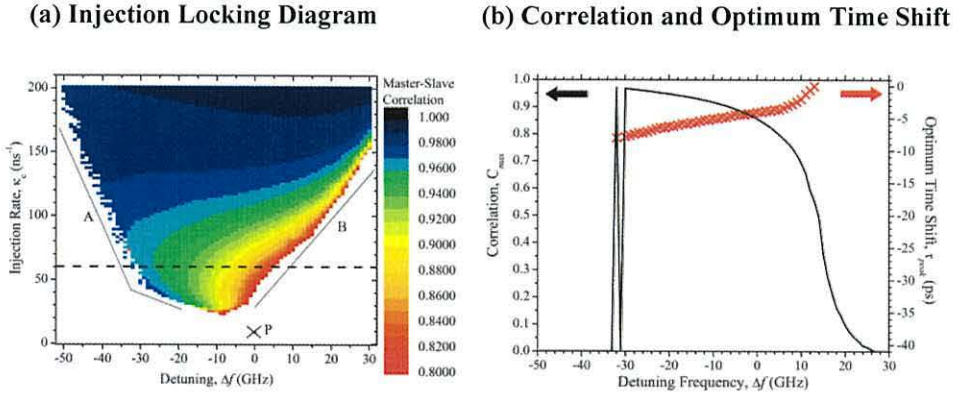

Figure 3.9. (a)- Optical intensity injection locking diagram. (b) - Correlation (red line) and optimum time shift (crosses) for $\kappa_c = 60\text{ns}^{-1}$.

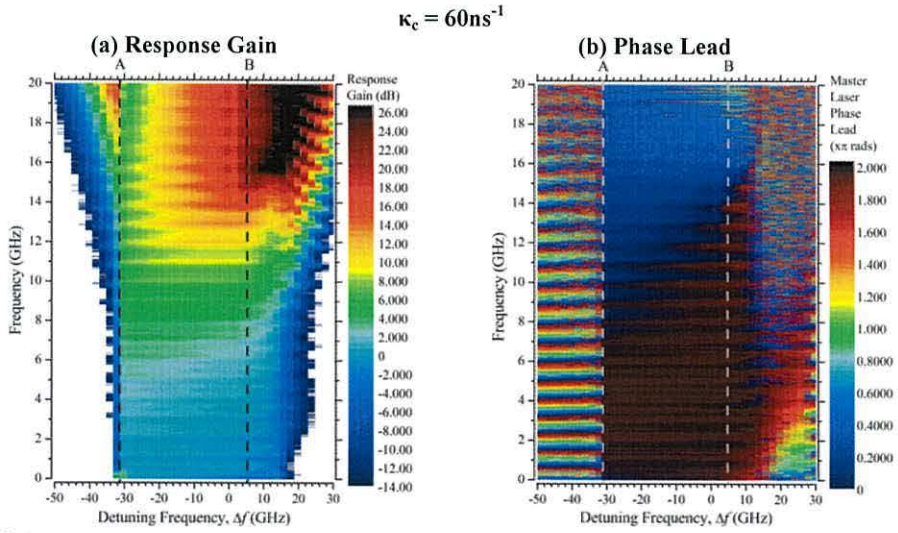

Figure 3.10. Frequency domain optical intensity injection locking diagrams for constant injection rate $\kappa_c = 60\text{ns}^{-1}$.

For increasing negative detuning frequencies to the left of line A in Figure 3.10 (a) there is an area of very strong optical intensity attenuation (white area in Figure 3.10

(a)) over a wide frequency range including around the relaxation oscillation frequency, indicating no intensity synchronization.

In Figure 3.10 (b) the phase lead clearly differentiates the negative detuning boundary of the injection locking region, on one side of the boundary there are large periodic variations in the phase, while on the other side the expected phase locking is seen. The change between these two regions is abrupt. The other boundary is less distinct in Figure 3.10 (b) where a gradual loss in the phase locking and the increased high frequency distortion seen in Figure 10 (a) both contribution to a gradual loss of synchronisation quality.

It is clear that the injection locking boundary identified in the frequency domain analysis, Figure 3.10, coincide with those seen in the time domain correlation and optimum time shift, Figure 3.9.

Between lines A ($\Delta f = -30\text{GHz}$) and B ($\Delta f = 6\text{GHz}$) in Figure 3.10 (a) the optical intensity response gain profile (H_A) remains uniform and relatively unchanged for the most important high power frequencies close to the relaxation oscillation frequency ($f_{relax} = 3.85\text{GHz}$). In addition, very little change is observed in the phase difference, Figure 3.10 (b), as the detuning frequency is changed from $\Delta f = -30\text{GHz}$ to $\Delta f = 6\text{GHz}$. The synchronization quality is dominated by the small changes in the response gain profile.

However, an increase in the high frequency ($f > 7\text{GHz}$) gain in the slave laser is observed (from green to red, left to right between A and B in Figure 3.10 (a)). This

increase in high frequency distortion as the frequency detuning increases results in a decrease in the optical intensity correlation across the range and is in agreement with the time domain correlation results of Figure 3.9 (a) and (b). The high frequency distortion is causing the deterioration in the correlation.

For strong positive detuning frequencies, to the right of line B in Figure 3.10 (a), the gradual increase in high frequency distortion continues up to $\Delta f = 14\text{GHz}$. Beyond this significant attenuation around the relaxation oscillation frequency ($f_{relax} = 3.85\text{GHz}$) is introduced and optical intensity synchronization is lost.

The loss of synchronization above $\Delta f = 14\text{GHz}$ is also observed in the master laser phase lead, Figure 3.10 (b), where significant variation in the phase difference is observed and hence synchronization is lost. This gradual deterioration in the synchronization is exactly what is observed in the time domain correlation, Figure 3.9.

In summary, for a fixed injection rate and varied frequency detuning the locked and unlocked region are identified in the frequency domain by the following features. The injection locking region has a flat response gain profile and zero phase shift. As the detuning frequency is increased across the injection locking region an increasing amount of high frequency distortion is observed above the relaxation oscillation frequency and as a result the measured correlation is reduced. Outside the injection locking region significant attenuation or gain of the optical intensity and variation in the response gain and phase lead profiles is also observed.

3.6.4 Synchronization Trends due to Injection Rate Increases

The injection locking diagram is again reproduced, Figure 3.11 (a), to aid the comparison. The superimposed vertical red line in Figure 3.11 (a) indicates a constant detuning frequency $\Delta f = -22\text{GHz}$. The correlation and optimum time shift for $\Delta f = -22\text{GHz}$ is also shown in Figure 3.11 (b) by the black line and red crosses respectively.

The optical intensity response gain (H_A) and master phase lead ($\Delta\varphi_A$) spectral profiles are presented in Figure 3.12 (a) and (b) respectively for a slave laser injection rate ranging from $\kappa_c = 5\text{ns}^{-1}$ to $\kappa_c = 200\text{ns}^{-1}$ for a constant detuning frequency $\Delta f = -22\text{GHz}$. Line A ($\kappa_c = 38\text{ns}^{-1}$) is superimposed on Figure 3.12 to represent the corresponding optical intensity injection locking boundary identified in Figure 3.11 (a). Line C ($\kappa_c = 60\text{ns}^{-1}$) is also superimposed to aid the following discussion.

For weak slave laser injection, low injection rates to the left of line A ($\kappa_c = 38\text{ns}^{-1}$) in Figure 3.12, the important spectral components close to the relaxation oscillation frequency are subject to significant attenuation (dark blue areas in Figure 3.12 (a)) and variation in the spectral phase lead (large variations in colour in Figure 3.12 (b)). This indicates a complete loss of synchronization for weak slave laser injection rates to the left of line A in Figure 3.12 and this unlocked state is indeed exactly what is observed in the time domain correlation, Figure 3.11.

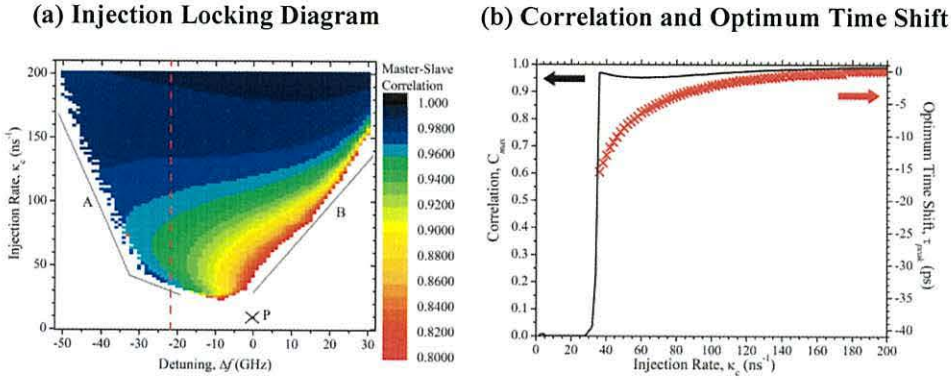

Figure 3.11. (a) - Optical intensity injection locking diagram. (b) - Correlation (red line) and optimum time shift (crosses) for Δf = -22GHz.

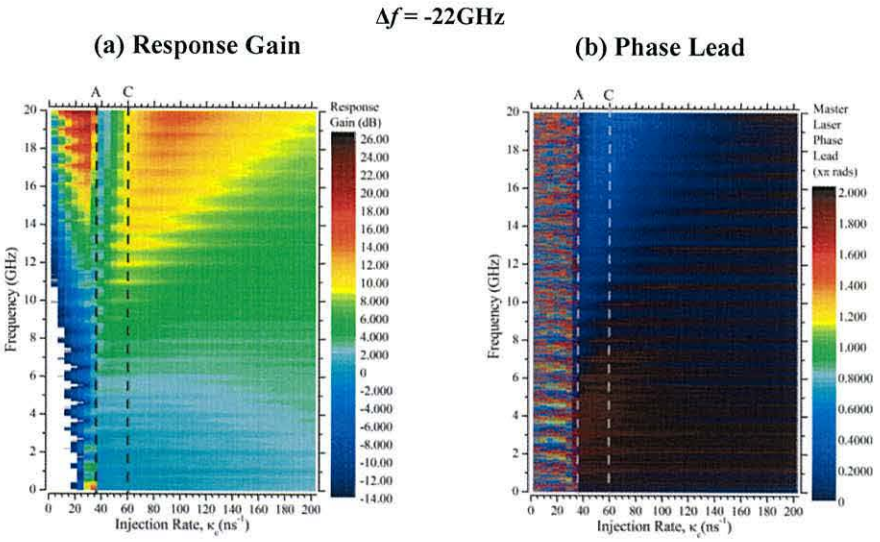

Figure 3.12. Frequency domain optical intensity injection locking diagrams for constant detuning frequency Δf = -22GHz.

The region between $\kappa_c = 38\text{ns}^{-1}$ and $\kappa_c = 60\text{ns}^{-1}$, lines A and C in Figure 3.12 (a), is markedly different to the rest of the figure and corresponds to the small region of high quality synchronization at low injection rates seen in Figure 3.11 and discussed in Section 2.5.2.2.

Immediately to the right of line A in Figure 3.12 (a) for $\kappa_c = 38\text{ns}^{-1}$ there is an abrupt change in the response gain and essentially all the spectral components of interest experience unity gain. As the injection rate is increased towards line C, $\kappa_c = 60\text{ns}^{-1}$, additional high frequency ($f = 7\text{GHz}$) structure, indicated by increased gain, is seen in Figure 3.12 (a). This indicates that the synchronization decreases gradually between $\kappa_c = 38\text{ns}^{-1}$ and $\kappa_c = 60\text{ns}^{-1}$ and this is exactly what is seen in Figure 3.11.

The spectral phase lead profile, Figure 3.12 (b), does not vary considerably between $\kappa_c = 38\text{ns}^{-1}$ (line A) and $\kappa_c = 60\text{ns}^{-1}$ (line B). It is therefore the response gain that has greatest effect upon the optical intensity synchronization quality within this area.

Immediately to the right of line C, $\kappa_c > 60\text{ns}^{-1}$, there is considerable high frequency gain (red area in Figure 3.12 (a)) along with considerable variation in the phase difference profile (light blue area in Figure 3.12 (b)) which results in a local minimum in the correlation, Figure 3.11 (a) and (b).

As the injection rate is increased further the level of high frequency distortion decreases in Figure 3.12 (a) and there is less deviation from zero in the master laser phase lead in Figure 3.12 (b). This indicates that the number of spectral components that are synchronized in the slave laser increases with injection rate for $\kappa_c > 60\text{ns}^{-1}$ (right of line C in Figure 3.12) and hence the quality of the synchronization increases gradually, and this is exactly what is seen in the correlation, Figure 3.11 (a) and (b).

3.7 Conclusions

The average master and slave spectra for injection locking synchronization have been constructed and the response gain and master laser phase lead calculated. A flat response gain profile and master laser phase lead of zero has been shown to occur when good quality synchronization is achieved.

The master laser optical intensity spectrum of the single simulation has much greater variation in the spectral power than the average and shows that the chaos spectrum varies considerably with time. The study of a single simulation, Section 3.4, identified the high power spectral components in the master laser optical intensity. The high power spectral components of the master laser, close the relaxation oscillation frequency, are subject to uniform response gain and zero phase shift that indicates a good synchronization with the slave laser.

The low power spectral components of the master laser optical intensity have also been studied in the single simulation spectrum and they show large variation in response gain and phase lead. The low power frequency components are therefore not well reproduced in the slave laser and are not synchronized. It is the variations in the reproduction of the low power spectral components that causes the small variations in synchronization quality observed in the injection locking region.

The variation in the master laser output spectral power has been demonstrated for two specific frequencies, Section 3.4.2. If the spectral power is sufficiently high it is accurately reproduced in magnitude and phase in the slave laser. When the spectral

power is low the synchronization of the component is lost. At any point in time a spectral component may or may not be locked. However, during injection locking there are enough spectral components of sufficient power to ensure synchronization is maintained.

In Chapter 2 it was shown that the correlation of the carrier dynamics is higher than that of the optical intensity at low injection rates and positive detuning frequencies. The frequency domain analysis in this chapter has shown that the carriers and optical intensity are both subject to the same flat response gain profile for the important high power components and a small amount of distortion at frequencies above the relaxation oscillation frequency. The slower carrier dynamics, where a greater proportion of spectral power is below the relaxation oscillation frequency, results in a higher correlation as they are affected less by the high frequency distortion introduced in the slave laser. The important, high power, chaotic components are subject to a flat response in both the carrier and optical intensity.

Chaos injection locking diagrams in the frequency domain have been introduced and trends compared with the time domain based diagram. The trends observed in the time domain correlation are also observed in the frequency domain and can be explained by the changing slave laser frequency response. The frequency based injection locking diagrams show that even though there is little chaotic power at frequencies above the relaxation oscillation the changes in correlation observed in the injection locking region are highly dependent upon the these frequencies since significant distortion is introduced in the slave laser.

3.8 Bibliography

[1] R Lang and K Kobayashi, "External optical feedback effects on semiconductor injection properties," *IEEE J. Quantum Electron.*, vol. 16, pp. 347-355, 1980.

[2] William H Press, Brian P Flannery, Saul A Teukolsky, and William T Vetterling, *Numerical Recipes: The Art of Scientific Computing.*: Cambridge University Press, 1987.

[3] S Peters-Flynn, P S Spencer, S Sivaprakasam, I Pierce, and K A Shore, "Identification of the Optimum Time-Delay for Chaos Synchronization Regimes of Semiconductor Lasers," *IEEE J. Quant. Elect.*, vol. 42, pp. 427-434, 2006.

[4] MW Lee, K A Shore, J Paul, "Effect of chaos pass filtering on message decoding quality using chaotic external-cavity laser diodes," *Opt. Lett.*, vol. 29, pp. 2497-2499, 2004.

[5] A Murakami and K A Shore, "Analogy between optically driven injection-locked laser diodes and driven damped linear oscillators," *Phys Rev A*, vol. 73, p. 043804, 2006.

[6] K Kawashima,K Atsuki, A Murakami, "Cavity resonance shift and bandwidth enhancement in semiconductor lasers with strong light injection," *IEEE J. Quantum Electron.*, vol. 39, pp. 1196-1204, 2003.

Chapter 4

Current Modulation Response of Semiconductor Lasers in the Coherence Collapse Regime

4.1 Introduction

Following Pecora and Carroll's study of chaos synchronization [1] Cuomo and Oppenheim proposed an electronic system based on the Lorenz equations that would mask speech within the fluctuations produced at the transmitter and then decoded at the receiver [2].

The decoding process is reliant on chaos synchronisation, whereby the receiver reproduces, or locks to, the chaotic fluctuations of the transmitter and this process is broadly similar in nature to CW injection locking. Several physical systems have demonstrated chaos synchronization and recently semiconductor laser diodes have received much attention in this regard.

Synchronized chaotic laser diodes have also been used to form hardware based secure communications system that masks the message within the chaotic fluctuations of the master laser. The slave laser preferentially locks to the chaotic fluctuations of the

master laser, effectively filtering out the masked message. By then comparing the dynamics of the master and slave lasers it is possible to extract the message [3-6]. This message extraction process is commonly referred to as 'Chaos Pass Filtering' [7,8] and has been the subject of some discussion. The extraction process in the receiver laser diode will be examined in the following chapters.

In this chapter the current modulation of the semiconductor laser diode with and without optical feedback from an external mirror is studied. The laser diode without external optical feedback is referred to as the solitary laser. The laser subject to external optical feedback from an external mirror is referred to as the external cavity laser (ECL). The ECL is identical to that simulated in Chapters 2 and 3 except for the applied current modulation. This chapter focuses on the transmitter laser of the complete transmitter/receiver communications system.

The aim of this chapter is to gain further insight into the current modulation response of a semiconductor laser diodes operating in the coherence collapse regime.

Firstly, to set a baseline for later discussion, the current modulation response of the stable solitary laser will be determined. A simple periodic sinusoidal current modulation is applied and a large range of modulation frequencies and depths are tested to create the modulation response - as well as providing a baseline these preliminary current modulation calculation also serve to validate the approach. An external mirror is then introduced and the laser is subject to same external optical feedback levels as those studied in Chapters 2 and 3.

4.2 Theoretical Framework

In this chapter the current modulation of the solitary laser and ECL are simulated using the enhanced Lang-Kobayashi rate equation model, outlined in Sections 4.2.1 and 4.2.2 respectively. The closed form solutions for the current modulation response of the solitary laser and subject to external optical feedback have previously been derived based on a small signal analysis and linear gain [9], however it is not clear that these solutions fully encapsulation the dynamics of a destabilised current modulated ECL.

4.2.1 Solitary Laser - Current Modulation

Figure 4.1 shows the schematic of the solitary laser with periodic sinusoidal current modulation.

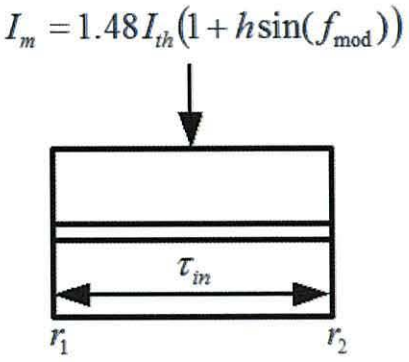

Figure 4.1. Schematic of sinusoidal current modulation of the solitary laser.

The complex field amplitude E_m of the solitary laser can be described using the following rate equation,

$$\frac{dE_m(t)}{dt} = \frac{1}{2}(1+i\alpha)\left[G_m(t) - \frac{1}{\tau_P}\right]E_m(t) \qquad 4.1$$

The carrier, N_m, and gain, G_m, equations are as used in Chapters 2 and 3,

$$\frac{dN_m(t)}{dt} = \frac{I_m}{e} - \frac{N_m(t)}{\tau_N} - G_m(t)\left|E_m(t)\right|^2 \qquad 4.2$$

The nonlinear gain is given by,

$$G_m(t) = \frac{g_0(N_m(t) - N_0)}{1+\varepsilon\left|E_m(t)\right|^2} \qquad 4.3$$

The laser drive current, I_m, is modulated with a periodic sinusoidal message. The modulation frequency is given by f_{mod} and the modulation depth given by h,

$$I_m = 1.48I_{th}\left(1 + h\sin(f_{\text{mod}})\right) \qquad 4.4$$

4.2.2 External Cavity Laser - Current Modulation

The ECL is subject to optical feedback from an external mirror, Figure 4.2. The external cavity dimensions and mirror feedback rate are $\kappa_m = 10\text{ns}^{-1}$, and external cavity round trip time $\tau_{ex} = 1\text{ns}$.

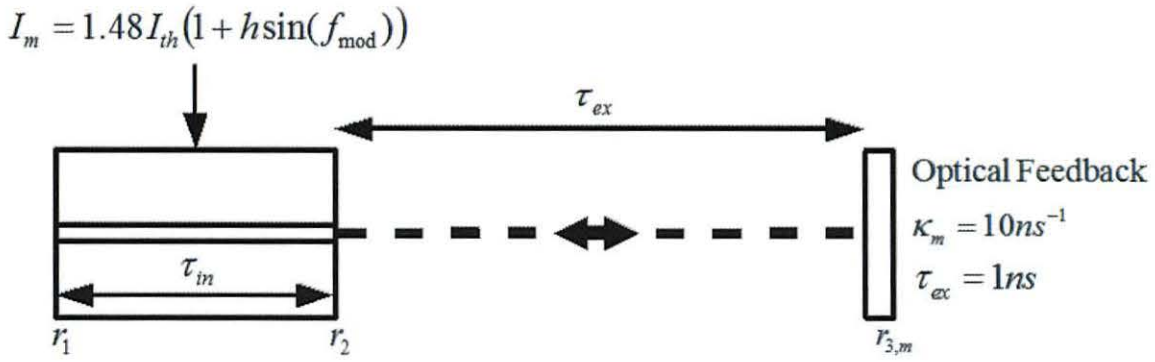

Figure 4.2. Schematic of sinusoidal current modulation of laser diode subject to optical feedback from an external mirror.

The complex field amplitude E_m, Eqn. 5, of the ECL is dependent upon the optical feedback and the additional term is included in the rate equation to describe this effect,

$$\frac{dE_m(t)}{dt} = \frac{1}{2}(1+i\alpha)\left[G_m(t) - \frac{1}{\tau_P}\right]E_m(t) + \kappa_m E_m(t-\tau_{ex,m})e^{-i\omega_m \tau_{ex,m}} \qquad 4.5$$

The carrier and gain are given by Eqn. 2 and 3 and the same drive current modulation as for the solitary laser is applied, Eqn. 4. All the parameter values are outlined below in the numerical framework.

4.3 Numerical Framework

For each modulation depth, h, tested the message applied to the drive current is swept through a range of modulation frequencies. Ten modulation depths from $h = 0.03\%$ to $h = 20\%$ are tested and in each case the modulation frequency is swept through 525 steps from 0.02GHz to 20GHz.

For the current modulated solitary laser the spectral power at the modulation frequency for each simulation is collated to obtain the modulation response. The modulation response of the solitary laser for a single modulation depth is created from 525 individual simulations.

The average spectral power, for the modulated ECL, at each modulation frequency is calculated from the results of 50 simulations each with different initial conditions and therefore a different route to chaos. The average spectral power at the modulation frequency is used to observe the general, time averaged, effect of the fluctuating chaotic power on the modulation. The ECL output characteristic for a single modulation depth is collated from the results of 262,500 simulations.

The current modulation response of the ECL will be compared to the average spectral power of the un-modulated ($I_m = 1.48I_{th}$) master laser (ECL) in Chapter 3.

4.3.1 Parameter Set

Table 4.1 details the parameter set used in the following numerical simulations. .

Parameter	Symbol	Value
ECL drive current (Un-modulated)	I_m	$1.48I_{th}$
ECL drive current (Modulated)	I_m	$1.48I_{th}(1+h\sin(f_{\mathrm{mod}}))$
Modulation Frequency	f_{mod}	0.02GHz – 20GHz
Modulation Depth	h	0.03% – 20%
Linewidth enhancement factor	α	5
Carrier lifetime	τ_N	2ns
Photon lifetime	τ_P	2ps
Internal cavity round-trip time	τ_{in}	7ps
ECL external cavity round-trip time	τ_{ex}	1ns
Linear gain coefficient	g	$1.5\text{x}10^{-8}\text{ps}^{-1}$
Gain saturation coefficient	ε	$5\text{x}10^{-7}$
Carrier number at transparency	N_0	$1.5\text{x}10^{8}$
Wavelength	λ	780nm
Facet reflectivity	r_1, r_2	0.548
Solitary laser feedback rate	κ_m	0
ECL feedback rate	κ_m	10ns^{-1}

Table 4.1. Parameter set used in the numerical simulations..

4.4 Current Modulated Solitary Laser Simulation Results

The solitary laser response to sinusoidal modulation of the drive current is now presented for a wide range of frequencies and modulation depths. Solitary laser optical intensity response curves, representing constant modulation depth, for modulation frequencies from $f_{mod} = 0.02\text{GHz}$ to $f_{mod} = 20\text{GHz}$ are presented in Figure 4.3. The following modulation depths are presented: $h = 0.03\%$ (black line), $h = 0.2\%$ (green line), $h = 1\%$ (cyan line), $h = 5\%$ (yellow line), $h = 20\%$ (purple line). This work acts as merely a base line to aid future analysis on the more complex modulated ECL output.

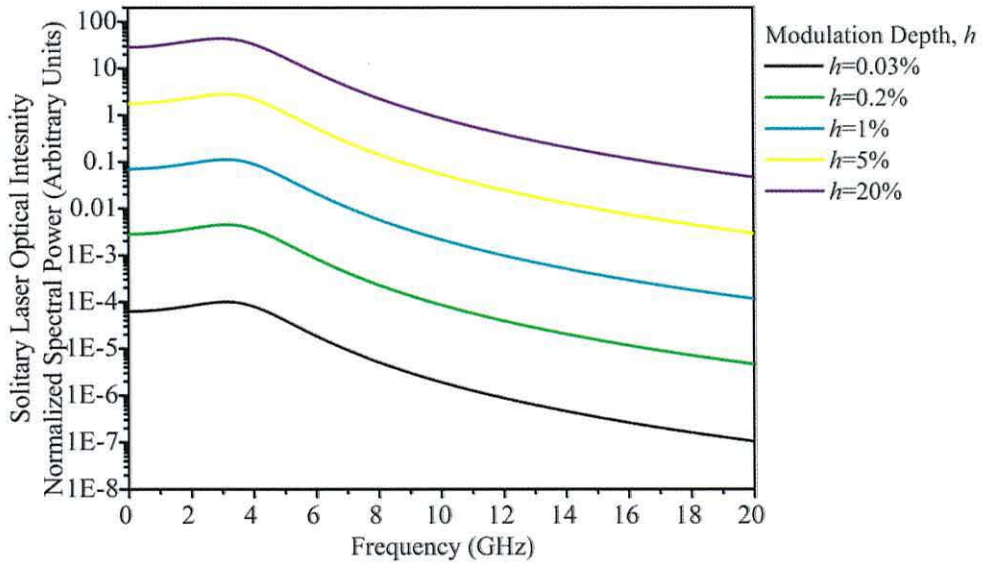

Figure 4.3. Current modulated solitary laser optical intensity output spectrum. Modulation depths: *h = 0.03%* (black line), *h = 0.2%* (green line), *h = 1%* (cyan line), *h = 5%* (yellow line), *h = 20%* (purple line).

The solitary laser current modulation response profiles in Figure 4.3 are identical for each modulation depth. The maximum spectral power is observed at the relaxation oscillation frequency, $f_{\text{mod}} = f_{relax} = 3.85\text{GHz}$. The modulation response drops off significantly above the relaxation oscillation frequency. At $f_{\text{mod}} = 20\text{GHz}$ the spectral power is approximately three orders of magnitude less than the maximum. This spectral response shows that a more complex message consisting of a wide spectral range will therefore be distorted when applied to even the solitary laser. Message components applied close to the relaxation oscillation receive gain with respect to the lower and higher message frequencies.

The optical intensity spectral power at the message frequency of the modulated solitary laser is plotted against the modulation depth in Figure 4.4 for four modulation frequencies; $f_{\text{mod}} = 2.4\text{GHz}$, $f_{\text{mod}} = 5.3\text{GHz}$, $f_{\text{mod}} = 7.2\text{GHz}$, $f_{\text{mod}} = 9.1\text{GHz}$. A linear relationship between the optical intensity spectral power and square of the modulation depth is observed in Figure 4.4.

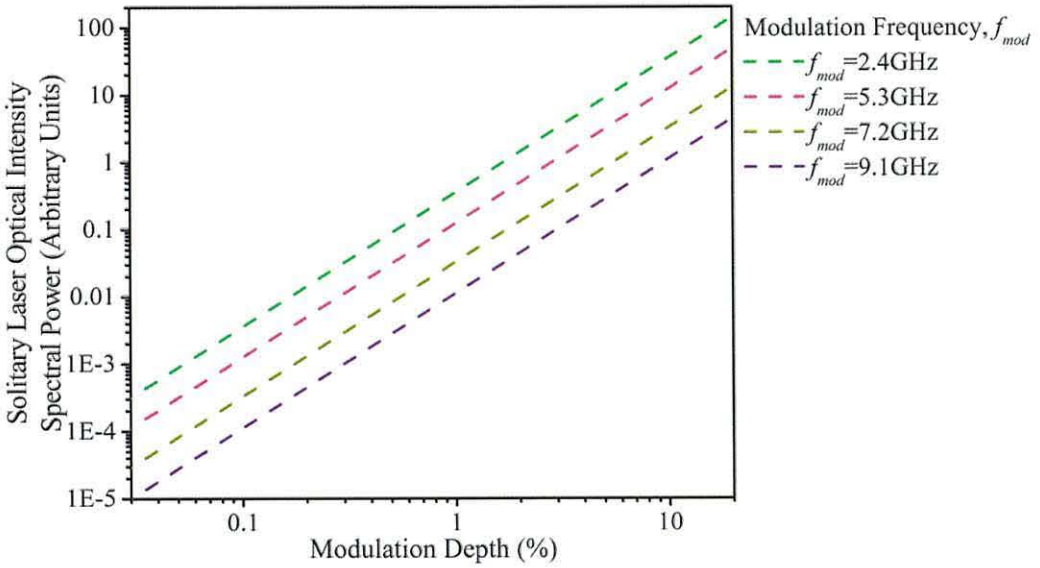

Figure 4.4. Optical spectral power versus modulation depth for sinusoidal current modulation of a solitary laser.

4.5 Current Modulated ECL Simulation Results

An external mirror is now added to the laser to provide optical feedback. The external mirror feedback rate, κ_m, and external cavity round trip time, τ_{ex}, are given in Table 1.

The current modulation response of the ECL is calculated using the average of 50 simulations each with unique initial conditions in order to gain the general time average effect of the chaotic fluctuations on the modulation process.

The current modulation response is presented in Figure 4.5 for a range of modulation depths. The same modulation depths as those used in Section 4.4.1 are presented for the chaotic laser, Figure 4.5.

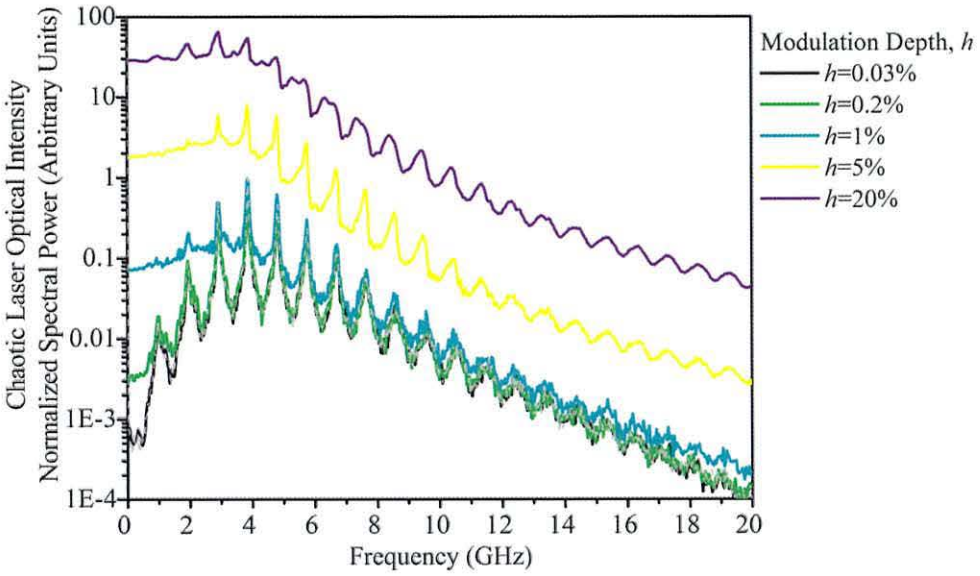

Figure 4.5. Current modulated ECL optical intensity output spectrum. Modulation depths: *h = 0.03%* (black line), *h = 0.2%* (green line), *h = 1%* (cyan line), *h = 5%* (yellow line), *h = 20%* (purple line).

The average optical intensity spectrum of the un-modulated ($I_m = 1.48I_{th}$) ECL is also superimposed on Figure 4.5 as the grey dashed line

The modulated ECL optical intensity output spectrum broadly follows the characteristic of the modulated solitary laser, Figure 4.3, but also contains local maxima at the external cavity roundtrip frequency. For the lowest modulation depth $h = 0.03\%$ (black line) the applied message has a negligible effect upon the chaotic power and is indistinguishable from the un-modulated case (grey line) in Figure 4.5.

The optical intensity characteristic of the modulated ECL, Figure 4.5, will now be compared to the solitary laser modulation response and the un-modulated ECL average chaotic output. The average chaotic output of the un-modulated ECL is a very good

approximation to the background chaos that is used to mask the message in the modulated ECL.

The spectral characteristic for a modulation depth $h = 0.03\%$ in the solitary laser (Figure 4.3, black line) is at least an order of magnitude lower in spectral power than the un-modulated ECL chaotic power (Figure 4.5, grey line). The chaos dominates the output and the applied signal is insignificant. It is unclear in Figure 4.5 whether this low power message is even present in the output, if the message is present it is effectively masked by the background chaos, which resembles noise.

For low frequency sinusoidal messages, $f_{mod} < 1\text{GHz}$, applied to ECL the magnitude of the background chaos (Figure 4.5, grey line) is low relative to the modulated solitary laser output (Figure 4.3). Because of this difference the message dominates the output for relatively low modulation depths. This can clearly be seen in Figure 4.5 for $h = 0.2\%$ (green line) where the message power is significantly higher than the chaotic background noise (grey line) for $f_{mod} < 1\text{GHz}$. A greater modulation depth is required at higher frequencies $f_{mod} > 1\text{GHz}$ before the message power dominates the background chaos.

For higher modulation depths h =5% and h=20% (Figure 4.5, yellow and purple lines respectively) the output characteristic is different for frequencies close to local minima or maxima in the un-modulated ECL output spectrum (Figure 4.5, grey line). For modulation frequencies that coincide with local minima the modulated ECL output closely follows that of the current modulated solitary laser modulation response. For

modulation frequencies coinciding with the local maxima the modulated ECL output has greater spectral power than the current modulated solitary laser characteristic due to constructive interference from the external mirror feedback.

These observations and the relationship between the output spectral power and the applied modulation depth will now be examined further by looking firstly at the modulation frequencies that coincide with the local minima in the average spectrum of the un-modulated ECL and, secondly with the modulation frequencies that coincide with the local maxima in the average spectrum of the un-modulated ECL.

4.5.1 Analysis of Chaotic Laser Modulation

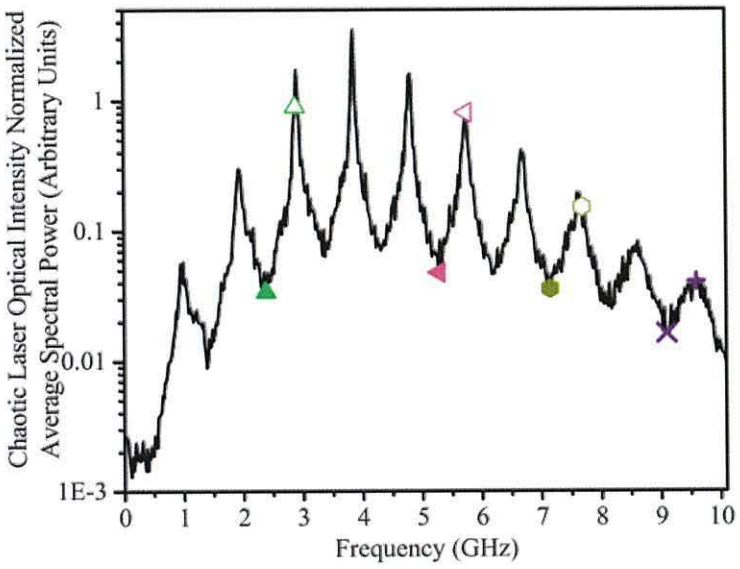

Figure 4.6. Average chaos spectrum of 50 simulations for un-modulated laser subject to external optical feedback.

The modulation frequencies to be examined further are given by the scatter points in Figure 4.6. Filled symbols represent modulation frequencies close to local minima in the average un-modulated chaos spectrum (black line) and are discussed in Section 4.4.2.2. Hollow symbols represent modulation frequencies close to local maxima in the average un-modulated chaos spectrum and are discussed in Section 4.4.2.3.

4.5.1.1 Local Minima in the Modulation Response

The current modulated ECL optical spectral power versus modulation depth is presented in Figure 4.7 for message frequencies that coincide with the local minima in the average spectrum of the un-modulated ECL i.e. where the low background noise at

the message frequency is low. Each scatter point in Figure 4.7 represents a point on the output characteristic of Figure 4.5. The dashed lines in Figure 4.7 are the solitary laser modulation characteristics, taken from Figure 4.4.

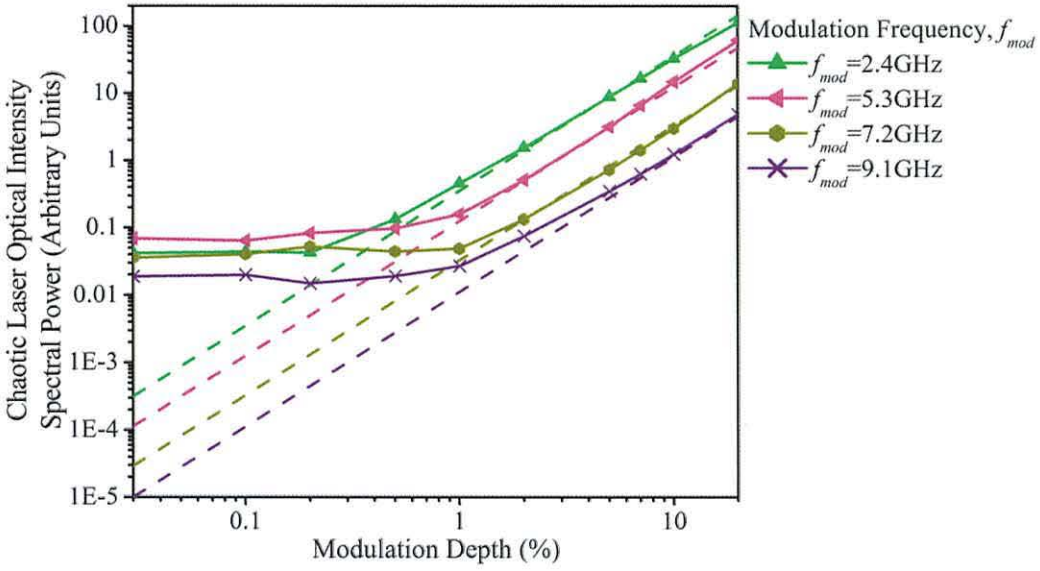

Figure 4.7. Optical spectral power versus modulation depth for sinusoidal current modulation of solitary laser. The modulation frequencies coincide with local minima in the average un-modulated chaotic laser output. The dashed lines give the current modulation response of a solitary laser.

Three regions of operation can be identified from Figure 4.7:

I – weak modulation

II – intermediate modulation

III – strong modulation

and are described in detail below.

A region of constant output power is observed in Figure 4.7 for a range of low modulation depths. The range of modulation depths for which the output power is

constant is dependent upon the modulation frequency and determined by the difference between the message power and the background chaos. For example, for $f_{mod} = 2.4\text{GHz}$ the spectral power is constant for $h = 0.03\%$ to $h = 1\%$ and for $f_{mod} = 9.1\text{GHz}$ the flat response extends from $h = 0.03\%$ to $h = 0.2\%$.

In Region I the chaotic background chaos is the dominant component in the output power at the modulation frequency and hence a region of constant output power, greater than the solitary laser current modulation response is observed in Figure 4.7. The message is indistinguishable in the ECL output from the chaotic background noise.

For a range of modulation depths above Region I the message power and chaotic fluctuations of the background chaos are of the same order of magnitude and both have a similar effect upon the output. For example, Region II is identified in Figure 4.7 for $f_{mod} = 2.4\text{GHz}$ within the range $0.2 < h < 2\%$ and for $f_{mod} = 9.1\text{GHz}$ within the range $1 < h < 7\%$.

The average output power is above that predicted for a current modulated solitary laser (Figure 4.7, dashed lines), but fluctuates due to the contribution made by the background chaos of the ECL. At any moment in time the message or chaotic background noise may dominate in the output and this is likely to affect the quality of the extraction in the receiver.

For very strong modulation depths the current modulation response of the ECL closely follows the solitary laser current modulation characteristic. For example in Figure 4.7 region III is observed for $f_{mod} = 2.4\text{GHz}$ at modulation depths $h \geq 2\%$ and for

f_{mod} = 9.1GHz at modulation depths $h \geq 7\%$. The chaotic background noise is insignificant in the output and the optical power is linearly related to the square of the modulation depth, as previously seen in the solitary laser case

The regions described above are dependent upon both the modulation frequency and modulation depth. The regions are determined by the difference in the solitary laser current modulation response and the un-modulated chaotic laser response.

4.5.1.2 Local Maxima in the Modulation Response

The current modulated ECL optical intensity spectral power versus modulation depth is presented in Figure 4.8 for message frequencies that coincide with the local maxima in the average spectrum of the un-modulated ECL. The local maxima correspond to harmonic frequencies of the ECL. Four modulation frequencies are presented in Figure 4.8; f_{mod} = 2.9GHz - green line, f_{mod} = 5.7GHz - magenta line, f_{mod} = 7.7GHz - dark yellow line, f_{mod} = 9.6GHz - purple line. The lines in Figure 4.8 represent a vertical section through Figure 4.5. The corresponding solitary laser current modulated responses are denoted by the dotted lines in Figure 4.8.

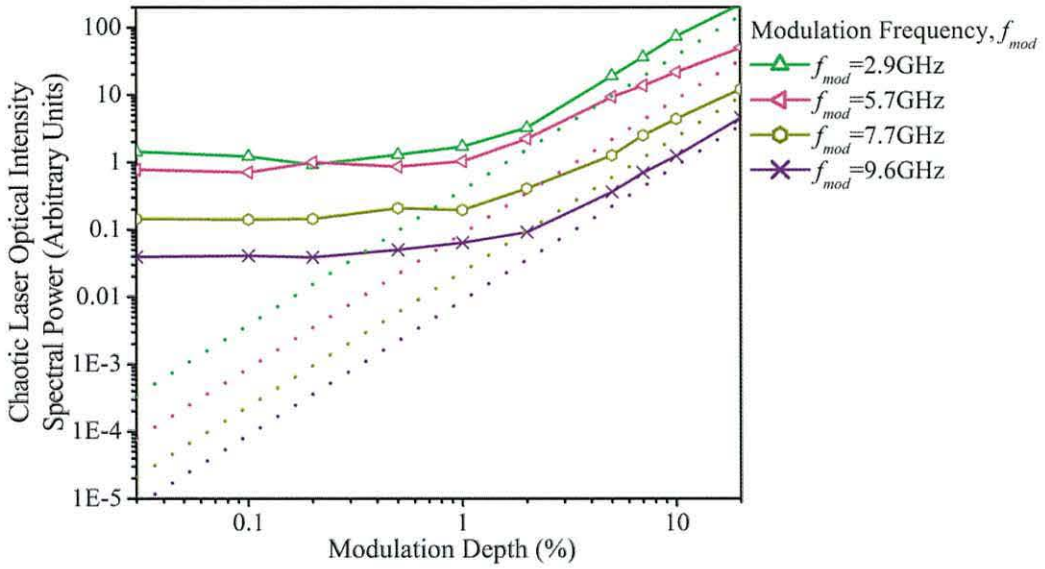

Figure 4.8. Optical spectral power versus modulation depth for sinusoidal current modulation of solitary laser. Modulation frequencies coincide with local maxima in the average un-modulated chaotic laser output. The dotted lines denote the solitary laser modulation response.

Region I, constant optical intensity output spectral power, for low modulation depths is observed in Figure 4.8. For example, for $f_{\mathrm{mod}} = 2.9\mathrm{GHz}$ the constant output power is observed at modulation depths $h \leq 1\%$ and for $f_{\mathrm{mod}} = 9.6\mathrm{GHz}$ at modulation depths $h \leq 2\%$.

Again, as for messages applied at the local minima, Region II is observed for intermediate modulation depths where both the applied message and background chaos have a significant effect upon the output of the current modulated ECL.

The output power in Region III is dominated by the applied message. The output power of the modulated ECL (Figure 4.8, solid lines) remains higher than that of the modulated solitary laser (Figure 4.8, dotted lines) but is observed to be asymptotic to it for high modulation depths. The additional output power of the modulated ECL (solid

lines) is due to constructive interference introduced by the optical feedback from the external mirror. For example, Region III is observed for f_{mod} = 2.9GHz at modulation depths $h \geq 2\%$ and for f_{mod} = 9.6GHz at modulation depths $h \geq 3\%$.

Three regions are again observed, however, much larger modulation depths are required to move from Region I to Region II and Region III is never fully realised.

4.6 Conclusions

The current modulation of the external cavity laser creates three regions of operation:

Region I: At very low modulation depths the power applied via the modulation of the drive current is very small and the optical intensity at the modulation frequency is dominated by the background chaos. The message is indistinguishable from the chaotic background noise and is therefore not effectively applied. This implies that it will be difficult to extract the message at the receiver.

Region II: For intermediate modulation depths both the chaotic background noise and modulation significantly affect the output spectral power. The simulations were performed using the average chaotic background noise and therefore give an aggregate spectral profile. However, the spectral characteristic at any given moment will be dependent upon the fluctuating chaotic background noise and therefore the message will become distorted. At any point in time the message or background chaos may dominate the output of the current modulated external cavity laser.

Region III: For message frequencies applied close to local minima in the average chaotic background noise, at high modulation depths the message is large enough to dominate over the corresponding chaotic background noise and the overall modulation response follows that of the solitary laser. Messages applied to the ECL close to local maxima in the average chaotic background noise have additional power due to constructive interference via optical feedback from the external mirror.

For a message to appear consistently in amplitude in the time domain it must be applied with a modulation depth sufficient to allow its spectral power to dominate over that of the fluctuating chaotic carrier. If the message is to be effectively applied it is not effectively masked by the background chaos.

4.7 Bibliography

[1] L M Pecora and T L Carroll, "Synchronization in chaotic systems," *Phys. Rev. Lett.*, vol. 64, no. 8, pp. 821-824, 1990.

[2] K M Cuomo and A V Oppenheim, "Circuit implementation of synchronized chaos with applications to communications," *Phys. Rev. Lett.*, vol. 71, no. 1, pp. 65-68, July 1993.

[3] J-P Goedgebuer, L Larger, and H Porte, "Optical Cryptosystem Based on Synchronization of Hyperchaos Generated by a Delayed Feedback Tunable Laser Diode," *Phys. Rev. Lett.*, vol. 80, no. 10, pp. 2249-2252, March 1998.

[4] S Hayes, C Grebogi, and E Ott, "Communicating with chaos," *Phys. Rev. Lett.*, vol. 70, no. 20, pp. 3031-3034, 1993.

[5] A Sanchez-Diaz, C Mirasso, P Colet, and P Garcia-Fernandez, "Encoded Gbit/s digital communications with synchronized chaotic semiconductor lasers," *IEEE J. Quant. Electron.*, vol. 35, pp. 292-297, 1999.

[6] S Sivaprakasam and K A Shore, "Message encoding and decoding using chaotic external-cavity diode lasers," *IEEE J. Quant. Electron.*, vol. 36, pp. 35-39, 2000.

[7] A Murakami and K A Shore, "Chaos-pass filtering in injection-locked semiconductor lasers," *Phys. Rev. A*, vol. 72, no. 5, p. 053810, 2005.

[8] J Paul, M W Lee, and K A Shore, "Effect of chaos pass filtering on message decoding quality using chaotic external-cavity laser diodes," *Opt. Lett.*, vol. 29, pp. 2497-2499, 2004.

[9] A Murakami and K A Shore, "Analogy between optically driven injection-locked laser diodes and driven damped linear oscillators," *Phys Rev A*, vol. 73, p. 043804, 2006.

Chapter 5

Chaos Communications System

5.1 Introduction

There has been a considerable amount of work devoted to developing a secure optical communication system based on masking data within the chaotic dynamics of a semiconductor laser [1-3]. In order to extract the message from the chaotic optical carrier wave it is essential that the chaotic dynamics are accurately reproduced in the receiver. This can be achieved by synchronizing the dynamics of the receiver (slave) laser diode to the chaotic dynamics of the external cavity laser (ECL) transmitter (master), as discussed in Chapters 2 and 3. This synchronization process can be achieved by injecting an appropriate amount of the signal from the transmitter into the receiver, in doing so the receiver laser preferentially locks to the chaotic dynamics of the transmitter laser only. By then comparing the transmitter and receiver signals it is possible to extract the message. This message extraction process is commonly referred to as 'Chaos Pass Filtering' (CPF) and has been subject of some discussion [4-6]. The term Chaos Pass Filtering has been widely adopted as a convenient shorthand notation for the message extraction process used in both experimental and theoretical studies of

secure communications schemes. It should be borne in mind that CPF is merely a convenient label for a process which is not well understood.

This chapter builds upon the investigation of sinusoidal current modulation of the transmitter (master) laser by introducing a receiver laser that is subject to optical injection from the current modulated transmitter laser, Figure 5.1.

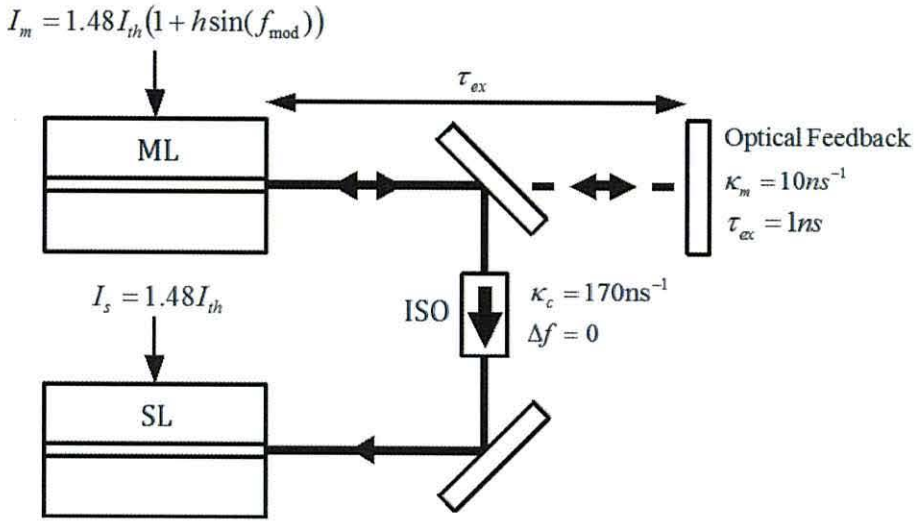

Figure 5.1. Schematic of the transmitter (ML) and receiver (SL) laser configuration. Transmitter

message is only reliably extractable for high modulation depths, Region III, the message is unmasked and the security of the transmitted message is poor.

Murakami's investigation of CPF, [5], suggests that the optical modulation response of the receiver laser is independent of the modulation depth. It will be shown that this is only true for high modulation depths where the message dominates the corresponding chaotic spectral power. The investigation into lower modulation depths presented in this chapter shows that the message and chaotic power generated by the optical feedback interact and hinder the extraction of low power messages.

In the transmitter it is the current modulation response which is of importance, however, in the receiver it is the optical modulation response that is of interest. The two types of modulation response have different characteristics and the aim here is to determine how these differences affect the extraction of the message via chaos pass filtering.

5.2 Review of Numerical Model

The semiconductor laser diode dynamics are again modelled using an enhanced form of the Lang-Kobayashi [7] rate equations, as described in Chapter 2 and replicated below,

$$\frac{dE_m(t)}{dt} = \frac{1}{2}(1+i\alpha)\left[G_m(t) - \frac{1}{\tau_P}\right]E_m(t) + \kappa_m E_m(t-\tau_{ex,m})e^{-i\omega_m\tau_{ex,m}} \quad 5.1$$

$$\frac{dE_s(t)}{dt} = \frac{1}{2}(1+i\alpha)\left[G_s(t) - \frac{1}{\tau_P}\right]E_s(t) + \kappa_s E_s(t-\tau_{ex,s})e^{-i\omega_s\tau_{ex,s}} + \kappa_c E_m(t)e^{i\Delta\omega t} \quad 5.2$$

$$\frac{dN_{m,s}(t)}{dt} = \frac{I_{m,s}}{e} - \frac{N_{m,s}(t)}{\tau_N} - G_{m,s}(t)\left|E_{m,s}(t)\right|^2 \quad 5.3$$

$$G_{m,s}(t) = \frac{g_0(N_{m,s}(t) - N_0)}{1 + \varepsilon\left|Em,s(t)\right|^2} \quad 5.4$$

The transmitter (receiver) laser optical intensity $P_m(t)$ $(P_m(t))$ is related to the electric field $E_{m,s}(t)$ via the relation,

$$P_{m,s}(t) = \left(\frac{\hbar\omega_{m,s}}{\tau_P}\right)\left|E_{m,s}(t)\right|^2 \quad 5.5$$

The transmitter laser drive current is modulated with simple sinusoidal messages with frequency f_{mod} and modulation depth h,

$$I_m = 1.48I_{th}\left(1 + h\sin(f_{\text{mod}})\right) \quad 5.6$$

The message is extracted in the receiver by subtraction of the optical intensity dynamics of the receiver from the transmitted dynamics $P_{m-s}(t)$,

$$P_{m-s}(t) = P_m(t) - P_s(t) \tag{5.7}$$

The complex Fast Fourier Transform (FFT) of the transmitter laser optical intensity $\Im[P_m(t)]$ provides a magnitude and phase, A_m and φ_m respectively,

$$\Im[P_m(t)] = A_m(f)e^{i\varphi_m(f)} \tag{5.8}$$

The receiver laser dynamics are shifted by the optimum time shift τ_{opt} for chaos injection locking synchronization and the FFT then gives,

$$\Im[P_s(t+\tau_{opt})] = A_s(f)e^{i\varphi_s(f)} \tag{5.9}$$

The spectral power of the transmitter and receiver optical intensity output $A_m(f)$ and $A_s(f)$ are used to calculate the optical intensity response gain $H_A(f)$ for the system [5,8] defined as,

$$H_A(f) = 10\log_{10}\frac{A_s(f)}{A_m(f)} \tag{5.10}$$

The transmitter and receiver spectral phases, φ_m and φ_s respectively, are unwrapped and transmitter laser phase lead is determined. The spectral phase difference is defined as,

$$\Delta\varphi = \varphi_m - \varphi_s \tag{5.11}$$

5.3 Numerical Framework

5.3.1 Simulation Parameters

Parameter	Symbol	Value	
Transmitter Drive Current (Un-modulated)	I_m	$1.48I_{th}$	
Transmitter Drive Current (Modulated)	I_m	$1.48I_{th}(1+h\sin(f_{\mathrm{mod}}))$	
Modulation Frequency	f_{mod}	0.02GHz – 20GHz	
Modulation Depth	h	0.03% – 20%	
Receiver Drive Current	I_s	$1.48I_{th}$	
Receiver Laser Injection Rate	κ_c	$170\mathrm{ns}^{-1}$	
Receiver Laser Detuning Frequency	Δf	0	
Transmitter Laser Feedback Rate	κ_m	**No Feedback**	**ECL**
		0	$10\mathrm{ns}^{-1}$
Transmitter Laser External Cavity Round Trip Time	τ_{ex}	1ns	
Receiver Laser Feedback Rate	κ_s	0	

Table 5.1. Parameter set used in the numerical simulation.

The same open-loop transmitter (master) – receiver (slave) laser configuration is assumed as that outlined in Chapters 2 and 3 and is illustrated in Figure 5.1. The difference here is that a message is now applied to the transmitter laser drive current,

Eqn. 5.6, as in Chapter 4. In order to determine the full system modulation response two cases will be considered

A baseline result will be obtained assuming the transmitter laser has no external optical feedback ($\kappa_m = 0$) as a precursor to simulating a transmitter subject to optical feedback from an external mirror (ECL) with feedback rate $\kappa_m = 10\text{ns}^{-1}$ and external cavity round trip time $\tau_{ex} = 1\text{ns}$.

Each combination of optical modulation depth, h, and frequency, f_{mod}, is applied separately and the average response calculated from 50 simulations, each with different initial conditions. The modulation frequency is swept through 525 steps from 0.02GHz to 20GHz and ten modulation depths ranging from $h = 0.03\%$ to $h = 20\%$. The transmitter and receiver laser output characteristic for a single modulation depth is therefore created from 26250 individual simulations. The average response gives the overall long-term spectral characteristic of the system. The modulation depth is not increased beyond $h = 20\%$ to ensure that the applied drive current does not fall below the threshold current.

For all the simulations the receiver laser drive current will remain constant $I_s = 1.48I_{th}$ and coupling parameters of $\kappa_c = 170\text{ns}^{-1}$ and $\Delta f = 0$ will be used to ensure good quality injection locking synchronization. The optical intensity correlation for chaos synchronization, with no message applied, is $C_P = 0.989$ with optimum time shift $\tau_{ex} = 0$.

5.4 Optical Modulation Response

5.4.1 Simulation Results - Transmitter and Receiver

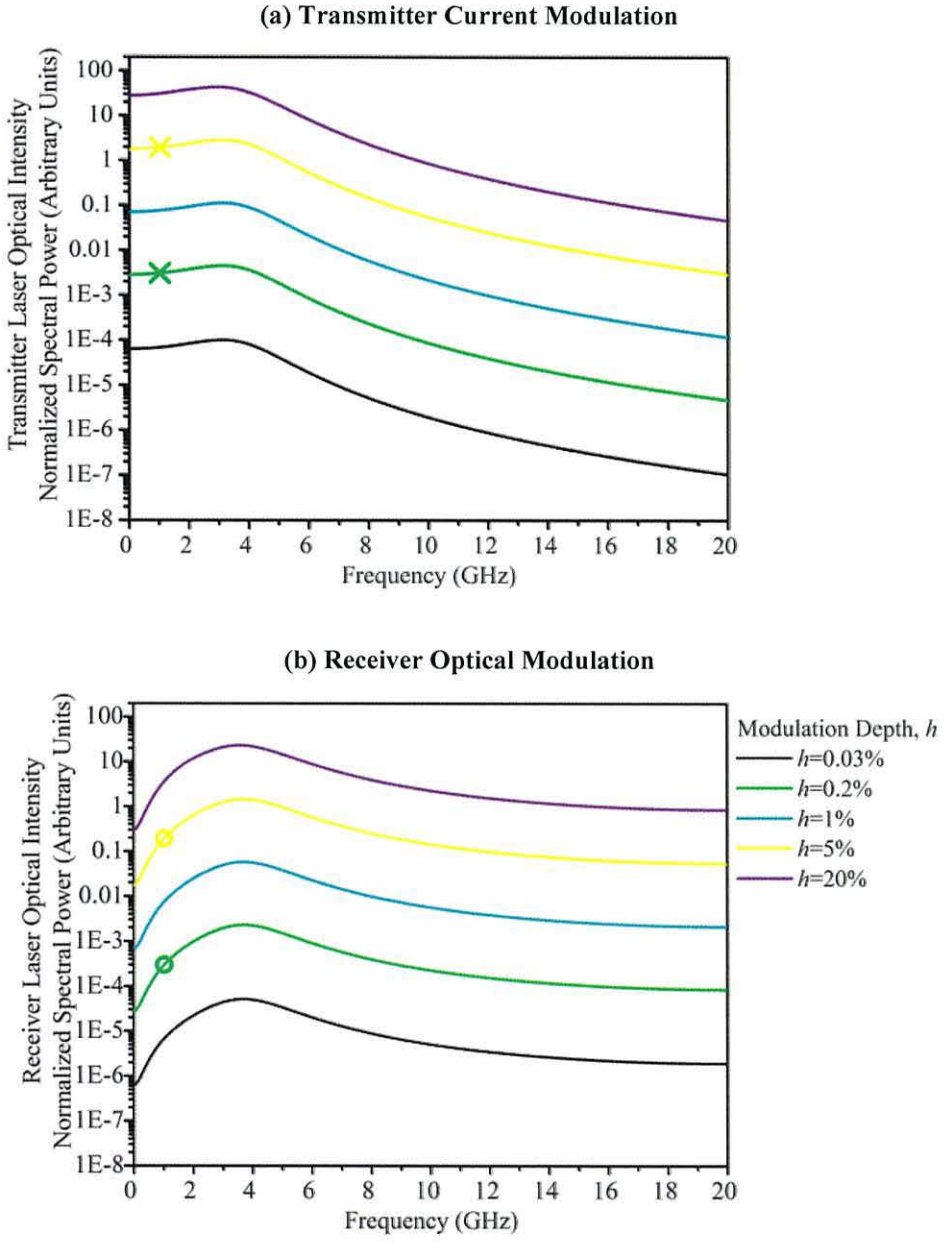

Figure 5.2. Optical intensity output spectra of Transmitter with no optical feedback (a) and Receiver (b) laser diodes for current modulated transmitter laser. Modulation depths: *h = 0.03%* (black line), *h = 0.2%* (green line), *h = 1%* (cyan line), *h = 5%* (yellow line), *h = 20%* (purple line).

Chapter 5 – Chaos Communications System

The current modulation response of a solitary laser has previously been determined, Chapter 4 and is reproduced here in Figure 5.2 (a). The receiver optical modulation response to the current modulated output of the transmitter is shown in Figure 5.2 (b).

The maximum spectral power in the current (Figure 5.2 (a)) and optical (Figure 5.2 (b)) modulation characteristic is close to the solitary laser relaxation oscillation frequency, $f_{relax} = 3.85\text{GHz}$. However, the current and optical modulation characteristic profiles are significantly different. The spectral power of the current modulation response drops off rapidly for frequencies above the relaxation oscillation frequency, Figure 5.2 (a), whereas, the spectral power of the optical modulation response drops off most rapidly for frequencies below the relaxation oscillation frequency, Figure 5.2 (b).

It is this difference in the current and optical modulation response that allows the extraction of the message via chaos pass filtering. The frequency dependent gain or attenuation of the message in the receiver laser allows the message to be extracted from the well synchronized background chaotic noise. This work essentially provides a baseline for future comparisons with the system of current modulated ECL and receiver laser.

5.4.2 Simulation Results - Response Gain and Phase Lead

(a) Optical Intensity Response Gain

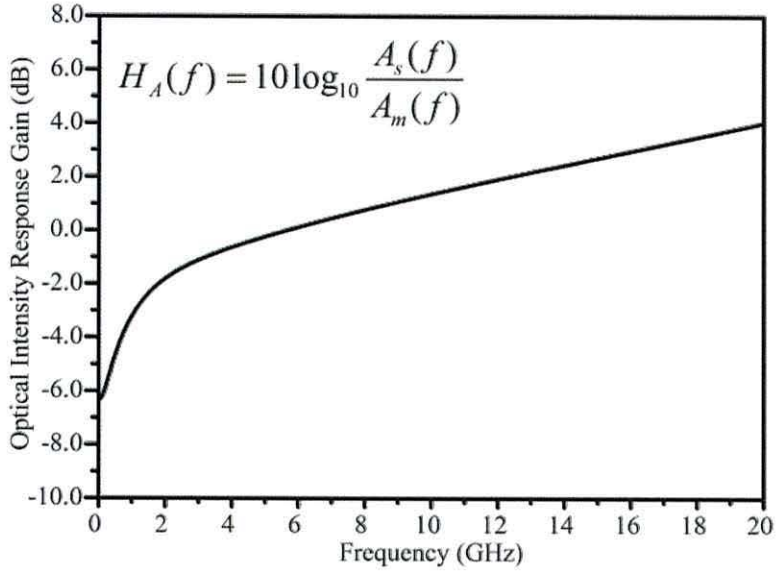

(b) Transmitter Phase Lead

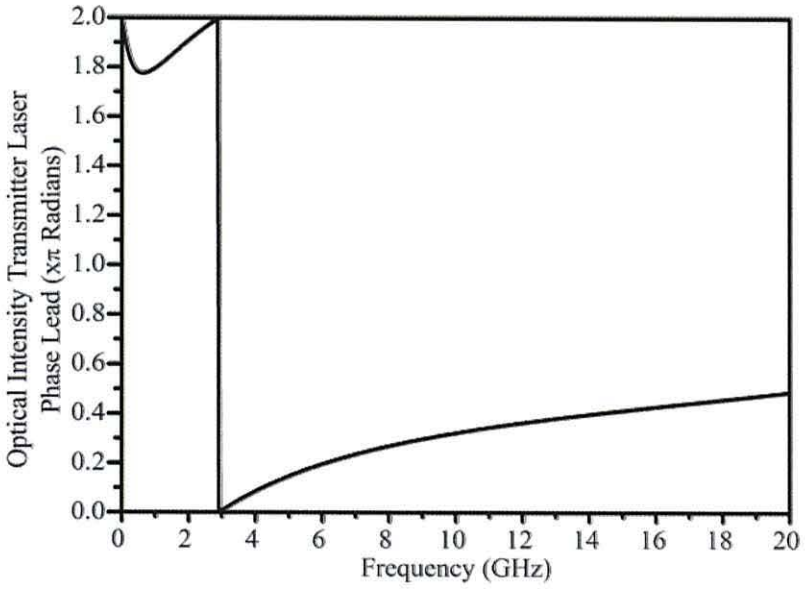

Figure 5.3. Optical intensity response gain (a) and transmitter laser phase lead (b) for transmitter laser current modulation. The receiver laser injection rate is $\kappa_c = 170\text{ns}^{-1}$.

The optical intensity response gain, (Eqn. 10), is calculated for the system using the current and optical modulation characteristics shown in Figure 5.2 (a) and (b) respectively. The response gain profiles for current modulation of the transmitter laser without external feedback are identical for every modulation depth ($h = 0.03\% - 20\%$) simulated. The response gain for $h = 5\%$ is given Figure 5.3, where signal attenuation (gain) is observed for frequencies below (above) the relaxation oscillation frequency.

Figure 5.3 (b) presents the transmitter laser phase lead at the message frequency. Very little phase difference between the transmitter and receiver lasers is observed close to the relaxation oscillation frequency. For message frequencies below the relaxation oscillation frequency the message in the transmitter laser leads the receiver laser by close to 2π radians. This is actually a large transmitter laser phase lead rather than a small receiver laser phase lead, since it is impossible for the receiver to anticipate the transmitted message. An increasing transmitter laser phase lead is observed for frequencies above the relaxation oscillation frequency. Figure 5.3 (b) indicates that the maximum phase distortion for a broad band message is 0.7π radians.

5.5 External Cavity Laser Transmitter

The transmitter laser is now subject to external optical feedback from an external mirror. The optical feedback creates a chaotic output that is injected into the receiver laser and the chaotic dynamics are synchronized. The ECL transmitter laser feedback rate, external cavity round trip time and the receiver laser coupling parameters, injection rate and detuning frequency are the same as those used in Chapters 2 and 3.

5.5.1 Single Simulation - Optical Spectral Power

The current modulated transmitter ECL and receiver laser optical intensity spectra are given by the black and red lines respectively in Figure 5.4 (a) for weak modulation, $h = 0.2\%$, of the 1GHz message. The transmitter ECL and receiver laser spectra are presented in Figure 5.4 (b) for strong modulation, $h = 5\%$. The transmitter (cross) and receiver (circle) laser spectral power for the current modulated transmitter laser without optical feedback is superimposed for comparison in Figure 5.4 (a) and (b) by green and yellow points respectively. These points correspond to the matching points in Figure 5.2.

For weak modulation, $h = 0.2\%$, the transmitter laser spectral power at the message frequency (Figure 5.4 (a) – black line) is close to the power of the neighbouring chaotic background . The background chaos at the message frequency is approximately one order of magnitude larger than the transmitter laser with no optical feedback (Figure 5.4 (a) – green cross). The background chaotic noise dominates under these conditions.

(a) Weak Modulation - $h = 0.2\%$

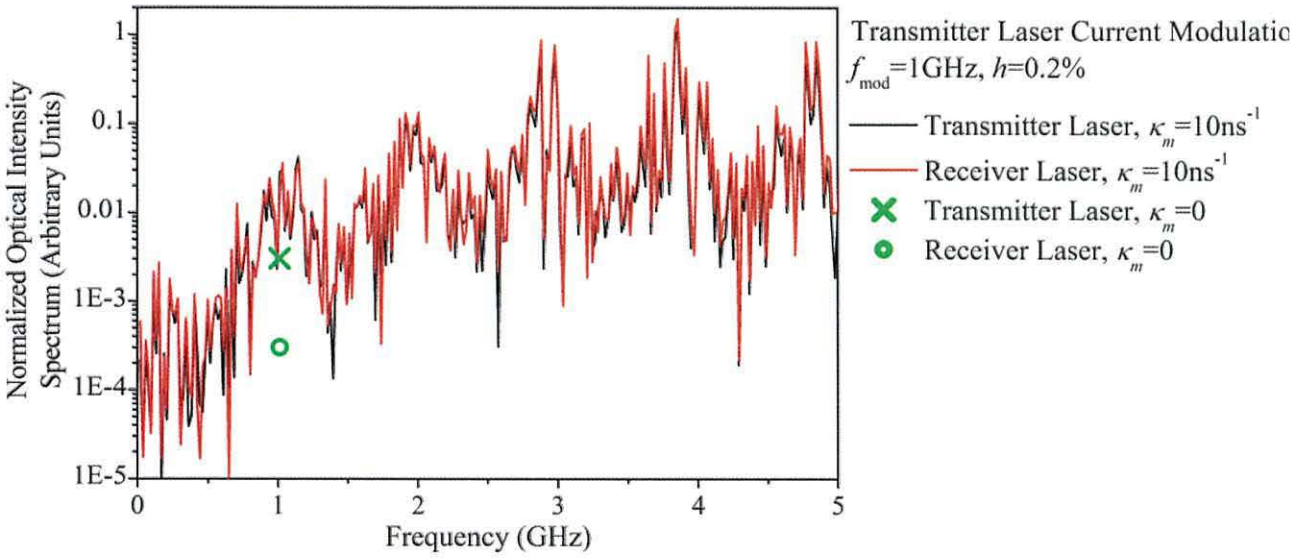

(b) Strong Modulation - $h = 5\%$

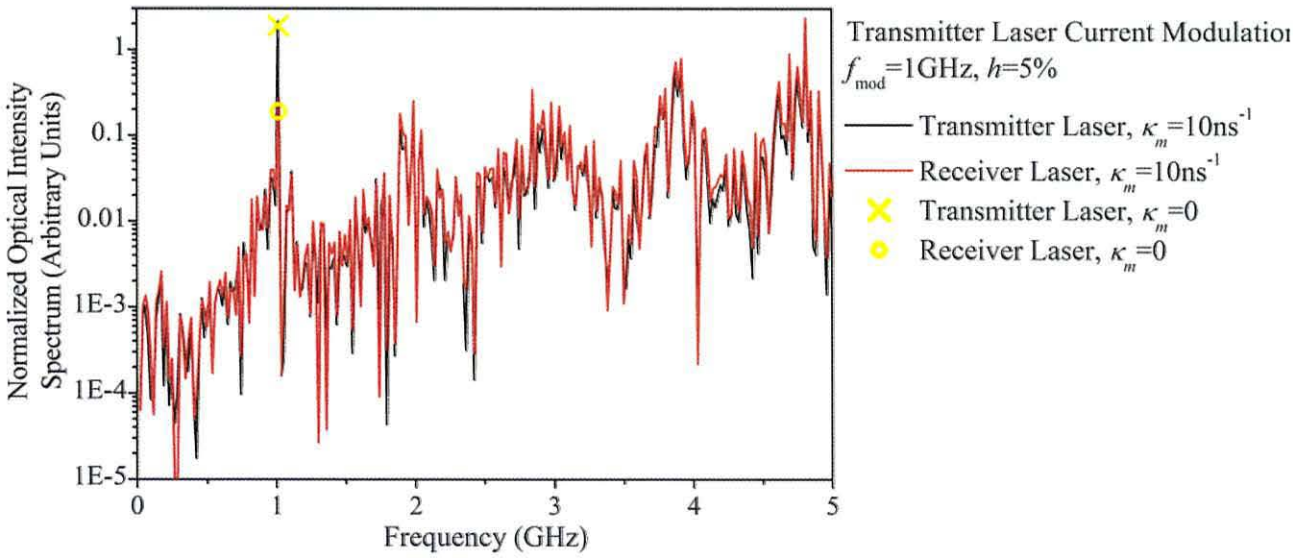

Figure 5.4. Transmitter (black) and receiver (red) laser optical intensity spectra for a single simulation with weak (a - $h = 0.2\%$) and strongly (b - $h = 5\%$) applied 1GHz sinusoidal message.

The receiver laser spectral power at the message frequency (Figure 5.4 (a) – red line) for weak modulation is comparable to the power of the background chaos and the transmitted power (Figure 5.4 (a) – red line). The receiver is synchronized to the chaotic dynamics of the transmitter and not the message. It is therefore reasonable to expect that message extraction would be impossible via chaos pass filtering.

The spectral power of the ECL transmitter for the strong modulation, $h = 5\%$, (Figure 5.4 (b), black line) is considerably larger (approximately two orders of magnitude) than the neighbouring spectral components of the background chaos. The ECL transmitter spectral power (Figure 5.4 (b), black line) at the message frequency is now essentially the same as for the transmitter without optical feedback (Figure 5.4 (b) – yellow cross). This is because the message power now dominates over the background chaos component in the ECL transmitter output. The small power increase in the ECL case is due to constructive interference of the optical feedback.

In Figure 5.4 (b) the spectral power of the message in the receiver is comparable to the modulated transmitter with (red line) and without optical feedback (yellow circle). This is because the message component dominates over the background chaos in the transmitter output. The message is attenuated in the receiver laser, Figure 5.4 (b), and therefore it is reasonable to assume the message would be easily extracted via chaos pass filtering. However, the message is clearly visible in the output spectrum of the ECL with strong current modulation (Figure 5.4 (b), black line) indicating that the message is not masked by the chaos.

5.5.2 Single Simulation - Transmitter Optical Intensity

(a) Weak Modulation - $h = 0.2\%$

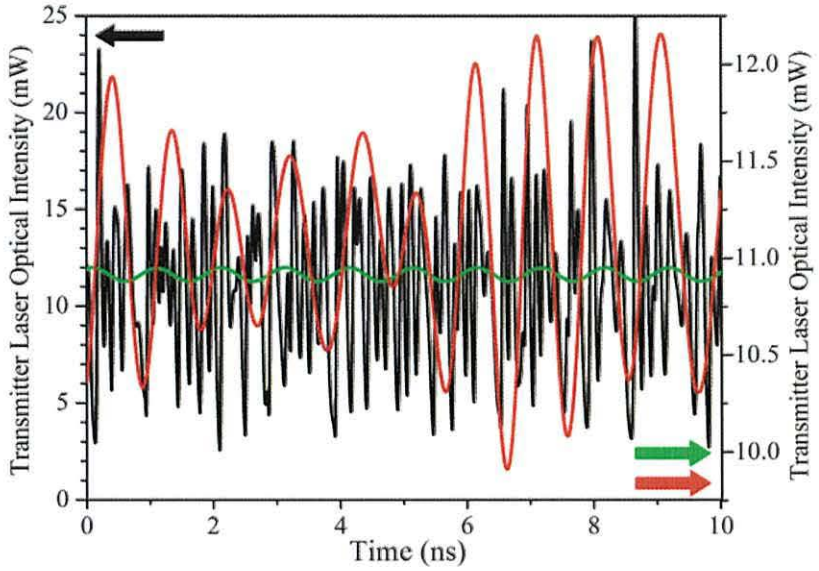

(b) Strong Modulation - $h = 5\%$

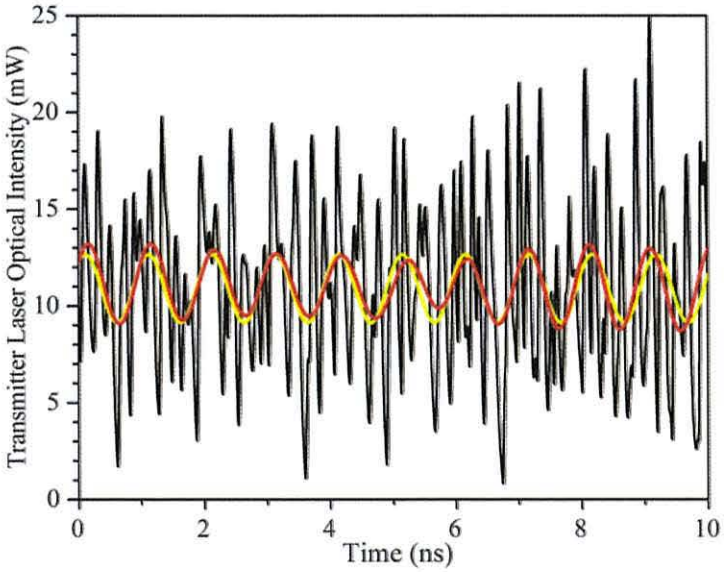

Figure 5.5. Current modulated transmitter laser output with (black line) and without (a – green, b - yellow) optical feedback. 1.25GHz low pass filter of modulated chaotic output (red line).

Chapter 5 – Chaos Communications System

The temporal dynamics of the optical intensity of current modulated ECL will now be compared to the current modulated transmitter laser without optical feedback. The ECL is current modulated with a 1GHz message and the optical intensity output is shown as the black lines in Figure 5.5 (a) and (b) for weak $(h = 0.2\%)$ and strong modulation $(h = 5\%)$ respectively.

The optical intensity of the current modulated ECL is post-processed with a first-order low-pass filter with cut-off frequency $f_{cut-off} = 1.25\text{GHz}$ to see if simple filtering can extract the message. The output of the low-pass filter for the current modulated ECL is given by the red lines in Figure 5.5 (a) and (b) for weak $(h = 0.2\%)$ and strong modulation $(h = 5\%)$ respectively. The optical intensity of the current modulated ECL without optical feedback is also presented in Figure 5.5 (a) and (b) by the green and yellow lines for weak and strong modulation respectively.

For weak modulation the message is not evident within the background chaotic noise (black line, Figure 5.5 (a)). Fluctuations of greater amplitude are observed at the message frequency (Figure 5.5 (a), red line) than for the transmitter without optical feedback (Figure 5.5 (a), green line). This shows that the chaotic background component in the ECL dominates the weakly $(h = 0.2\%)$ applied message. If the ECL transmitter is not modulated, the low-pass filtered output is essentially the same as the red line in Figure 5.5 (a). This indicates that the current modulation is not apparent in the chaotic dynamics of the ECL. Under these conditions the message is securely

masked and cannot be extracted by a naive eavesdropper filtering the output. However, it is not clear whether chaos pass filtering can extract the message either.

The result of the low pass filter of the ECL transmitter optical intensity (red line, Figure 5.5 (a)) for the stronger modulation $h = 5\%$ closely follows the output dynamics of the transmitter laser when not subject to optical feedback (yellow line, Figure 5.5 (a)). The filtered output shows a consistent amplitude and phase across the 10ns time range and closely matches the applied message and output of the transmitter laser without optical feedback. This shows the background chaos component is insufficient to mask the message at the stronger modulation depth. However, this also means that there is a possibility that the simple message applied here may be successfully extracted by a naive eavesdropper as predicted in the frequency domain, Figure 5.4 (b).

5.5.3 Optical Intensity Response Gain

(a) Weak Modulation - $h = 0.2\%$

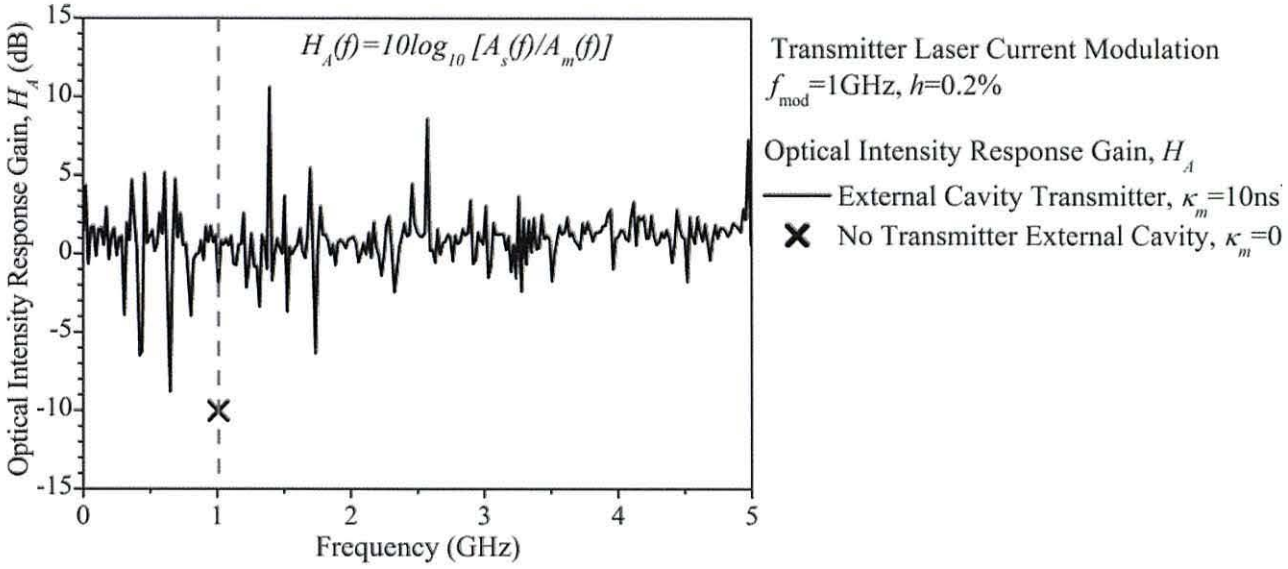

(b) Strong Modulation - $h = 5\%$

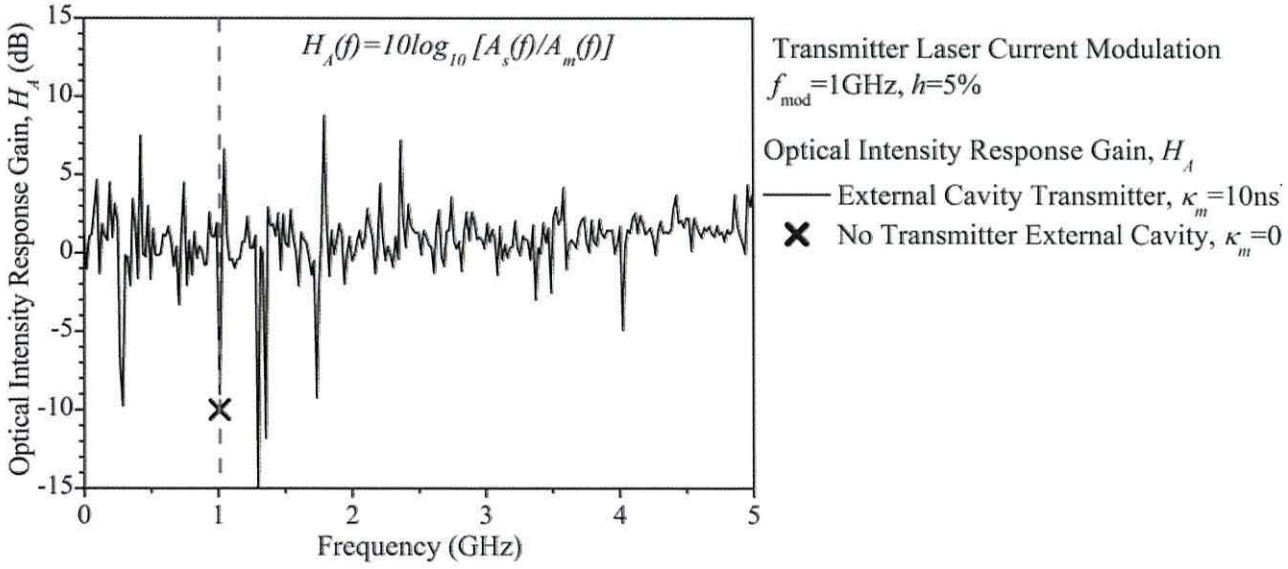

Figure 5.6. Response gain for ECL transmitter modulated with a 1GHz message and (a) – weak modulation, $h = 0.2\%$ (b) – strong modulation, $h = 5\%$.

The optical intensity response gain, calculated using (5.10), for the weak $(h = 0.2\%)$ and strong $(h = 5\%)$ modulation of the 1GHz message is given by the black lines in Figure 5.6 (a) and (b) respectively. The spectral component corresponding to the message is highlighted by the superimposed grey dashed vertical line. The response gain for the case of the current modulated transmitter laser without optical feedback is indicated by the black cross in Figure 5.6 (a) and (b) and corresponds to the same point on the solid line of Figure 5.3 (a).

The response gain at the message frequency for weak current modulation of the ECL (Figure 5.6 (a), black line) is very close to that of the surrounding background chaos. This is to be expected since the transmitted message power was undistinguishable from the background chaos in Figure 5.4 (a). The spectral power at the message is dominated by the chaotic component and there is a significant 8dB difference in the response gain of the transmitter laser with and without external feedback (Figure 5.6 (a), black cross). This indicates that the weakly applied message will not be successfully extracted via subtraction of the optical intensity dynamics in the receiver laser.

The stronger modulation $h = 5\%$ provides sufficient power to dominate over the background chaos of the transmitter laser, Figure 5.4 (b). This means the chaotic spectral component at the message frequency is insignificant and the response gain is very close to that for the modulated transmitter laser without optical feedback, (Figure 5.6 (b), black cross). The chaotic amplitude fluctuations are negligible and the message is predicted to be easily extracted from the background chaotic in the receiver laser.

The largest chaotic fluctuations in the response gain, Figure 5.6, correspond to very low power chaotic components and hence do not have a significant impact upon the extraction process, as described in Chapter 3.

The extraction of the message via subtraction of the optical intensity in the time domain is studied in the following section in order to confirm the observations and predictions of the frequency domain discussed above.

5.5.4 Message Extraction

(a) Weak Modulation - $h = 0.2\%$

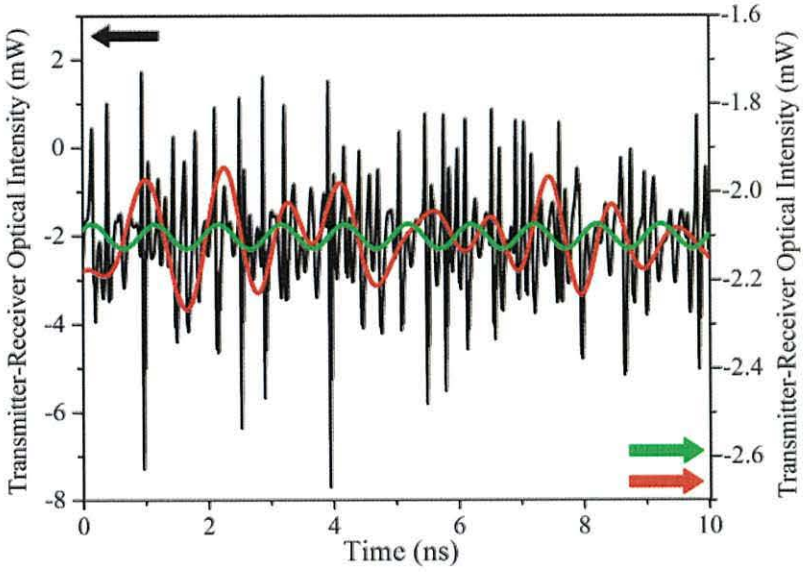

(b) Strong Modulation - $h = 5\%$

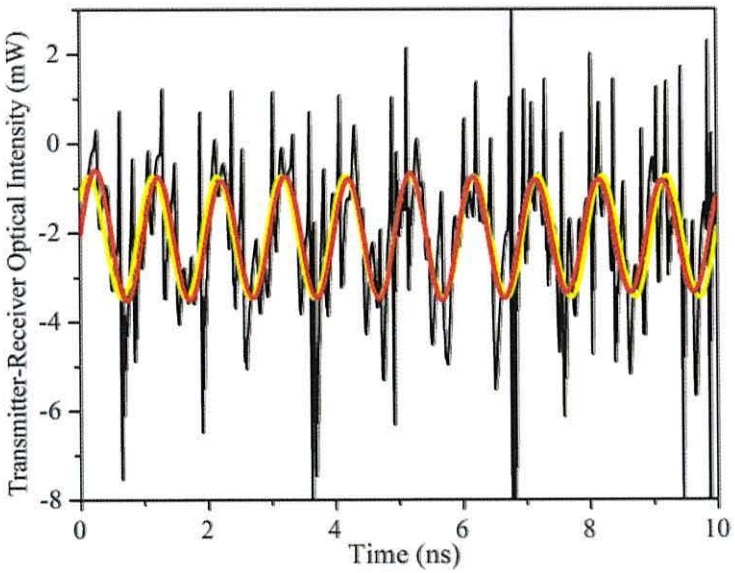

Figure 5.7. Subtraction of ECL transmitter and receiver optical intensities for weak (a - $h = 0.2\%$) and strong (b - $h = 5\%$) modulation of the transmitter laser output with (black line) and without (a – green, b - yellow) optical feedback. The 1.25GHz low pass filter of the subtraction is given by the red line.

The extraction process, (5.7), is examined for the weak $(h = 0.2\%)$ and strong $(h = 5\%)$ application of the 1GHz message to the ECL transmitter drive current. The message is extracted in the receiver laser via subtraction of its optical intensity from the incoming transmitter laser optical intensity. Successful extraction of the message may be defined as a good reproduction of the applied message. For the sinusoidal messages employed here, a constant amplitude and phase is required. The message must be extracted from the optical intensity subtraction, $P_{m-s}(t)$, without prior knowledge of the message.

The subtraction of the receiver laser dynamics from the transmitter laser dynamics is given by the black lines in Figure 5.7 (a) and (b). The message is not evident in the extracted signal for the weakly applied message (Figure 5.7 (a), black line). The strongly applied message is visible in the extracted signal (Figure 5.7 (b), black line) and can then be improved by applying a low-pass filter.

A first order low pass-filter with cut-off frequency, $f_{cut-off} = 1.25\text{GHz}$, is applied to the optical intensity subtraction of the strongly applied message and its output is given by the red line in Figure 5.7 (b). The quality of the extracted 1GHz message is very good with constant amplitude and phase. The extracted message (Figure 5.7 (b), red line) closely follows the extracted message for a transmitter laser without optical feedback (Figure 5.7 (b), yellow line).

The weakly applied message is securely transmitted but cannot be extracted via chaos pass filtering. The low frequency content of the subtraction will now be studied to show

that the background chaos is dominant at the message frequency. A first order low pass-filter with cut-off frequency, $f_{cut-off} = 1.25\text{GHz}$, is applied to the optical intensity subtraction of the weakly applied message and its output is given by the red line in Figure 5.7 (a). The output of the filter can be compared to the extraction from the system employing a transmitter laser without optical feedback, given by the green line in Figure 5.7 (a). Much larger amplitude fluctuations are observed in the filter output for the ECL transmitter system (Figure 5.7 (a), red line) as a result of the background chaos. Hence, the message is not recoverable.

The investigation of single message frequencies presented so far has shown how the frequency domain techniques can be used to give an indication of the security of the transmission and the quality of extraction. This will now be extended to a large range of frequencies and modulation depths.

5.6 Average Optical Modulation Response

(a) Transmitter

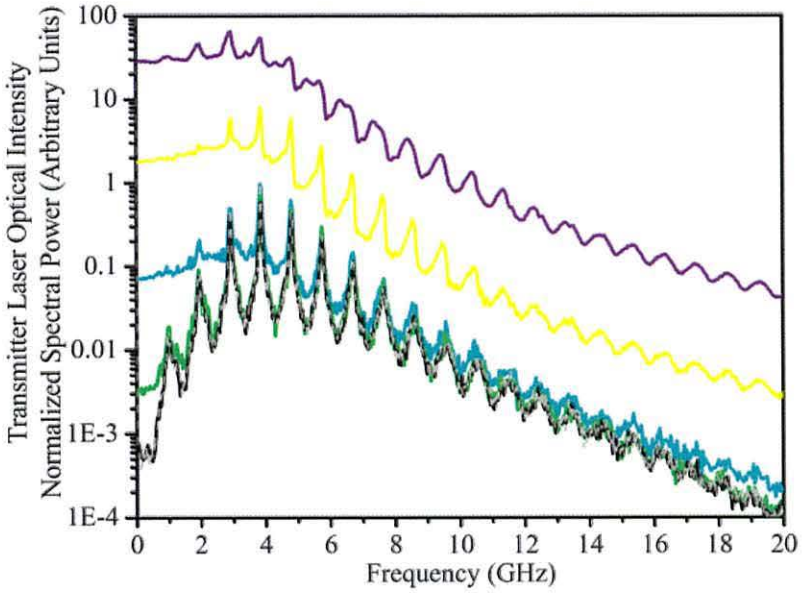

(b) Receiver

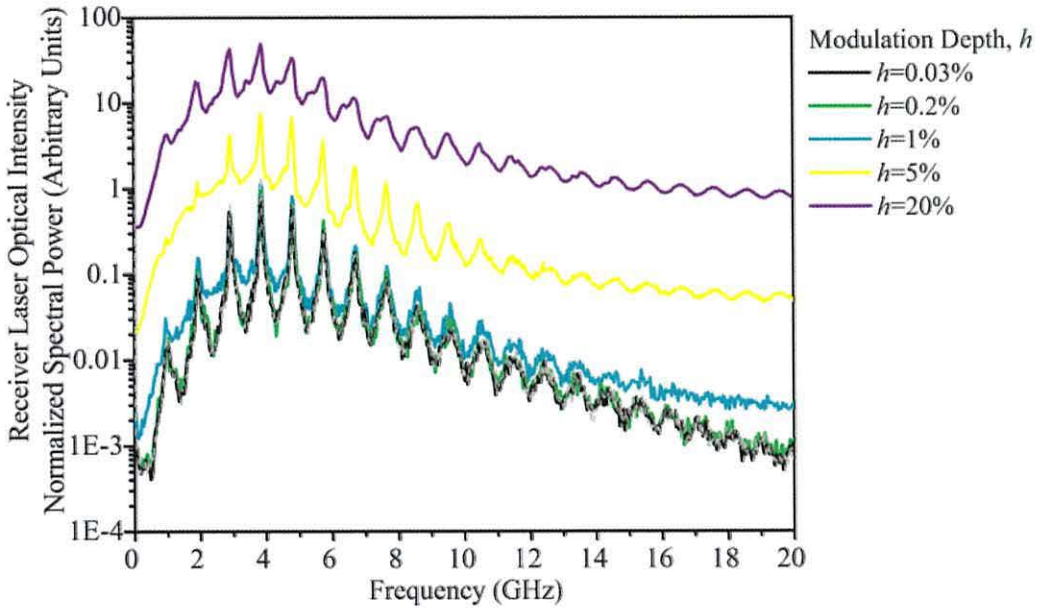

Figure 5.8. Optical intensity spectra of current modulated ECL transmitter (a) and receiver (b). Modulation depths: *h = 0.03%* (black line), *h = 0.2%* (green line), *h = 1%* (cyan line), *h = 5%* (yellow line), *h = 20%* (purple line).

The averaged optical modulation response of the receiver laser will now be presented. The optically injected signal is derived from an ECL transmitter subject to current modulation. The modulation frequency is swept through 525 steps from 0.02GHz to 20GHz and ten modulation depths ranging from $h = 0.03\%$ to $h = 20\%$.

The current modulated ECL transmitter laser optical intensity output characteristic as presented in Chapter 4 are reproduced here, Figure 5.8 (a), for comparison with the receiver laser optical modulation response shown in Figure 5.8 (b).

The modulation depth $h = 0.03\%$ (black line) is indistinguishable from the dominant background chaos (grey line) in both the transmitter and receiver optical intensity.

5.6.1 Response Gain and Transmitter Phase Lead

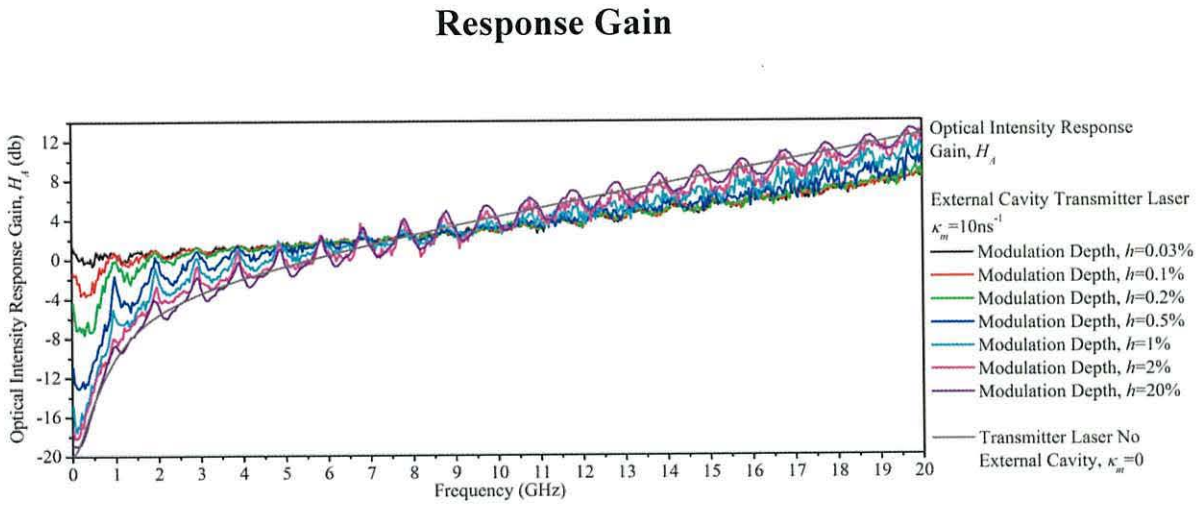

Figure 5.9. Optical intensity response gain for sinusoidal current modulation of ECL transmitter.

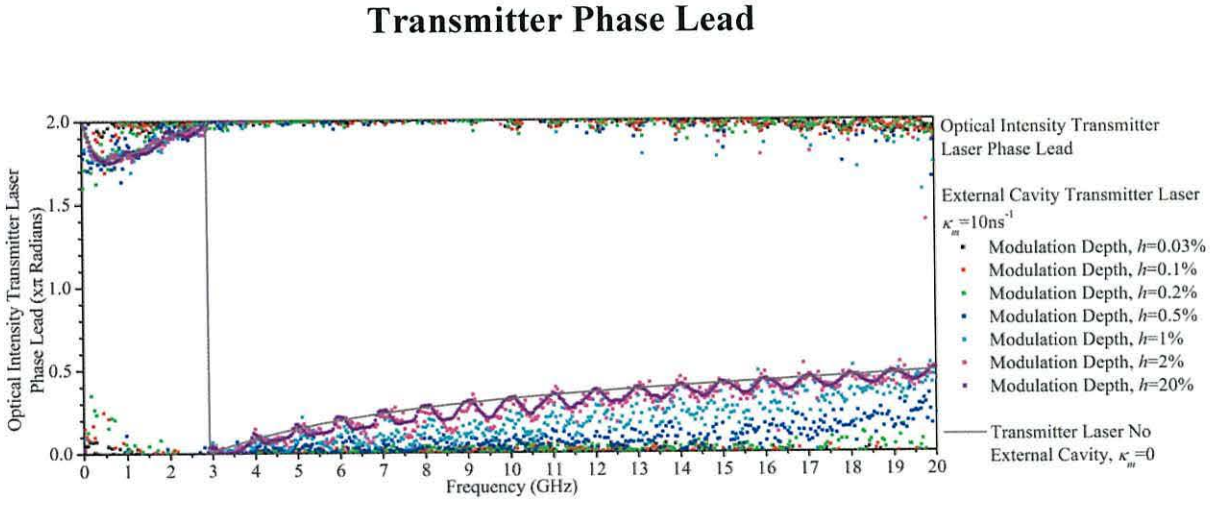

Figure 5.10. Transmitter phase lead at message frequency for sinusoidal current modulation of ECL transmitter.

The transmitter and receiver modulation characteristics, Figure 5.8 (a) and (b), are now used to construct the response gain of the system, Eqn. 5.10, for the range of tested modulation depths. The optical intensity response gain of the receiver laser subject to optical injection from a current modulated ECL transmitter is presented in Figure 5.9. The transmitter laser phase lead is presented in Figure 5.10.

The response gain and transmitter phase lead characteristics for current modulation of the transmitter laser without optical feedback, Figure 5.3, are superimposed as grey lines in Figures 5.9 and 5.10 respectively for comparison.

The response gain and phase lead characteristics of the lowest modulation depth tested $h = 0.03\%$, (Figures 5.9 and 5.10, black line), follow the profile of chaos injection locking synchronization characteristic of the un-modulated ECL transmitter and receiver (Chapter 3, Figure 3.3). This is because the applied message power is very weak and does not have significant effect upon the output.

As the modulation depth is increased, the message power has greater effect upon the output and the response gain and phase lead profiles move towards the expected modulation response, namely, that of the current modulation of the system with a transmitter laser without optical feedback (grey lines, Figures 5.9 and 5.10). The response at the intermediate modulation depths is determined by both the message power and chaotic fluctuations. The message cannot then be reliably extracted as both

the amplitude and phase of the transmitter output can fluctuate significantly and hence at any point in time either the message or background chaos may be dominant.

For the highest modulation depth tested $h = 20\%$ the response gain and phase lead closely follows the characteristics for the system employing current modulation of the transmitter laser without optical feedback. The response gain and phase lead deviate most from the expected modulation characteristic at frequencies close to local maxima in the average background chaos due to constructive interference in the ECL.

The three regions of operation observed above in the response gain will now be compared to the three regions described for modulation of the master laser in Chapter 4 to see if they coincide. The implications on the security of the transmitted message and the possibility of extraction in the receiver will then be discussed.

5.7 Message Security and Extraction

Three regions of operation were identified in Chapter 4 for the current modulation of the ECL drive current.

- Region I: At very low modulation depths the output is dominated by the background chaos. The message component is indistinguishable from the chaotic carrier.
- Region II: For intermediate modulation depths the message power and the background chaos have significant impact upon the output spectral power. The

time varying chaotic component results in time varying spectral power at the message frequency.

- Region III: For very high modulation depths the output power is dominated by the message power. The background chaos is insignificant and the ECL transmitter laser output is very close to that of the transmitter without optical feedback.

The system response gain will be compared to the observations made of the transmitter laser output characteristic and the regions described above. The quality of extraction in the receiver laser can also be related to the degree of security observed in the transmitter laser output spectrum.

The findings of Chapter 4 will now be directly compared with the system response gain for three modulation frequencies. Figure 5.11 (a) presents $f_{\text{mod}} = 1\text{GHz}$, as discussed earlier in Section 5.6, the message frequency coincides with a local maximum in the average background chaos. Figure 5.11 (b) presents $f_{\text{mod}} = 1.4\text{GHz}$ applied at a local minima in the average background chaos. Figure 5.11 (c) presents $f_{\text{mod}} = 2.9\text{GHz}$ which coincides with a high power local maximum in the average background chaos.

The three regions identified in Chapter 4 are denoted by the two vertical dashed lines and the diagonal dashed line denotes the solitary laser modulation response in Figure 5.11. In each case the solid black line denotes the modulation response of the ECL transmitter. The response gain curves (magenta, red, yellow) all show a rapid decrease

in magnitude in Region II and relatively constant values in Regions I and III. Clearly both techniques identify three distinct regions.

Within Region I for low modulation depths the message is effectively masked by the background chaos but cannot be extracted in the receiver laser. In Region II the chaotic fluctuations of the background noise play a significant role in the transmitter output; when the background chaos is low the message can be successfully extracted, however, when the background chaos is high the message is lost and cannot be extracted. In Region III the message power is dominant over the corresponding background chaos component and can be easily extracted in the receiver. However, the dominant message power means that the security of the transmission is compromised and it is possible for an eavesdropper to intercept the message. The message can only be reliably extracted over time if the system is operating in Region III.

In summary, it has been shown that in order to successfully extract the message at the receiver the message power must be dominant over the background chaos. Consequently the message is not effectively masked in the transmitted signal and may be successfully intercepted by an eavesdropper.

(a) – f_{mod}=1GHz - Low chaotic power local maximum

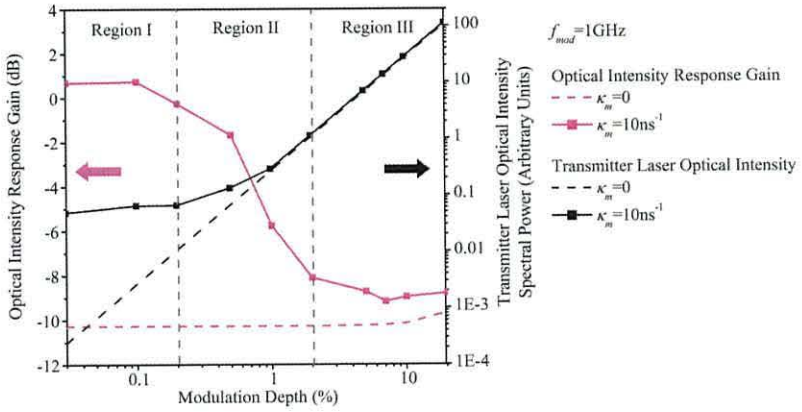

(b) – f_{mod}=1.4GHz - Low chaotic power local minimum

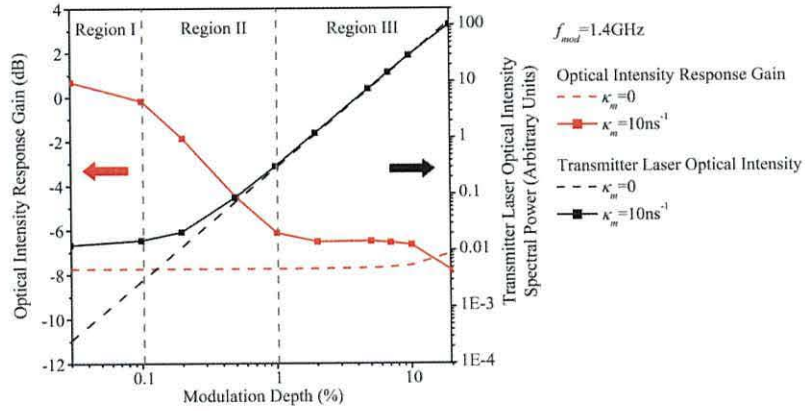

(c) – f_{mod}=2.9GHz - High chaotic power local maximum

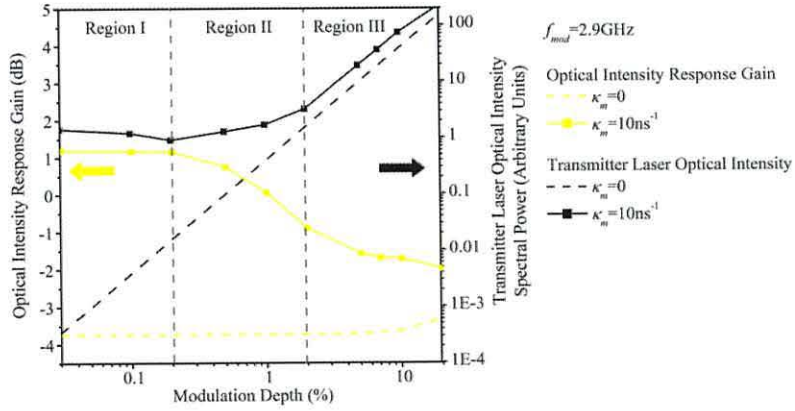

Figure 5.11. Transmitter optical intensity spectral power and system response gain versus modulation depth for sinusoidal current modulation of transmitter with and without optical feedback.

5.8 Conclusions

This investigation has shown that the frequency domain techniques presented provides additional insight into the modulation process. The transmitter laser spectrum shows how well the message is applied to the transmitted optical intensity and the resultant security of the message transmission. The response gain provides a good measure of the message security and the quality of the extraction possible.

Chaos Pass Filtering

The differences in the current and optical modulation responses result in a frequency dependent attenuation or gain. It has already been shown that the important chaotic components are subject to a flat response gain characteristic in the receiver (slave) laser. The frequency dependent attenuation or gain of the transmitter current modulation and the flat chaos response give rise to the chaos pass filtering effect that allows the message to be extracted by subtraction of the transmitter and receiver optical outputs.

Message Security and its Implication for Message Extraction

It has been shown that only messages with a high modulation depth (within Region III) can be reliably extracted in the receiver laser via chaos pass filtering. However, the large spectral power required to dominate over the coincident chaos background spectral power means that there is a possibility of message interception by an eavesdropper. A low power message can be applied and successfully masked amongst the dominant background chaos, but it has been shown that this weak message is also

indistinguishable from the background noise in the receiver and cannot be successfully extracted.

The frequency dependent attenuation and gain, as well as, the phase difference in the recovered message have implications for more complex messages. If a more complex message, consisting of a range of frequencies, is applied the recovered message will be distorted by the chaos pass filtering process.

In the following Chapter a more realistic communications type message made up of a pseudo random bit stream consisting of a range of spectral content will be studied.

5.9 Bibliography

[1] A Argyris et al., "Chaos-based communications at high bit rates using commercial fibre-optic links," *Nature*, vol. 438, pp. 343-346, 2005.

[2] J Ohtsubo, "Chaos synchronization and chaotic signal masking in semiconductor lasers with optical feedback," *IEEE J. Quantum Electron.*, vol. 38, pp. 1141-1154, 2002.

[3] J Paul, M W Lee, and K A Shore, "Effect of chaos pass filtering on message decoding quality using chaotic external-cavity laser diodes," *Opt. Lett.*, vol. 29, pp. 2497-2499, 2004.

[4] I Fischer, Y Liu, and P Davis, "Synchronization of chaotic semiconductor laser dynamics on subnanosecond time scales and its potential for chaos communication," *Phys. Rev. A*, vol. 62, no. 1, p. 011801, June 2000.

[5] A Murakami and A Shore, "Chaos-pass filtering in injection locked semiconductor lasers," *Phys. Rev. A*, vol. 72, p. 053810, 2005.

[6] A Murakami and K A Shore, "Energy transfer and message filtering in chaos communication using injection locked laser diodes," *Int. J. Micro. Opt. Technol.*, vol. 1, pp. 181-187, 2006.

[7] R Lang and K Kobayashi, "External optical feedback effects on semiconductor

injection properties," *IEEE J. Quantum Electron.*, vol. 16, pp. 347-355, 1980.

[8] S J Lea and P S Spencer, "Frequency domain analysis of the chaotic synchronization of injection-locked semiconductor lasers," *J. Opt. Quant. Electron.*

Chapter 6

Pseudo Random Bit Stream Message

6.1 Introduction

The pseudo random current modulation of a single-mode chaotic semiconductor laser was simulated by Mirasso et al in 1993 [1] and pattern effects in the output were investigated. Since then simulation and experimental investigations of a system consisting of chaotic transmitter laser with digital message current modulation and receiver laser have been studied by various groups [2-14].

The chaotic masking of the pseudo random message will be investigated further in this chapter using the time and frequency domain techniques developed in earlier chapters.

6.2 Pseudo Random Bit Sequence Current Modulation

A system consisting of Pseudo Random Bit Sequence (PRBS) current modulated transmitter laser (Tx) with no external feedback whose optical output is injected into the receiver laser (Rx) is presented in Figure 6.1.

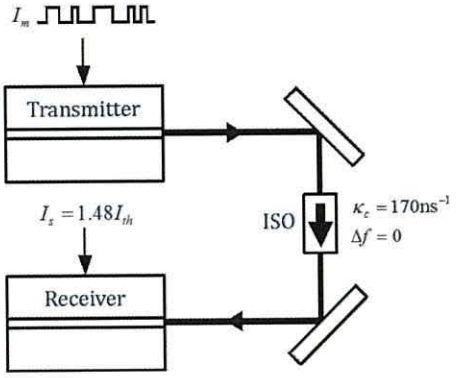

Figure 6.1. Schematic of transmitter laser subject to PRBS current modulation and receiver laser subject to optical injection from the transmitter.

The optical output of the transmitter laser will be studied to determine the accuracy of the message encoded and quality of the message extraction in the receiver laser. This will provide a baseline performance indicator against which sinusoidal modulation (Chapters 4 and 5) and PRBS current modulation of an external cavity transmitter laser (Section 6.3) will be assessed.

6.2.1 Numerical Framework

The PRBS current modulated transmitter output from a single simulation will be investigated with $(\kappa_m = 10\text{ns}^{-1})$ and without $(\kappa_m = 0)$ an external mirror.

The pseudo random bit stream message is created using a shift register technique [15] which allows two different bit rates to be examined in one simulation.

A low bit level (0) is represented by a transmitter drive current of $I_m = 1.48I_{th}$ and a modulation depth, h, is used to represent a high bit level (1). Two modulation depths

are used in the following investigation; a weak modulation of $h = 5\%$ and a strong modulation of $h = 10\%$. Each bit transition occurs instantaneously.

For a modulation depth $h = 5\%$ the message bit rate, R, cannot be increased above $R = 5\text{Gbit/s}$ without compromising the quality of the message encoding. If the bit rate exceeds this maximum limit ($R = 5\text{Gbit/s}$) the steady state value of the optical intensity will not be reached and the message will not be successfully modulated onto the transmitter laser's optical intensity.

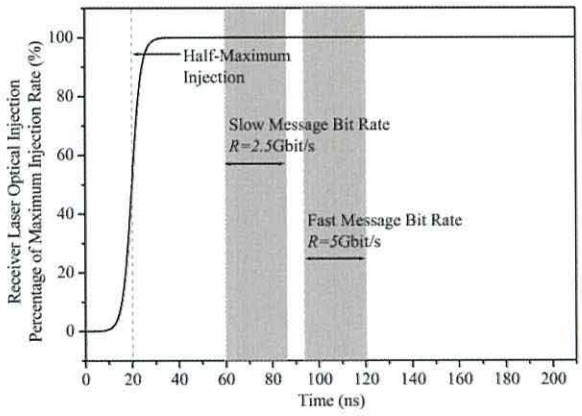

Figure 6.2. Percentage of maximum receiver laser injection rate.

Two time periods of the simulation are studied and these correspond to a slow bit rate, $R = 2.5\text{Gbit/s}$, and a fast bit rate, $R = 5\text{Gbit/s}$. The slow bit rate occurs during the time period 59ns-85ns and the fast bit rate between 94ns-120ns, Figure 6.2. The Fast Fourier Transform window is now reduced to 26ns to allow separate analysis of the slow and fast bit rates.

The slave laser injection rate and detuning frequency are kept constant throughout the simulation and all the other parameters are taken from Table 3.1.

6.2.2 Transmitter PRBS Performance

The optical intensity of the PRBS current modulated transmitter laser (without optical feedback, $\kappa_m = 0$) is given by the black lines in Figures 6.3 and 6.4 for the slow (R = 2.5GBbit/s) and fast (R = 5GBbit/s) bit rate sections of the message respectively. The modulated transmitter injection current is superimposed in Figures 6.3 and 6.4 for comparison.

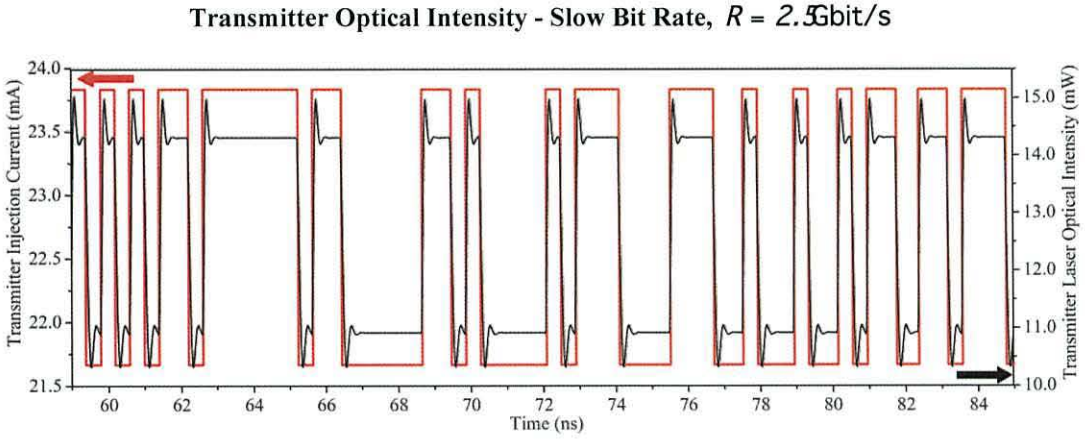

Figure 6.3. Optical intensity (black line) of transmitter laser subject to PRBS current modulation (red line).

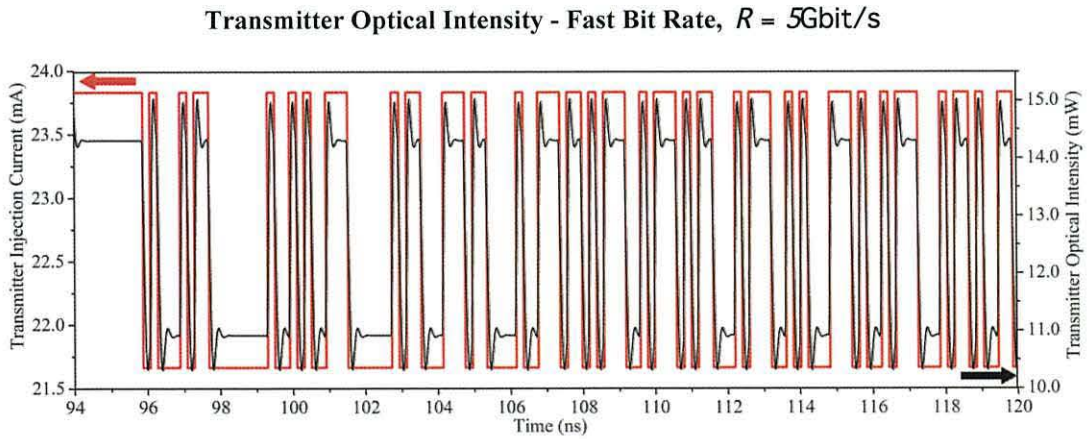

Figure 6.4. Optical intensity (black line) of transmitter laser subject to PRBS current modulation (red line).

The applied message (Figures 6.3 and 6.4, red line) is well reproduced in the optical intensity (Figures 6.3 and 6.4, black line) of the transmitter laser for both slow and fast message bit rates. An overshoot in the optical intensity is observed at each bit transition but this quickly decays to the steady state value optical intensity of a (0) or (1).

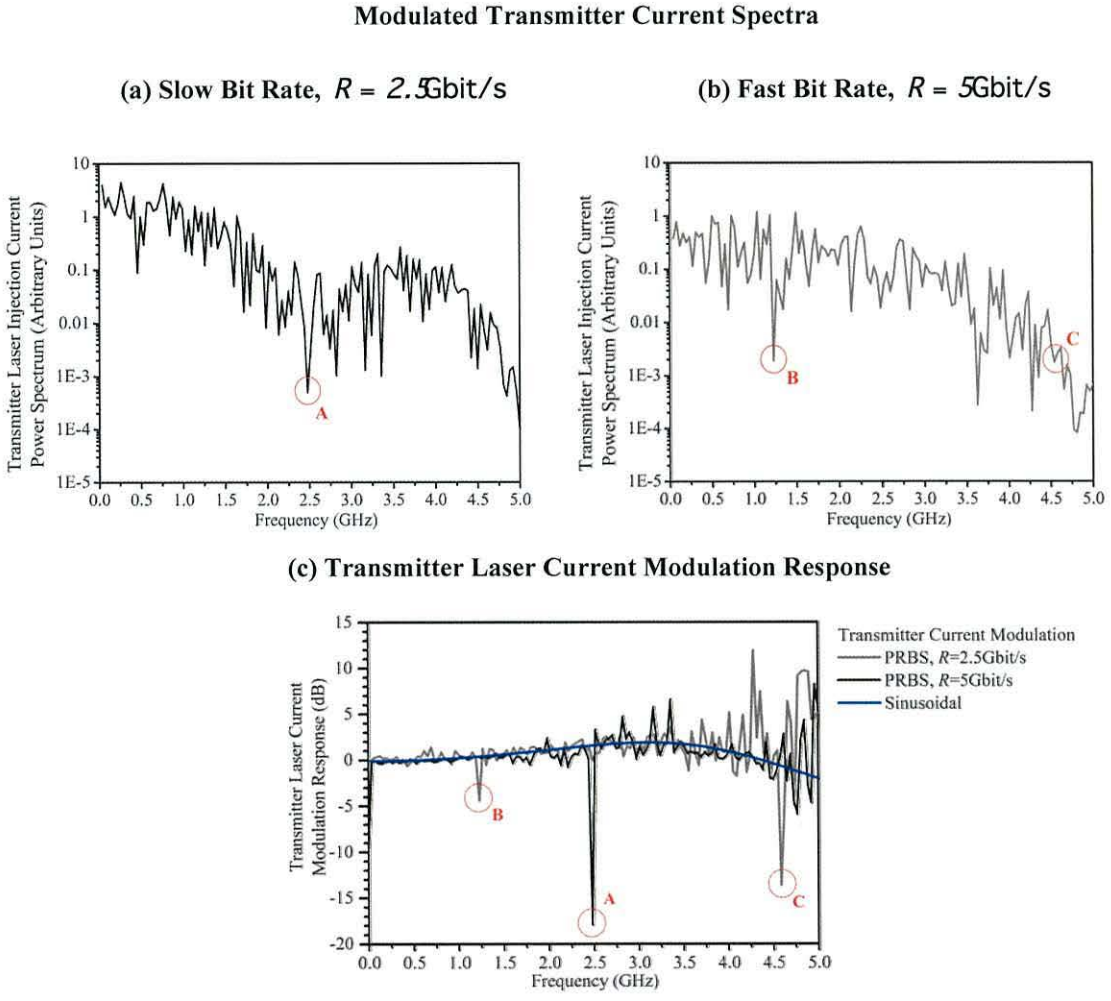

Figure 6.5. Power spectra of PRBS modulated current for slow (a) and high (b) bit rate sections of the message. (c) - Transmitter laser PRBS modulation response (slow (black line) and fast (grey line) bit rates) and sinusoidal modulation response (blue line).

The power spectrum of the modulated drive current (Figures 6.3 and 6.4, red line) is presented in Figure 6.5 (a) and (b) respectively. The modulated drive current spectrum

of the 26ns time period from 59ns to 85ns with message bit rate $R = 2.5\text{Gbit/s}$ is shown by the black line in Figure 6.5 (a) and the time period from 94ns to 120ns with bit rate $R = 5\text{Gbit/s}$ is shown by the grey line in Figure 6.5 (b). Figure 6.5 (a) and (b) show the anticipated *sinc* envelope expected for the square pulse bit rates used with nulls at $f = 2.5\text{GHz}$ $(R = 2.5\text{Gbit/s})$ and $f = 5\text{GHz}$ $(R = 5\text{Gbit/s})$. The longer duration pulses of the lower bit rate $(R = 2.5\text{Gbit/s})$ result in a narrower *sinc* function than that of the higher bit rate $(R = 5\text{Gbit/s})$. The modulation response of the PRBS modulated transmitter will now be compared to that of a sinusoidal modulation.

The transmitter laser response characteristic to the PRBS modulated drive current is given by the black and grey lines in Figure 6.5 (c) for bit rates $R = 2.5\text{Gbit/s}$ (59ns-85ns) and $R = 5\text{Gbit/s}$ (94ns-120ns) respectively. The sinusoidal modulation characteristic of the solitary laser is given by the blue line in Figure 6.5 (c). The optical intensity of the PRBS modulated transmitter (Figure 6.5 (a) and (b)) and sinusoidal modulated transmitter (Chapter 4, Figure 4.3) are normalized to the lowest sinusoidal frequency tested in Chapter 4, $f_{\text{mod}} = 0.02\text{GHz}$ so that the overall characteristics may be compared.

The modulation response characteristic of the PRBS modulated transmitter (Figure 6.5 (c), grey lines) closely follows that for sinusoidal modulation (Figure 6.5 (c), blue line) for the high power message components identified in Figure 6.5 (a) and (b).

The low power spectral components of the message are not well reproduced in the transmitter laser optical intensity; examples are indicated by points A, B, C in Figure

6.5. The indicated spectral components (A, B, C) deviate significantly from the sinusoidal modulation response (Figure 6.5 (c), blue line). These low power spectral components are not well reproduced in the transmitter laser and account for the degradation of the message in the transmitter output seen in Figures 6.3 and 6.4.

6.2.3 Receiver PRBS Response

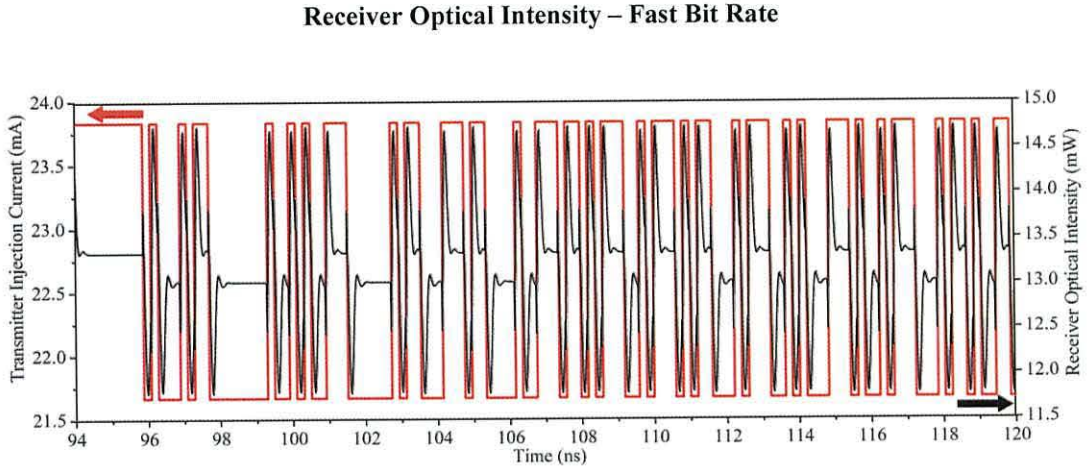

Figure 6.6. Receiver laser optical intensity (black line). Transmitter laser PRBS current modulation (red line), fast bit rate R = 5Gbit/s.

The current modulated transmitter laser optical intensity is now injected into the receiver laser and the quality of the message extraction is examined. The receiver laser is subject to strong injection from the transmitter laser with injection rate $\kappa_c = 170\text{ns}^{-1}$ and zero detuning $\Delta f = 0$. The receiver laser optical intensity is presented for the high bit rate, R = 5Gbit/s, time period 94ns-120ns in Figure 6.6. The bit transitions of the message are observed in the receiver laser optical intensity in Figure 6.6.

A large overshoot in the optical intensity is observed in the receiver, Figure 6.6, at each bit transition as in the transmitter. The matched and damped relaxation oscillation frequency quickly decays to the steady state value. The difference in the optical intensity between low and high bit levels is much smaller in the receiver than in the transmitter but is sufficient to allow very good message extraction via subtraction of the laser output intensities, $P_m(t) - P_s(t)$.

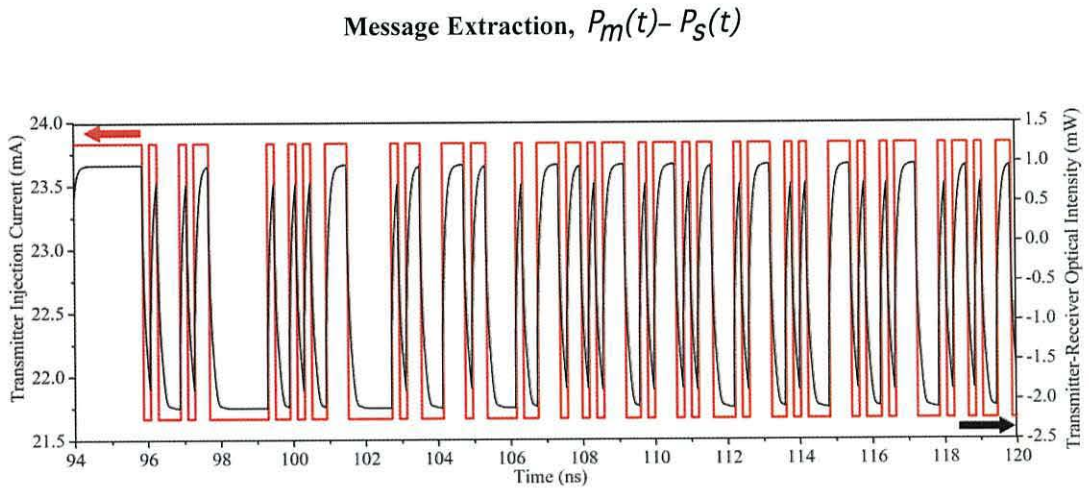

Figure 6.7. Message extraction (black) via subtraction, $P_m(t) - P_s(t)$, in the receiver laser. Transmitter laser PRBS current modulation (red), fast bit rate R = 5Gbit/s.

The optical intensity extraction $P_m(t) - P_s(t)$ in the receiver is presented in Figure 6.7 (black line) and accurately reproduces the message applied at the transmitter (red line). The extraction shows the maximum extraction quality expected. The smoothing of the bit transitions observed in the extracted message, Figure 6.7, is due to two processes. The transmitter distorts the high frequency components of the current modulated

message and the receiver's frequency dependent optical modulation response further distorts the injected signal.

The response gain for the transmitter – receiver system with PRBS current modulation of the transmitter is presented for a single simulation in Figure 6.8 for the two Fast Fourier Transform windows shown in Figure 6.2. The response gain for the slow bit rate, $R = 2.5\text{Gbit/s}$ (59ns-85ns), is given by the black line in Figure 6.8. The grey line in Figure 6.8 gives the response gain for the second Fast Fourier Transform window with message bit rate $R = 5\text{Gbit/s}$, (94ns-120ns). The system response gain for sinusoidal current modulation of the transmitter laser without optical feedback (Chapter 5, Figure 5.3) is also superimposed as the blue line in Figure 6.8. Chaos injection locking with no current modulation (Chapter 3 Figure 3.2(a)) is given by the green line in Figure 6.8.

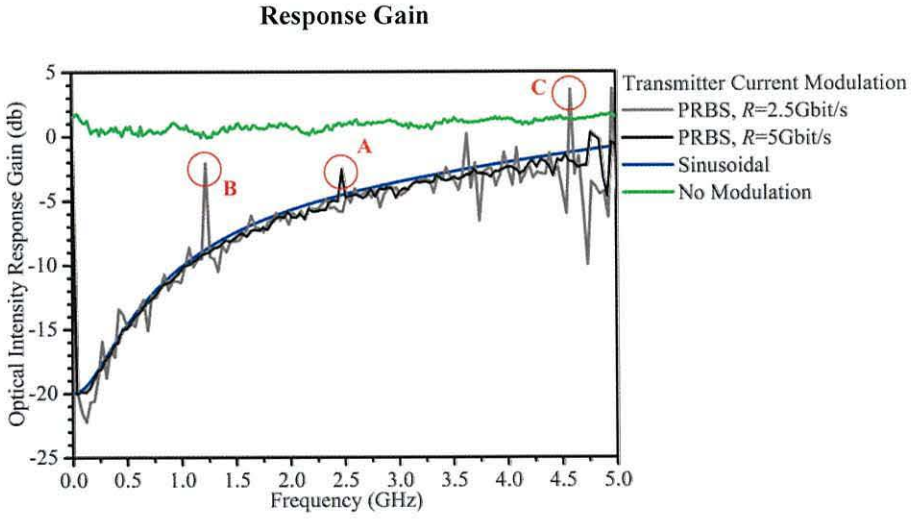

Figure 6.8. Response gain for slow (black) and high (grey) bit rate sections of the PRBS message applied to the transmitter drive current. Response gain for sinusoidal modulation (blue) and injection locking synchronization (green).

The response gain profiles of the PRBS message (Figure 6.8, black and grey lines) closely follow the response gain profile of sinusoidal current modulation (Figure 6.8, blue line) and receive a frequency dependent attenuation and gain. This response allows both the slow (R = 2.5Gbit/s) and fast (R = 5Gbit/s) messages to be extracted in the time domain via subtraction of the optical intensity dynamics in the receiver. The system response to the message is significantly different from the response to chaos injection (Figure 6.8, green line) and predicts that the PRBS message, if applied with sufficient power in the ECL transmitter, will be extractable in the receiver. The largest deviations, A, B, C, from the expected response gain for a current modulated message correspond to the low power spectral components of the message identified in Figure 6.5.

6.2.4 Summary

The high power spectral content of the Pseudo Random Bit Sequence message experiences the same transmitter response as sinusoidal modulation. The response gain for the transmitted PRBS message is also identical to that of sinusoidal messages and it is therefore anticipated that the message may be extracted from the background chaos when an external cavity laser transmitter is employed.

The message is distorted in the transmitter in two ways. Firstly, the frequency dependent current modulation response attenuates the higher frequency content. Secondly, the low power spectral components of the message are also not well

reproduced. However, the overall distortion introduced by the transmitter was shown to be small.

The frequency dependent attenuation or gain of the message in the receiver allows the extraction of the message via subtraction of the optical intensity dynamics. However, for messages consisting of significant spectral bandwidth the frequency dependence of both the transmitter current modulation response and receiver optical modulation response will introduce distortion to the message. In the case of the pseudo random bit message used here the level of distortion is very small and the message is easily recovered.

6.3 External Cavity Transmitter Laser PRBS Performance

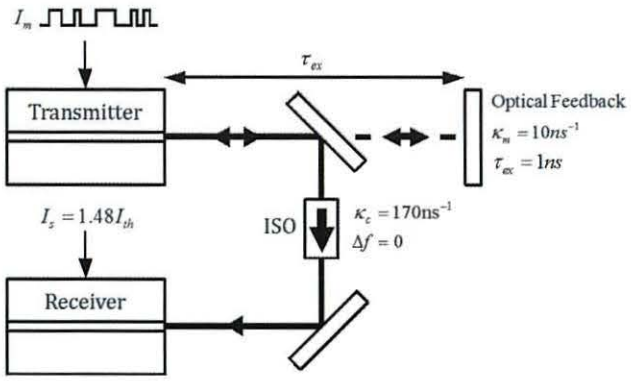

Figure 6.9. Schematic of external cavity transmitter laser subject to PRBS current modulation and receiver laser subject to optical injection from the transmitter.

An external mirror is added to the transmitter laser, shown in Figure 6.9, and provides optical feedback creating a chaotic carrier to mask the message. The optical feedback rate $\kappa_m = 10\text{ns}^{-1}$ and external cavity round trip time $\tau_{ex} = 1\text{ns}$ are the same as those used in the previous investigations. The pseudo random bit sequence message applied to the external cavity transmitter laser drive current is identical to that applied to the transmitter laser in the preceding section. Two cases will be presented:

- Case (i) - Strong modulation with modulation depth $h = 10\%$, as used for the transmitter without optical feedback, of the slow bit rate $(R = 2.5\text{Gbit/s})$ section of the message 59ns-85ns.
- Case (ii) - Weak modulation with modulation depth $h = 10\%$ of the fast bit rate $(R = 5\text{Gbit/s})$ section of the message 94ns-120ns.

Chapter 6 – Pseudo Random Bit Stream Message

The message extraction process in the receiver laser will be examined as well as the possibility that the message may be successfully intercepted by a naive eavesdropper using the time and frequency domain techniques developed in Chapters 2 to 5.

6.3.1 Best Case Scenario - Strong Modulation and Slow Bit Rate

6.3.1.1 Time Domain Analysis

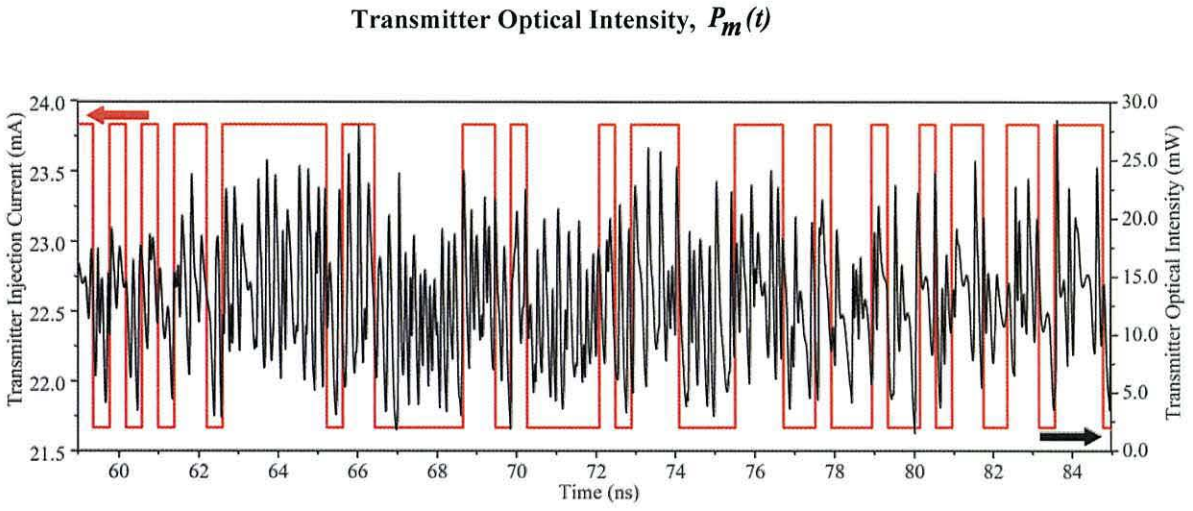

Figure 6.10. Optical intensity of transmitter laser subject to external optical feedback and strong current modulation ($h = 10\%$) of pseudo random bit sequence message.

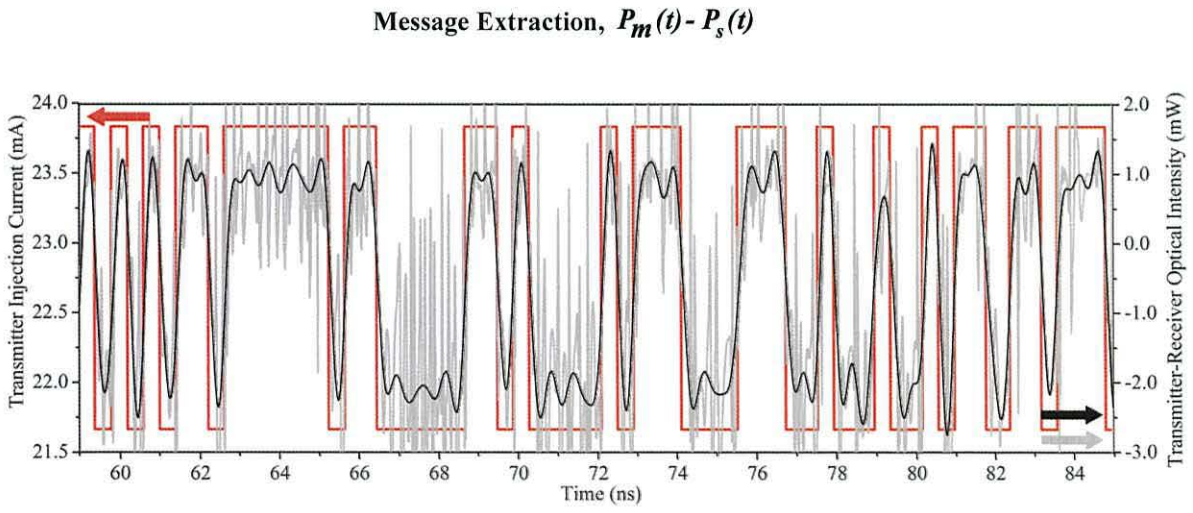

Figure 6.11. Extraction of message via subtraction of receiver output optical intensity from transmitted optical intensity.

Figure 6.10 presents the master laser optical intensity (black line) for the time range 59ns to 85ns with maximum message bit rate $R = 2.5\text{Gbit/s}$. The modulated transmitter drive current is superimposed in Figure 6.10 as the red line. The strong message modulation, $h = 10\%$, results in appreciable changes in the chaotic mean optical power. The mean optical intensity is significantly higher when a high bit level is encoded compared to a low bit level for the strong modulation, $h = 10\%$, employed here. The masking of the message is poor and the security of the transmission is weak.

The modulated ECL transmitter is injected into the receiver laser with injection rate $\kappa_c = 170\text{ns}^{-1}$ and zero detuning $\Delta f = 0$. The subtraction of the receiver intensity dynamics from the transmitter laser dynamics, $P_m(t) - P_s(t)$, is given by the grey line in Figure 6.11. The extracted message is low pass filtered with cut-off frequency $f_{cut-off} = 2.5GHz$ and is given by the black line in Figure 6.11. Excellent message recovery is achieved, as expected, for the strong modulation employed. The output of the low pass filter retains the majority of the message spectral content including the most important high power components while removing the high frequency noise and unsynchronized chaotic components.

6.3.1.2 Frequency Domain Analysis

(a) ECL Tx and Rx Optical Intensity Spectra

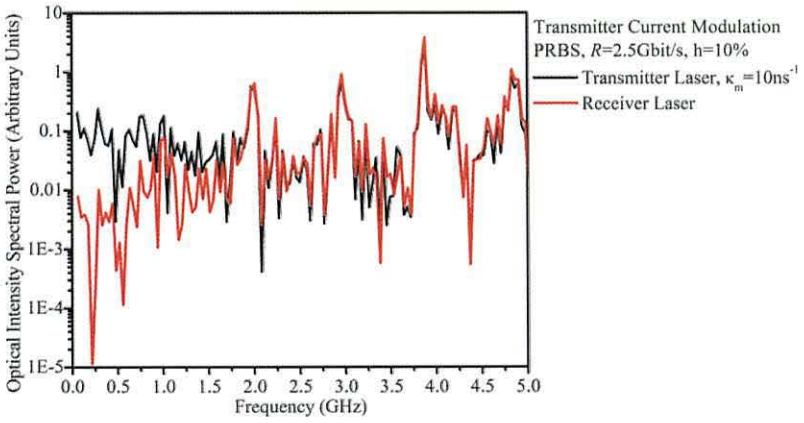

(b) Optical Intensity Response Gain

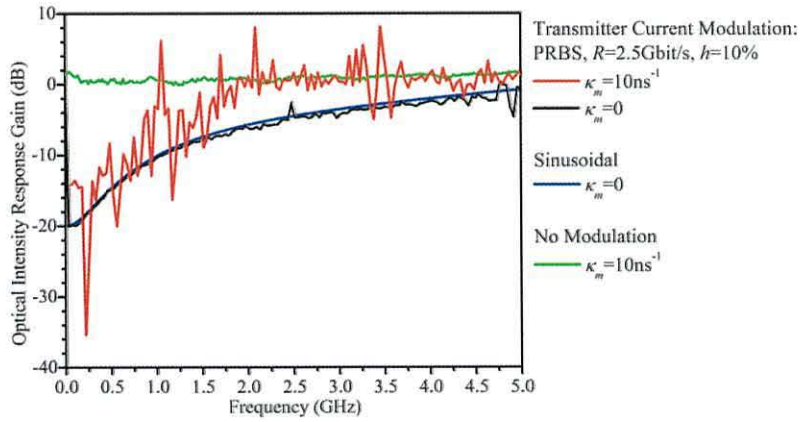

Figure 6.12. (a) Tx (black) and Rx (red) optical intensity output spectra for PRBS current modulation of ECL Tx. (b) System response gain for PRBS current modulation of ECL Tx (red), PRBS current modulation of Tx (black), sinusoidal current modulation of Tx (blue), injection locking synchronization (green).

Figure 6.12 (a) presents the optical intensity spectrum of the PRBS modulated ECL transmitter (black line) and the receiver laser (red line) for the time period 59ns to 85ns shown in Figure 6.11.

For chaos injection locking the slave spectrum closely follows that of the master. The areas of the master spectrum for which the message dominates the background chaos can, therefore, be identified by a power difference in the master and slave spectra.

It is clear in Figure 6.12 (a) that the transmitter spectral power (black line) for frequencies $f < 2\text{GHz}$ is much greater than in the receiver laser (red line). The spectral power for frequencies $f < 2\text{GHz}$ is dominated by the message and the background chaotic noise is negligible in comparison. For frequencies $f \geq 2\text{GHz}$ the master and slave spectra are closely aligned because message power is not sufficient to perturb the background chaotic noise. The transmitter and receiver lasers are synchronized for the majority of the spectral content $f \geq 2\text{GHz}$.

The response gain of the system for chaos masking of the PRBS modulated transmitter laser with slow bit rate, $R = 2.5\text{Gbit/s}$, and strong modulation, $h = 10\%$ will now be compared to the response gain of injection locking synchronization, simple sinusoidal modulation and PRBS modulation of the transmitter laser with no external mirror, Figure 6.12 (b).

The system response gain for the PRBS modulated ECL transmitter is given by the red line Figure 6.12 (b). The response gain for the same PRBS message applied to the transmitter laser with no external mirror is given by the black line in Figure 6.12 (b)

(from Figure 6.8, grey line) and the response gain for sinusoidal modulation of the transmitter laser is given by the blue line in Figure 6.12 (b) (from Chapter 5, Figure 5.3 (a)). Chaos injection locking with no current modulation (Chapter 3 Figure 3.2(a)) is given by the green line in Figure 6.12 (b). The dominant message components in the transmitter output identified in Figure 6.12 (a) $(f < 2GHz)$, have a response gain (Figure 6.12 (b), red line) close to the expected modulation response (blue and black lines, Figure 6.12 (b)). Frequencies upto and above the Nyquist frequency of $f_{Nyquist} = 1.25\text{GHz}$ follow the expected modulation response and as such it is anticipated that the message may be extracted via chaos pass filtering and this is exactly what is seen in Figure 6.11.

The response gain (Figure 6.12 (b), red line) for $f \geq 2\text{GHz}$ closely follows the average characteristic for chaos injection locking synchronization (green line, Figure 6.12 (b)) except for a few spectral components of the message that have sufficient power to dominate the local minima in the background chaotic noise, e.g. close to $f = 3.5\text{GHz}$ and $f = 4.5\text{GHz}$. Above approximately 2GHz the majority of the message power is insufficient to perturb the background chaotic noise, as observed in Figure 6.12 (a), and cannot be recovered in the receiver. The loss of message components $f \geq 2\text{GHz}$ suggests that the extracted signal should experience a small amount of distortion and this is exactly what is seen in Figure 6.11.

6.3.1.3 Naive Eavesdropper

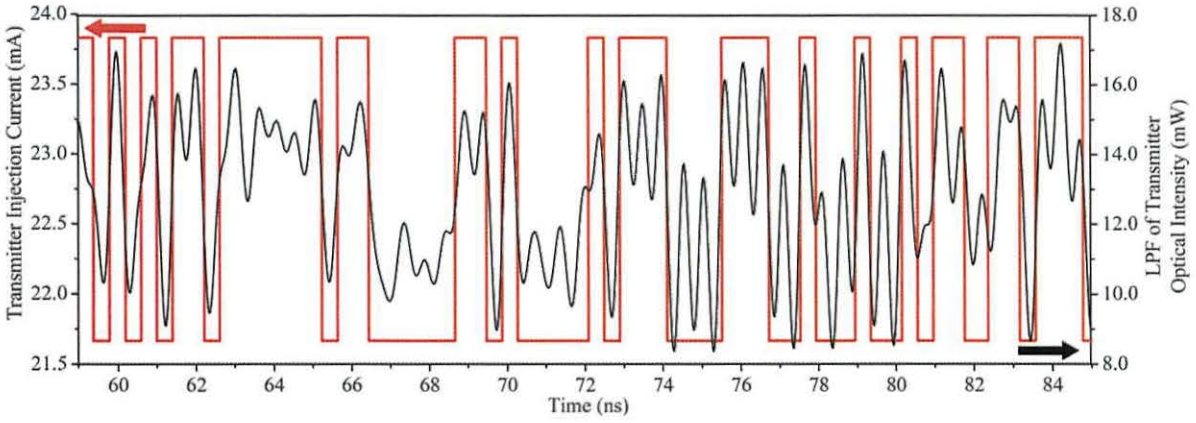

Figure 6.13. Low pass filter of transmitted optical intensity with cut-off frequency $f_{cut-off} = 2.5\text{GHz}$.

The dominant message components observed in the transmitter spectrum Figure 6.12 (a) suggests that the transmitted message is liable to interception by a naive eavesdropper. It will now been shown that a strongly modulated message is not effectively masked by the chaotic background noise produced in the ECL transmitter. Figure 6.13 presents the result of direct low pass filtering (cut-off frequency $f_{cut-off} = 2.5GHz$) of the transmitter laser output, thereby simulating a naive eavesdropper. The decoded message seen in Figure 6.13 (black line) shows that the strong modulation ($h = 10\%$) applied here does not allow the chaos to effectively mask the transmitted message.

6.3.1.4 Summary

The receiver response at a particular frequency is determined by the relative spectral power of the message and the background chaotic noise. If the power of the message component is dominant then it is subject to the same frequency dependent attenuation or gain as sinusoidal modulation of a transmitter without an external mirror. If the background chaotic noise component is dominant then the receiver synchronizes with the transmitter. The combination of these two processes allows the extraction of the message via chaos pass filtering [12].

6.3.2 Worst Case Scenario - Weak Modulation and Fast Bit Rate

6.3.2.1 Time Domain Analysis

A lower modulation depth of $h = 5\%$ is now considered for the time range 94ns - 120ns with a message bit rate of $R = 5\text{Gbit/s}$. The lower modulation depth and broader message spectrum should result in greater intermixing of the spectral components of the message and the background chaos. The masking, and hence, the security of the message is improved. The aim is to increase the security of the transmitted message while allowing extraction of the message in the receiver.

The improved chaotic masking should mean that the bit transitions are no longer clearly observed in the optical output as changes in the mean output power. In the frequency domain we expect the transmitted signal to contain fewer dominant message components.

However, as described above for strong modulation, a sufficient amount of the message spectrum must dominate the corresponding background chaotic noise in order to ensure successful extraction. Therefore, the quality of the recovered message is likely to deteriorate.

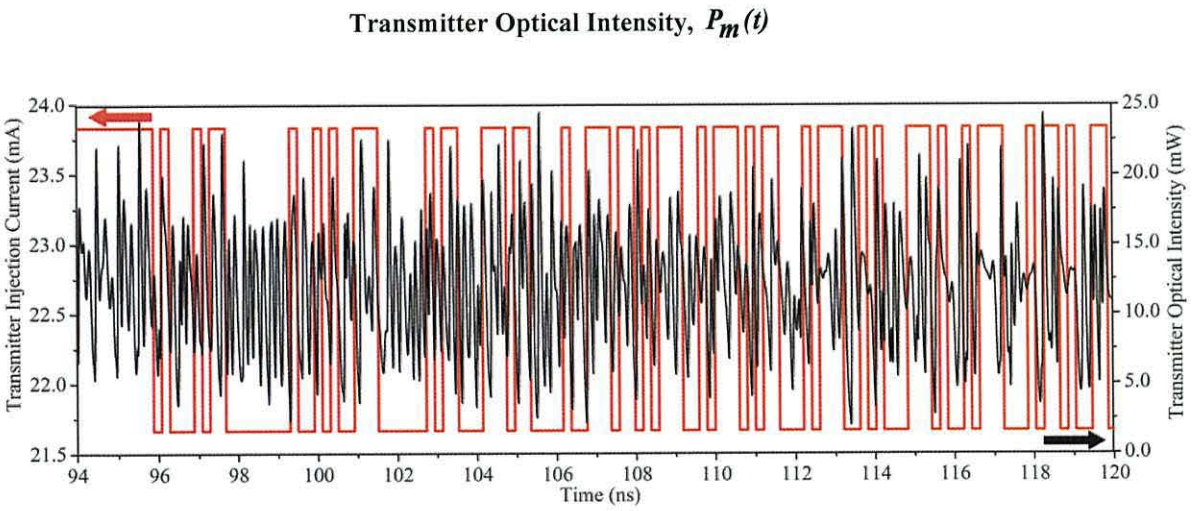

Figure 6.14. Optical intensity of transmitter laser subject to external optical feedback and weak current modulation (h = 5%) of pseudo random bit sequence message.

The optical intensity output of the PRBS modulated ECL transmitter is presented by the black line in Figure 6.14. The message applied to the transmitter drive current is given by the red line in Figure 6.14. The low modulation depth (h = 5%) and faster bit rate (R = 5Gbit/s) employed here means the intensity fluctuations due to the modulation are smaller and as a result are better masked by the fluctuations in the background chaotic noise, Figure 6.14, when compared to the strongly modulated slower rate message shown in Figure 6.10. Changes in the optical intensity at bit transitions are not evident in the optical intensity output, Figure 6.14. The bit rate of the message is sufficiently high so that the spectral range of the message coincides with significant chaotic spectral power.

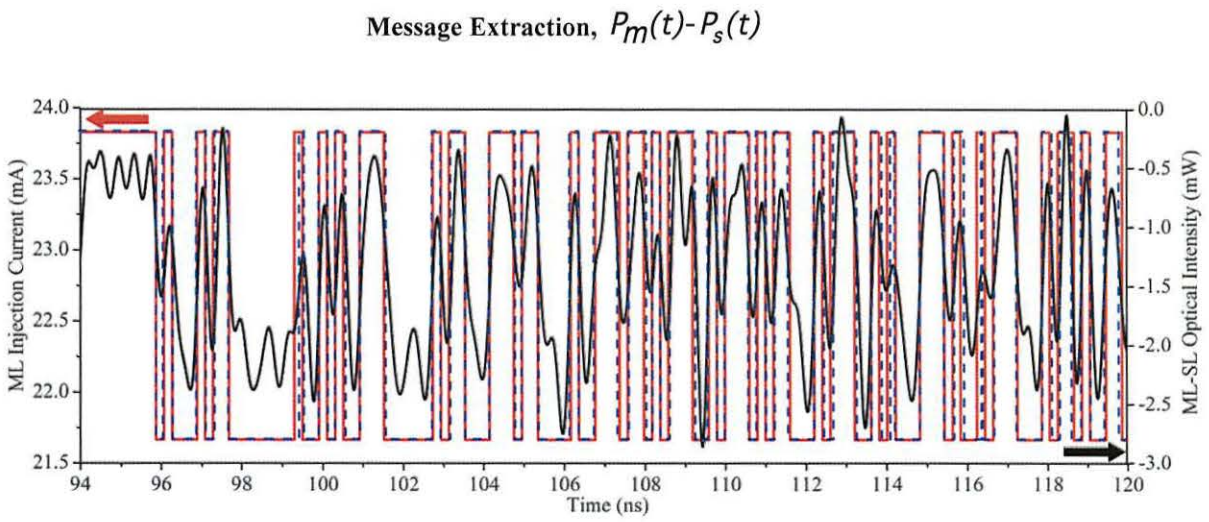

Figure 6.15. Extraction of message via subtraction of receiver output optical intensity from transmitted optical intensity.

The output message is extracted by subtracting $P_s(t)$ from $P_m(t)$ and then low-pass filtered with $f_{cut-off} = 3.5GHz$ and is shown by the black line in Figure 6.15.

The message is recovered by applying a threshold at the mean output of the low-pass filter. Above the threshold the message is 'high' and equal to or below the threshold the message is 'low'. The recovered message is given by the dashed blue line and can be compared to the applied message given by the red line, Figure 6.15. The message recovery in the receiver is good for low modulation depth $h = 5\%$ and bit rate $R = 5\text{Gbit/s}$.

6.3.2.2 Frequency Domain Analysis

(a) ECL Tx and Rx Optical Intensity Spectra

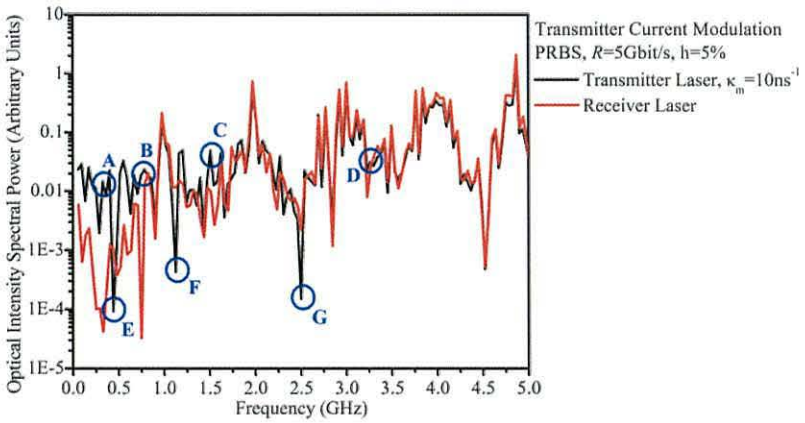

(b) Optical Intensity Response Gain

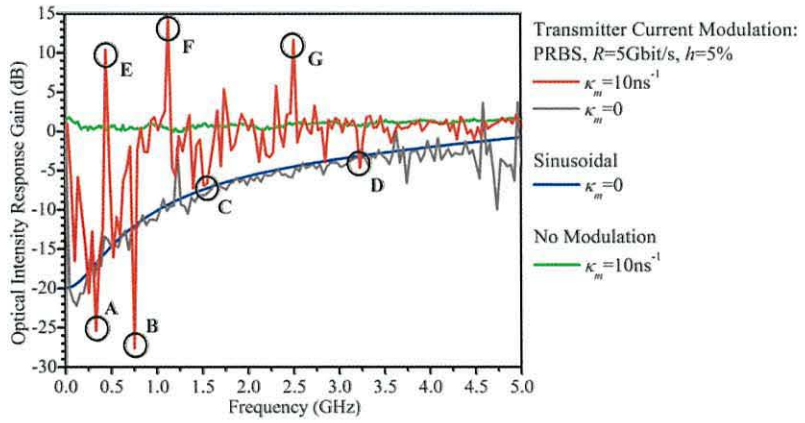

Figure 6.16. (a) Tx (black) and Rx (red) optical intensity output spectra for PRBS current modulation of ECL Tx. (b) System response gain for PRBS current modulation of ECL Tx (red), PRBS current modulation of Tx (black), sinusoidal current modulation of Tx (blue), injection locking synchronization (green).

The optical intensity spectra of the PRBS modulated ECL transmitter (black line) and receiver laser (red line) are presented in Figure 6.16 (a). The spectral components of the

message that have significantly more power than the background chaos can be seen in the transmitter spectrum, examples of which are denoted by points A-D in Figure 6.16 (a). Sections of the spectrum where the receiver closely follows the transmitter correspond to synchronization of the background chaos. Spectral components that correspond to low power message and background noise are also observed, given by points E-G in Figure 6.16 (a). These components are neither synchronized or subject to the expected attenuation or gain.

As expected, fewer dominant message spectral components are observed for the low modulation depth, Figure 6.16 (a), than for the high modulation depth, Figure 6.12 (a). Greater intermixing of dominant message and background chaos components is observed in Figure 6.16 (a). The local maxima in the background chaos at $f = 1\text{GHz}$ is now dominant at the lower modulation depth (cf. Figure 6.12(a)).

The system response gain for the PRBS modulated ECL transmitter is given by the red line Figure 6.16 (b). The response gain for the same PRBS message applied to the transmitter laser with no external mirror (Figure 6.16 (b), grey line) and the response gain for sinusoidal modulation of the transmitter laser (Figure 6.16 (b), blue line) are superimposed for comparison in Figure 6.16 (b). Chaos injection locking with no current modulation (Chapter 3 Figure 3.2(a)) is given by the green line in Figure 6.16 (b).

The high power message components including points A-D identified in Figure 6.16 (a) have response gains (Figure 6.16 (b), red line) close to the expected modulation

response of PRBS modulation of the transmitter with no external mirror (Figure 6.16 (b), grey line). The high power background chaos is synchronized in the receiver and closely follows the average response gain for un-modulated injection locking synchronization (Figure 6.16 (b), green line). The largest deviations from the message (Figure 6.16 (b), grey line) and synchronized chaos (Figure 6.16 (b), green line) response gain characteristics are denoted by points E-G in Figure 6.16 (b) and correspond to the same points in Figure 6.16 (a), identified as low power message and background chaos spectral components.

The high power spectral components of the message remain dominant even for the lower modulation depth $h = 5\%$ (and bit rate $R = 5\text{Gbit/s}$) and are subject to the expected attenuation in the receiver laser that allows the message to be successfully recovered. If the modulation depth is decreased further $(h < 5\%)$ the high power spectral components of the message no longer dominate over the background chaos and the message cannot be recovered by subtraction in the receiver.

6.3.2.3 Eavesdropper

If the transmission is monitored by an eavesdropper the overall structure of the chaotic carrier can be identified. The frequencies of the local maxima and minima in the chaotic background spectrum can be estimated and from this a series of filters can be used in an attempt to extract the message.

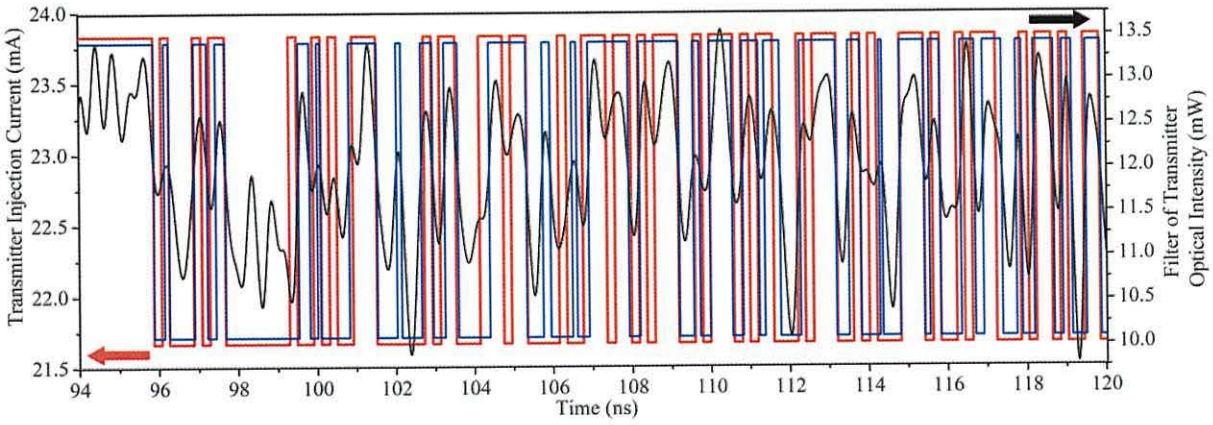

Figure 6.17. Attempted message extraction from filtration of transmitted optical intensity. Filter used: Low pass filter $f_{cut-off} = 2.5GHz$, band-stop filters $f_{1,low} = 0.9GHz$, $f_{1,high} = 1.2GHz$, $f_{2,low} = 1.7GHz$, $f_{2,high} = 2.3GHz$.

Even for this weak modulation there is significant power at low frequencies $f < 2GHz$ and the chaotic local maxima at $f = 1GHz$ and $f = 2GHz$ may be identified. Using this information the transmitter output intensity is filtered using a low pass filter with cut-off frequency $f_{cut-off} = 2.5GHz$ and band-stop filters with low and high frequency cut-off frequencies $f_{1,low} = 0.9GHz$, $f_{2,low} = 1.7GHz$ and $f_{1,high} = 1.2GHz$, $f_{2,high} = 2.3GHz$ respectively. The low pass filter removes the background chaos at frequencies at which the message is not expected to have significant power. The band-pass filters remove the chaotic maxima at $f = 1GHz$ and $f = 2GHz$ respectively. The result of the filters is given by the black line in Figure 6.17. The same threshold at the mean output of the filter is applied and the recovered message is given by the blue line in Figure 6.17. The message recovery from studying the transmitter output is poor in comparison to the receiver extraction.

The receiver laser is now, in essence, a complex band stop filter attenuating the high power message components. This makes it difficult for the message to be successfully extracted from the transmitted signal by an eavesdropper. However, the recovered message in Figure 6.17 could be improved by applying a threshold with error correction codes. There remains the possibility of extraction by an eavesdropper because the message components remain dominant in the transmitted signal in the chaotic masking communications system.

6.3.2.4 Summary

The low modulation depth employed here reduces the number of message components that are dominant in the transmitter output and therefore those that can be extracted in the receiver. However, sufficient message components remain to reconstruct the message in the receiver.

There is greater intermixing of the message and background chaotic noise components at the low modulation depth. The receiver synchronizes to the dominant chaotic components and attenuates the dominant message components. The difference in the receiver response to the message and the background chaos allows the message to be extracted by subtraction of the optical fields in the receiver. The greater intermixing of the message and background chaos means it is difficult for a naive eavesdropper to extract the message.

6.4 Conclusions

The more complex PRBS message investigated in this chapter is subject to the same response gain characteristic in the transmitter and receiver laser diodes as for simple sinusoidal messages.

The PRBS message applied to the transmitter suffers distortion in both the transmitter and receiver. The message is subject to a frequency dependent current modulation response in the transmitter and only the high power spectral components of the message are accurately encoded. In the receiver the broadband message is subject to a frequency dependent optical modulation response.

It has been shown that a message spectral component is extractable in the receiver if it has sufficient power to dominate the corresponding chaotic noise. However, a strongly applied message can be extracted by naive eavesdropper simply low-pass filtering.

A degree of security via chaotic masking has been observed for a low modulation depth and high bit rate message. For this worst case scenario the message is at the limit of extraction in the receiver laser via chaos pass filtering. The message is not easily extracted by an eavesdropper. However, the investigation performed here assumes ideal conditions with no transmission losses and very good quality transmitter – receiver chaos synchronization.

Chapter 6 – Pseudo Random Bit Stream Message

When applying a low modulation depth message, close to the limit of possible extraction where the best masking is achieved, the spectral structure of the background chaotic noise generated in the ECL transmitter needs to be considered to avoid losing important message components to dominant high power chaotic components.

6.5 Bibliography

[1] C R Mirasso, P Colet, and M San Miguel, "Pseudorandom word modulation of single-mode semiconductor lasers at GHz rates," *IEE Proceedings-J*, vol. 140, no. 1, pp. 26-29, February 1993.

[2] V Annovazzi-Lodi and S Donati, "Synchronization of Chaotic Injected-Laser Systems and Its Application to Optical Cryptography," *IEEE Journal of Quantum Electronics*, vol. 32, no. 6, pp. 953-959, June 1996.

[3] G D Van Wiggeren and R Roy, "Communication with chaotic lasers," *Science*, vol. 279, pp. 1198-1200, 1998.

[4] G D Van Wiggeren and R Roy, "Chaotic communications using time delayed optical systems," *International J. of Bif. and Choas*, vol. 9, pp. 2129-2156, 1999.

[5] C R Mirasso, P Colet, and P Garcia-Fernandez, "Synchronization of chaotic semiconductor lasers: application to encoded communications," *Phot. Tech. Lett.*, vol. 8, pp. 299-301, 1996.

[6] A Sanchez-Diaz, C Mirasso, P Colet, and P Garcia-Fernandez, "Encoded Gbit/s digital communications with synchronized chaotic semiconductor lasers," *IEEE J. Quant. Electron.*, vol. 35, pp. 292-297, 1999.

[7] S Sivaprakasam and K A Shore, "Message encoding and decoding using chaotic external-cavity diode lasers," *IEEE J. Quant. Electron.*, vol. 36, pp. 35-39, 2000.

[8] I Fischer, Y Liu, and P Davis, "Synchronization of chaotic semiconductor laser dynamics on sub-ns timescales and its potential for chaos communication," *Phys. Rev. A*, vol. 62, p. 011801, 2000.

[9] J Ohtsubo, "Chaos Synchronization and Chaotic Signal Masking in Semiconductor Lasers With Optical Feedback," *IEEE Journal of Quantum Electronics*, vol. 38, no. 9, pp. 1141-1154, September 2002.

[10] R Vicente, T Perez, and C R Mirasso, "Open- Versus Closed-Loop Performance of Synchronized Chaotic External-Cavity Semiconductor Lasers," *IEEE Journal of Quantum Electronics*, vol. 38, no. 9, pp. 1197-1204, September 2002.

[11] J-M Liu, H-F Chen, and S Tang, "Synchronized Chaotic Optical Communications at High Bit Rates," *IEEE Journal of Quantum Electronics*, vol. 38, no. 9, pp. 1184-1196, September 2002.

[12] A Murakami and K A Shore, "Chaos-pass filtering in injection-locked semiconductor lasers," *Phys. Rev. A*, vol. 72, no. 5, p. 053810, 2005.

[13] J Paul, M W Lee, and K A Shore, "Effect of chaos pass filtering on message decoding quality using chaotic external-cavity laser diodes," *Optics Letters*, vol.

29, no. 21, pp. 2497-2499, 2004.

[14] R Vicente, C R Mirasso, and I Fischer, "Simultaneous bidirectional message transmission in a chaos-based communication scheme," *Optics Letters*, vol. 32, no. 4, pp. 403-405, February 2007.

[15] William H Press, Brian P Flannery, Saul A Teukolsky, and William T Vetterling, *Numerical Recipes in C: The Art of Scientific Computing*, 2nd ed.: Cambrifge University Press, 1992.

Review of Thesis

Chapter 1 presented the semiconductor laser background theory required to create the numerical model outlined in Chapter 2.

The simulations of a master-slave configuration of semiconductor laser diodes were presented in Chapter 2. In this configuration the optical output of the master laser diode is injected into a slave laser diode. The master laser dynamics are driven to chaos by the addition of optical feedback from an external mirror. If a sufficient proportion of the master laser optical output is injected into the slave laser diode then the dynamics of the slave lock to those of the master and injection locking chaos synchronization is achieved. The operation of the numerical model was verified by simulating the widely studied phenomenon of chaotic injection locking and recreating the widely used chaos injection locking diagram – a composite plot created from a large number of simulations with different injection strength and detuning frequencies. The degree of temporal synchronization between the master and slave laser optical intensity, phase and carrier dynamics were determined using a cross-correlation function. The synchronization quality of the optical intensity, phase and carrier dynamics were compared for varying slave laser injection rates at zero detuning. The optical phase was shown to have the highest correlation followed by the carrier's then optical intensity.

The lower optical intensity correlation was attributed to high frequency distortion of the optical intensity dynamics.

Chaos synchronization was examined further in Chapter 3 using a new frequency domain technique. The injection locking diagrams of the carrier dynamic and for the current modulated system were also calculated for the first time.

Motivated by the eventual aim of simulating a chaotic communications system, the quality of the chaos synchronization has also been studied when the master laser (transmitter) is modulated. This systematic approach verified that good synchronization could still be achieved in the slave laser (receiver). The signals applied to the master laser drive current were shown to have very little effect upon the quality of the synchronization.

Chapter 3 examined chaos injection locking in the frequency domain. The output optical intensity spectra of the master and slave laser diodes were presented and the response gain and master laser phase lead characteristics were calculated. It was demonstrated that a flat response gain profile and master phase lead of zero for the high power spectral components, close to the relaxation oscillation frequency, were required for a good synchronization.

The study of individual simulations rather than ensemble averages identified the high power spectral components in the master laser and demonstrated for the first time that, at any moment in time, only a relatively small range of frequencies, close to the relaxation oscillation, were required for good quality synchronization. The largest

variation from the desired flat response gain profile and zero phase lead were observed for low power spectral components, these low power spectral components do not have sufficient power to be well reproduced in the slave laser and hence are not synchronized. This validates the conclusions gained from the averaged simulation outputs but emphasises that only a relatively small number of the high power components are required to be accurately reproduced in the slave laser at any instant in time to achieve a good synchronization.

The origin of the difference between the carrier and optical intensity time domain correlations was studied in the frequency domain and the difference attributed to their specific spectral characteristics. The majority of the spectral power of the carrier dynamics is located at low frequencies below the relaxation oscillation frequency. The response gain characteristic for both the carrier dynamics and optical intensity was shown to be identical but the slower dynamics of the carriers mean that a greater proportion of their spectral power is situated within the band of frequencies subject to the desired flat response gain. The distortion introduced in the slave laser at frequencies above the relaxation oscillation frequency therefore has less effect upon the carriers than the optical intensity.

For the first time, frequency domain based chaos injection locking diagrams were constructed by collating the results of a large number of response gain and phase lead characteristics with varying injection rates and detuning frequencies. The frequency based technique presented here provides added insight into the chaos synchronization process. Trends in synchronization quality observed using these frequency domain

techniques could then be compared to the traditional time domain methods. The trends observed in the time domain correlation were also observed in the response gain characteristic. The frequency based injection locking diagrams show that, even though there is little chaotic power at frequencies greater than the relaxation oscillation, the small changes in correlation observed in the injection locking region are highly dependent upon these low power high frequency components since a significant amount of distortion is introduced.

The addition of a message via the modulation of the semiconductor laser diode drive current was introduced in Chapter 4. Chapter 4 explored the current modulation of a solitary laser diode and then an external cavity laser diode operating in the coherence collapse regime. The frequency dependent output characteristic of the modulated solitary laser and ECL were presented. A difference is observed between the output characteristics of the current modulated solitary and ECL laser diodes. Message frequencies applied to the ECL drive current close to local maxima in the average chaos have additional power from constructive interference due to the optical feedback from the external mirror.

The degree to which the average background chaos and an applied sinusoidal message contribute towards the laser output was presented and for the first time three regions of operation were identified:

Region I – At very low modulation depths the message is not effectively applied and is indistinguishable from the background chaotic noise.

Region II – For intermediate modulation depths both the chaotic background noise and message have comparable spectral power and determine the output power at the applied message frequency. At any point in time the message or background noise can dominate the output depending upon the spectral power fluctuations of the chaotic background noise.

Region III – High modulation depths allow the message to dominate as the power fluctuations of the background noise become insignificant in the transmission at the message frequency.

Chapter 5 adds a receiver laser diode which is injected with the optical output of the modulated transmitter (master) laser diode. Frequency domain techniques were used to study: the chaotic masking of an applied sinusoidal message; the optical modulation of the receiver laser and the extraction of the message. The optical amplitude and phase modulation response of the receiver to the sinusoidal messages applied via current modulation of the transmitter were shown to be frequency dependent.

A strongly applied message may be extracted in the receiver laser via the phenomenon of chaos pass filtering. The response gain characteristic for chaos synchronization of a master and slave laser system as presented in Chapter 3 was compared to that of a chaos communication system. The differences in the optical and current modulation characteristics give rise to frequency dependent attenuation and gain of the message while the high power background chaos receives uniform gain in the receiver. This synchronization of the background chaos and attenuation or gain of the message allows

the message to be extracted in the receiver by subtraction of the receiver output from the incoming transmission.

The three regions of operation of the modulated ECL diode defined in Chapter 4 were then related to the quality of message extraction in the receiver:

Region I – At very low modulation depths the message is not effectively applied and is indistinguishable from the background chaotic noise. The applied message is effectively masked but is not extractable in the receiver.

Region II – For intermediate modulation depths both the chaotic background noise and message have significant effect upon the transmitted power at the applied message frequency. At any point in time the message or background noise may be dominant in the transmitter spectral output depending upon the chaotic power fluctuations of the background noise. The message cannot be consistently extracted in the receiver; for portions of the transmission where the background chaos is dominant the message is unrecoverable as for Region I, and for portions of the transmission for which the message component of the transmitter output is dominant the message is extractable in the receiver via chaos pass filtering, as for Region III.

Region III – High modulation depths allow the message to dominate and the power fluctuations of the background chaos become insignificant in the transmission at the message frequency. The dominant message component allows simple extraction of the message in the receiver.

There is, therefore, a trade off between security of the message and ease of extraction. A strongly applied message may be easily extracted via subtraction of the optical fields in the receiver laser but is susceptible to possible detection in the transmission by an eavesdropper. A securely applied message that is not distinguishable from the background noise is also indistinguishable from the chaos in the receiver and cannot be extracted successfully.

Using the frequency domain techniques developed in previous chapters, chapter 6 showed that the complex and more realistic message made up of a pseudo random bit sequence (PRBS) is subject to the same response in the transmitter and receiver lasers as for individually applied sinusoidal messages.

For messages applied with sufficient power to be successfully extracted in the receiver laser the following conclusions were drawn from the simulations. The time varying spectral content of the PRBS message is more difficult to identify in the transmission spectrum if the applied modulation depth is just high enough to operate in Region III. The modulation depth can be set such that sufficient spectral content of the PRBS message is applied within region III for successful reconstruction of the message in the synchronized receiver while the background chaos masks the message in the transmission. The message is not easily extracted however due to the interaction with the fluctuating spectral power of the background chaos some deterioration of the message at the receiver must be accepted if the message is to be securely transmitted.

Appendix

List of Publications

Journal Publications

1. Sam J. Lea and Paul S. Spencer. Frequency domain analysis of the chaotic synchronization of injection-locked semiconductor lasers. Opt Quant Electron. Springer. April 2008.

Conference Contributions

1. Sam J. Lea and Paul S. Spencer. Frequency domain analysis of the chaotic synchronization of injection-locked semiconductor lasers. PHASE, Metz, 28th – 30th March 2007.

3. Sam J. Lea and Paul S. Spencer. Nonlinear amplitude response of slave laser induces the chaos pass filtering effect in synchronized semiconductor laser diodes. CLEO/Europe, Munich, 17th – 22nd June 2007.

4. Sam J. Lea and Paul S. Spencer. Message Extraction. PICASSO Meeting, Berlin. 19th - 20th March 2009.

5. Sam J. Lea and Paul S. Spencer. Pseudo Random Bit Sequence Transmission in Chaos Communication Channel. SIOE, Cardiff. April 2009.

6. Sam J. Lea and Paul S. Spencer. Analysis of Experimental Data from a Chaos Communication Channel. SIOE, Cardiff. April 2009.